TIME-RESOLVED TUNABLE DIODE LASER DETECTION OF THE PRODUCTS OF THE INFRARED MULTIPHOTON DISSOCIATION OF CF_2HCl, $(CF_3)_2CO$, AND $CHCl_3$

by

JOHN JOSEPH ORLANDO, B.Sc.

A Thesis

Submitted to the School of Graduate Studies

in Partial Fulfilment of the Requirements

for the Degree

Doctor of Rhilosophy

© McMaster University

1987

TUNABLE DIODE LASER DETECTION OF THE PRODUCTS OF IRMPD

DOCTOR OF PHILOSOPHY (1987) McMASTER UNIVERSITY
(Chemistry) Hamilton, Ontario

TITLE: Time-resolved Tunable Diode Laser Detection of the Products of the Infrared Multiphoton Dissociation of CF_2HCl, $(CF_3)_2CO$, and $CHCl_3$

AUTHOR: John Joseph Orlando, B.Sc. (McMaster University)

SUPERVISOR: Dr. D.R. Smith

NUMBER OF PAGES: xx, 149

ABSTRACT

In the experiments described in thesis, tunable diode lasers are used to detect infrared absorption by the transient species produced in the infrared multiphoton dissociation (IRMPD) of CF_2HCl, $(CF_3)_2CO$, and $CHCl_3$.

The time-resolved infrared absorptions of CF_2 and HCl are detected following the IRMPD of CF_2HCl. Quantification of the HCl allows one to determine a CF_2 infrared absorption linestrength, $(9\pm2) \times 10^{-21}$ cm molecule^{-1} for the $^rQ_3(9)$ line. From this linestrength, the CF_2 ν_1 bandstrength is found to be $(3.4\pm0.8) \times 10^{-18}$ cm molecule^{-1}. The rate constant for CF_2 recombination to form C_2F_4 is found to be $(2.3\pm0.7) \times 10^{-14}$ cm^3 molecule^{-1} s^{-1}.

Time-resolved detection of CF_3, C_2F_6, and CO following the IRMPD of $(CF_3)_2CO$ establishes that the dissociation mechanism involves the production of one molecule of CO and two of CF_3. From this stoichiometry, the linestrength of the $^rR_{16}(20)$ CF_3 transition is found to be $(1.4\pm0.3) \times 10^{-20}$ cm molecule^{-1} and the CF_3 ν_3 bandstrength is then calculated to be $(8\pm2) \times 10^{-17}$ cm molecule^{-1}. The rate constant for CF_3 recombination is

measured to be (2.2±0.5) X 10^{-12} cm^3 $molecule^{-1}$ s^{-1} at or near the high pressure limit, while the rate constant for CF_3 reacting with O_2 and NO are found to be (2.1±0.5) X 10^{-29} and (2.8±0.7) X 10^{-29} cm^6 · $molecule^{-2}$ s^{-1}, respectively.

The use of TDLs in determining the isotopic selectivity of IRMPD processes is then analysed. The sensitivity of the technique is demonstrated in the detection of the DCl produced in the IRMPD of natural abundance $CDCl_3$ in $CHCl_3$. However, complications due to wall adsorption and desorption effects necessitate monitoring the DCl and HCl on a short timescale (tens of μs) to obtain meaningful quantitative information. It is shown that the CCl_4 and much of the HCl produced in the photolysis of $CDCl_3/CHCl_3$ mixtures is the result of isotopically non-selective reactions involving Cl atoms.

ACKNOWLEDGMENTS

I would like to thank the following people for their contribution to this thesis:

Dr. Don Smith, for his guidance throughout this work;

Dr. John Reid, for lending his expertise in the area of TDL analysis and for helpful discussions regarding all aspects of this work;

Atomic Energy of Canada Ltd., for the loan of the high repetition rate CO_2 laser;

Dr. John Johns of N.R.C., for confirming the method used in calculating the CF_2 bandstrength;

N.S.E.R.C., for financial support in the form of a post-graduate scholarship;

Mr. Carl Brown, for his collaboration in the development of the transient detection technique for CF_2 (Section 3.2) and CF_3 (Section 4.2) and in the measurement of the CF_3 recombination rate constant (Section 4.4.5), his general assistance throughout the course of this work and for making the lab an enjoyable place to work.

Mr. Paul Beckwith, for his collaboration in the development of the transient detection technique for CF_2

(Section 3.2), the development of DCI detection and, in particular, for collecting the data presented in Figure 5.4.

My parents and brother for their continual support;

The many friends who made my graduate life that much more rewarding;

Brian Fahie, for his advice and friendship, and especially Joan Fahie, for her help in proofreading this manuscript and for her constant support and friendship.

TABLE OF CONTENTS

	PAGE
ABSTRACT	iii
ACKNOWLEDGEMENTS	v
LIST OF FIGURES	x
LIST OF TABLES	xx
CHAPTER	
1 INTRODUCTION	1
1.1 General	1
1.2 The IRMPD Process	5
1.3 Theory of Infrared Absorption	24
1.4 Summary	28
2 EXPERIMENTAL	30
2.1 Introduction	30
2.2 Gases and Gas Handling Techniques	30
2.3 Photolysis and Stable Product Analysis Techniques	31
2.4 Time-resolved Detection of Transients with TDLs	40
2.5 Summary	47

3 IRMPD OF CF_2HCl 48

3.1 Introduction 48

3.2 Experimental 48

3.3 Photolysis Mechanism 52

3.4 Results and Discussion 55

3.4.1 CF_2 and HCl Vibrational Relaxation 55

3.4.2 Linestrength and Bandstrength Calculations 59

3.4.3 CF_2 Kinetics 66

3.5 Summary 68

4 IRMPD OF HEXAFLUOROACETONE 70

4.1 Introduction 70

4.2 Experimental 70

4.3 Previous Work 73

4.4 Results and Discussion 75

4.4.1 Photolysis Mechanism 75

4.4.2 Vibrational Relaxation of CF_3 80

4.4.3 Photolysis Yield as a Function of Fluence 80

4.4.4 CF_3 Linestrength and Bandstrength Calculations 81

4.4.5 CF_3 Kinetic Studies 85

4.5 Summary 92

5 IRMPD OF $CDCl_3/CHCl_3$ 95

5.1 Introduction 95

5.2 Experimental 96

5.3 Previous Work 98

5.4 Results and Discussion 104

5.4.1 Effect of Additives on Product Yield in $CDCl_3$ IRMPD 104

5.4.2 DCl/HCl Detection Following IRMPD of Chloroform 110

5.4.3 Time-Resolved TDL Detection of DCl/HCl 117

5.5 Summary 121

6 CONCLUSIONS 123

6.1 Introduction 123

6.2 Time-Resolved Detection with TDLs 124

6.3 Determination of the IRMPD Mechanism 125

6.4 Linestrength and Bandstrength Calculations 127

6.5 Kinetic Studies of Transient Species 129

6.6 Laser Isotope Separation 131

6.7 Summary 132

REFERENCES 133

APPENDIX A 148

LIST OF FIGURES

NO.		PAGE
2.1	Experimental design for static sample photolyses. The CO_2 laser beam is focussed by means of a 25 cm BaF_2 lens into the cell. Polyethylene sheets are used as necessary to obtain the desired CO_2 laser pulse energy.	32
2.2	Schematic diagram of TDL stable product analysis apparatus. The TDL beam is focussed into the cell by means of L_1, and then focussed onto the IR detector using L_2. The TDL beam is chopped by the mechanical chopper. Detection is done using a lock-in amplifier whose phase matches that of the chopper.	36
2.3	Calibration plots for CO and CO-$CHCl_3$ mixtures. Line A, showing detection of pure CO, gives a linestrength for R(8) in agreement with the literature. Line B shows the effects of pressure broadening	38

on the CO absorption coefficient. The data are consistent with a pressure-broadening coefficient of 8.0 X 10^{-5} cm^{-1} $Torr^{-1}$, as measured in our lab. Line C, with detection done on R(6), shows that the measured absorption coefficient (by either direct or second harmonic detection) is linear over a range of CO pressures of greater than three orders of magnitude. The inset defines the parameters I and I_o, used in the measurement of α_o.

2.4 Schematic of TDL transient detection apparatus. Lens L_1 is used to focus the TDL beam, while lens L_2 collimates the CO_2 laser beam. The two beams are combined on beamsplitter M_1 and focussed on L_3 into the capillary cell. The two beams are then separated on a diffraction grating, with the TDL beam then being focussed onto the infrared detector, and the CO_2 laser beam being focussed onto an energy meter. 41

2.5 Idealized schematic of the detector output in a transient detection experiment. In each modulation cycle, the absorption feature is sampled twice, once in each direction. 44

2.6 Demonstration of the advantages of background subtraction in TDL transient spectroscopy. Note that the subtraction removes the precursor absorptions and enhances the CF_2 signal. The CF_2 is produced by photolysis of 1.5 Torr of C_2F_3Cl, and both the signal and background represent the average of 50 scans. 46

3.1 FT-IR spectrum of 2 Torr of CF_2HCl. The pathlength is 10 cm, while the FT-IR resolution is set at 2 cm^{-1}. 50

3.2 Transient TDL absorption by HCl. The absorption feature monitored is P(9) at 2677.732 cm^{-1}. The HCl is produced by photolysis of 800 mTorr of CF_2HCl. 51

3.3 TDL spectrum of CF_2 in the region of 1243 cm^{-1}. The figure shows the absorption lines created in a microwave discharge by Davies et al.[38], and in our lab for comparison. The lower trace shows an expanded view of a portion of the spectrum. 53

3.4 TDL transient absorption spectrum showing the presence of the CF_2 triplet near 1243 cm^{-1}. CF_2 is produced by irradiation of 800 mTorr of CF_2HCl. The TDL sweeps over three CF_2 lines at a modulation frequency of 40 kHz. The strongest absorption line corresponds to about 20% absorption. The growth of the two outer lines relative to the central line of the triplet is attributed to rotational relaxation. The overall growth of the triplet is attributed to cascading of vibrationally excited CF_2 into the vibrational ground state. 58

3.5 CF_2 and HCl yields (in terms of the 61

absorption per cm, α_o) as a function of the average CO_2 laser fluence. The CF_2HCl pressure is 800 mTorr.

3.6 Partial pressure of CF_2 and C_2F_4 as a function of time following photolysis of 800 mTorr of CF_2HCl at an average CO_2 laser fluence of 17 J cm^{-2}. 63

3.7 Second order plot (the inverse of the CF_2 linecenter absorption coefficient, α_o, versus time) showing the decay of CF_2 via recombination. The data were obtained by photolysis of 800 mTorr of CF_2HCl with a peak CO_2 laser fluence of 17 J cm^{-2}. 67

4.1 FT-IR spectrum of 0.5 Torr of hexafluoroacetone. The spectrum is recorded at a resolution of 2 cm^{-1} over a pathlength of 10 cm. 72

4.2 Transient tunable diode laser absorption signal from CF_3 created in the IRMPD of hexafluoroacetone. The detection is done 77

on the $^{r}R_{16}(20)$ CF_3 absorption line at 1264.739 cm^{-1}.

4.3 Transient absorption near 1263 cm^{-1}, showing CF_3 decay immediately following the CO_2 laser pulse, and the growth of C_2F_6 at later times. 78

4.4 CO(+) and C_2F_6(□) yields from IRMPD of 600 mTorr hexafluoroacetone as a function of the average incident CO_2 laser fluence. The irradiations are done with the 10R(10) CO_2 laser line. 82

4.5 Plot of CF_3 absorption per cm at linecenter, α_o, as a function of CF_3 pressure. α_o for CF_3 is measured at a variety of CO_2 laser fluences, and the CF_3 pressure is obtained from the CO and C_2F_6 yields measured at each of these fluences and a knowledge of the dissociation stoichiometry. 83

4.6 Second order decay plot (the inverse of 90

	the absorption coefficient per cm versus time) for the recombination of CF_3. CF_3 is created from the IRMPD of 600 mTorr of hexafluoroacetone. The 10R(14) laser line, with a fluence of 34 J cm^{-2}, is employed.	
4.7	Plot of the inverse CF_3 half-life (ms^{-1}) versus the concentration of added O_2 or NO (Torr). CF_3 is created by the IRMPD of 600 mTorr of hexafluoroacetone at a CO_2 laser fluence of 34 J cm^{-2} (on 10R(10)).	91
5.1	An FT-IR spectrum of a mixture of 2.5 Torr $CDCl_3$ and 2.5 Torr $CHCl_3$, recorded in a 10 cm long Pyrex with a resolution of 4 cm^{-1}.	97
5.2	Plot of the product yield of CCl_4 and dissociation yield of $CDCl_3$ following the photolysis of 1 Torr $CDCl_3$ in the presence of additives. The irradiation is done on 10P(48), with a peak focal fluence of 10 J cm^{-2}. Errors are $\pm 1\sigma$.	106

Line A: CCl_4 yield following irradiation of 1 Torr $CDCl_3$ with 1 Torr Ar.
Line B: Upper limit of CCl_4 yield following irradiation of 1 Torr $CDCl_3$ with 1 Torr C_2F_4.
Line C: CCl_4 yield following irradiation of 1 Torr $CDCl_3$ with 1 Torr Cl_2.
Line D: CCl_4 yield following irradiation of 1 Torr $CDCl_3$ with 5 Torr Cl_2.
Line E: Average dissociation yield of $CDCl_3$ in the above experiments A through D. The difference in the dissociation yield in the four cases was not significant.

5.3 Relative DCl yield as a function of photolysis frequency following IRMPD of 1 Torr $CDCl_3$ in a 10 cm Pyrex cell. The peak focal fluence is 10 J cm^{-2} in all cases. The error bar represents $\pm 1\sigma$. 112

5.4 Successive scans taken of a 5 Torr sample of natural chloroform after irradiation with 100 pulses of 10P(38) and 10P(48) 114

radiation (about 10 J cm^{-2}). The increase in DCl concentration after irradiation with 10P(48) is attributed to IRMPD of naturally occurring $CDCl_3$ in the sample. The noise level is equivalent to about 0.8 ppm DCl.

5.5 Dissociation yield of $CDCl_3$ (lower line) and total (HCl + DCl) yield following the irradiation of a mixture of 0.1 Torr $CDCl_3$ and 1.9 Torr $CHCl_3$. The photolysis is performed at a peak focal fluence of 10 J cm^{-2} with the 10P(48) CO_2 laser line. The points labelled 1,2, and 3 represent the $CDCl_3$ dissociation yield in three separate experiments, while the points labelled a,b, and c represent the (HCl and DCl) yield in the same three experiments. 116

5.6 Transient HCl yield following the single pulse irradiation of an equimolar mixture of $CDCl_3$:$CHCl_3$:Ar (Line A) or $CDCl_3$:$CHCl_3$:C_2F_4 (Line B). The irradiation is performed with the 10P(38) 120

CO_2 laser line at a peak focal fluence of 16 J cm^{-2}. Errors are $\pm 1\sigma$.

LIST OF TABLES

NO.		PAGE
4.1	Initial half-life of CF_3 decay at various initial CF_3 concentrations, $(CF_3)_o$, formed in the IRMPD of hexafluoroacetone. The rate constant, k, for CF_3 recombination is reported for each trial in units of cm^3 $molecule^{-1}$ s^{-1}. The half-lives are estimated to within ± 5 μs, while $(CF_3)_o$ is estimated to $\pm 10\%$. Each entry in the table is the average of three separate trials, recorded under identical conditions.	87

CHAPTER 1

INTRODUCTION

1.1 General

The process of infrared multiphoton absorption and dissociation (IRMPA and IRMPD) of polyatomics by intense infrared laser radiation was first realized in the early 1970's.[1] In the years following, IRMPD has become the area of study of dozens of labs worldwide and has been extensively reviewed.[2-9]

IRMPD has become an important field of study for numerous reasons. Firstly, the process is quite general as over 100 molecules, ranging in size from 3 to 62 atoms, have been shown to dissociate under irradiation by high powered infrared (IR) lasers.[3] IRMPA is also an efficient method of producing molecules in highly excited vibrational states, allowing for the spectroscopic study of these excited levels.[2] The IRMPD process provides a convenient method of studying the unimolecular dissociation and isomerization of numerous species,[2] and is also a convenient method for production of various radicals whose subsequent reactions can then be studied.[3]

The most important practical application of IRMPD arises from the isotopic selectivity of the process. For example, deuterium enrichment factors of up to 20000 have been found for the selective dissociation of CDF_3 in the presence of CHF_3.[10] IRMPD has also found some application in chemical synthesis.[2]

During approximately the same time period over which the IRMPD process has been studied, the use of lead-salt tunable diode lasers (TDLs) in the detection of absorptions in the infrared has grown, as TDLs provide improved sensitivity and resolution over conventional grating and Fourier transform spectrometers.[11] The narrow linewidth of the TDL (typically less than .001 cm^{-1}) allows for the measurement of Doppler broadened absorption features without instrumental broadening. This narrow linewidth also provides for high specificity - the ability to distinguish between different molecules, including those differing only in their isotopic makeup. The high power per unit spectral range and the ability of the diode to be modulated provide for increased sensitivity. While TDLs have found numerous applications in the detection of gases in the atmosphere,[12] and in measuring high resolution infrared spectra,[13] their use in studying photochemical systems and, indeed, chemical reactions in general has to date been fairly limited.

In this thesis, the infrared multiphoton dissociation (IRMPD) of various halocarbons (CF_2HCl, $(CF_3)_2CO$, and $CDCl_3$) are studied by detecting the products of their dissociation with TDLs. In particular, a TDL absorption technique for monitoring IRMPD products over short timescales (tens of μs) has been developed in collaboration with C.E. Brown and P.H. Beckwith. Information regarding the photolysis and post-photolysis mechanisms of the above-mentioned halocarbons has been obtained. Also, infrared linestrengths and bandstrengths for the transient species, CF_2 and CF_3, have been measured for the first time, and kinetic studies on these species have been made. The time-resolved detection of DCl and HCl has led to information regarding the isotopic selectivity of the IRMPD of chloroform.

The remainder of this chapter provides a detailed description of the infrared multiphoton process in three stages - absorption through the discrete lower levels, absorption through the quasicontinuum, and absorption and dissociation in the continuum region above the dissociation limit. Also described in this chapter is the background theory required for quantitative analysis of the products of IRMPD by TDL absorption spectroscopy.

Chapter 2 provides a description of the general

experimental methods employed in this thesis, including gas handling, irradiation and standard TDL infrared detection procedures. Finally, the techniques used in the time-resolved detection of transient species with TDLs are described.

The results obtained from the time-resolved detection of HCl and CF_2 following IRMPD of CF_2HCl are discussed in Chapter 3. These results include a confirmation of the photolysis mechanism by direct detection of the preliminary dissociation products, and the determination of an infrared linestrength and bandstrength for CF_2 by quantification of the amount of CF_2 and HCl produced by a single CO_2 laser pulse. The second order decay constant for CF_2 combination is also measured.

Time-resolved detection of CF_3, CF_2, CF_4, C_2F_6, COF_2, and CO following IRMPD of hexafluoroacetone is described in Chapter 4. The IRMPD mechanism is conclusively established, and an infrared linestrength and bandstrength for CF_3 is obtained for the first time through quantification of the CO, C_2F_6, and CF_3 produced in the photolysis. Kinetic studies of CF_3 have also been made and are shown to compare favorably to results obtained by other methods.

The detection of DCl and HCl following IRMPD of

chloroform is described in Chapter 5. The DCl produced in the IRMPD of natural abundance $CDCl_3$ in $CHCl_3$ is detected by TDL absorption spectroscopy. Monitoring DCl and HCl production on short timescales with TDLs (to eliminate the effects of isotope exchange reactions and wall adsorption/desorption effects) leads to information on the isotopic selectivity of the IRMPD process. Evidence for the presence of isotopically non-selective radical reactions following IRMPD of chloroform is also presented.

Chapter 6 provides a review of the significant results presented in this thesis, and provides a basic outline for future research in these areas.

1.2 The Infrared Multiphoton Process

The IRMPD of polyatomics is a much studied process, with numerous theoretical and experimental investigations having been undertaken. Of the several review articles in print, the most extensive is that of Bagratishvili and co-workers, the general outline of which has been followed in writing this section.[2]

The IRMPD of a molecule involves the successive absorption of many photons (30-50) to a point above the dissociation limit, where unimolecular reaction can occur.

The process can be conveniently separated into three sections: the coherent absorption of the first few photons, the excitation of the molecule through the quasicontinuum, and the absorption of photons in the continuum region above the dissociation limit where unimolecular reaction can take place.

The excitation in the lower levels is perhaps the most difficult process to understand in a quantitative sense, because the spectroscopy of vibrational levels above v=2 or 3 is generally not known. Therefore, theories put forward to date are semi-quantitative in nature.[2] While the process would be simple to explain for a pure harmonic oscillator, real molecules are anharmonic. Thus, if the excitation frequency is in resonance with the first transition (from v=0 to v=1), then it is quickly out of resonance for the higher levels because of the anharmonic shift.

Experimental techniques used to study lower level excitation include double IR-IR resonance,[14] double IR-UV resonance,[15] Raman scattering,[16] and IR fluorescence.[17] The multiphoton absorption (MPA) process through the lower levels is usually discussed in terms of its frequency dependence and its intensity dependence. It has been found that the MPA process is strongly dependent on excitation frequency - that is, it involves resonant

transitions. It is this property that leads to the most important practical application of IRMPD, that of isotope separation. The MPA spectrum is generally broadened and shifted to lower energy (red-shifted) compared with the normal one-photon spectrum,[2] the amount of broadening and red-shifting increasing with increasing excitation intensity. These effects are due to the anharmonic nature of molecules, with each successive transition being shifted to the red of the previous one. For example, in the MPA spectrum of OsO_4, distinct peaks corresponding to successive anharmonic shifts of the excited ν_3 mode can be observed.[18]

Typically, CO_2 laser irradiation intensities of 10^6 - 10^8 W cm^{-2} are employed. The required intensity is dependent on the size of the molecule. Small molecules with large anharmonicities and low density of states require higher intensity than large molecules. For example, diatomics cannot be dissociated, and triatomics are very difficult. In small molecules, which cannot be dissociated, saturation is observed. That is, the average number of absorbed photons, $\bar{n}$, at first increases with laser power but quickly levels off as the transition from v=0 to v=1 is saturated. For larger molecules, such as SF_6, no saturation is observed. Instead, a smooth change

over from linear to multiphoton absorption takes place and a near linear dependence of $\bar{n}$ on laser power is observed. Saturation only sets in when dissociation of the molecule begins to occur. At lower temperatures, a greater than linear dependence of $\bar{n}$ on laser power is observed. Because less rovibrational states are occupied, less pathways for successive transitions are available and 2- and 3-photon processes become more important.[2]

An important experimental observation regarding the excitation of polyatomics is that two ensembles exist immediately following irradiation - one "hot" ensemble, and one "cold" ensemble. For example, when SF_6 is excited by a CO_2 laser, two peaks appear in a time-resolved Raman scattering experiment, one due to the cold ensemble, and another (shifted to lower energy) due to the hot ensemble. (Eventually, the two distributions collapse to one with collisional vibrational energy exchange). This observation is due to the fact that in the ground vibrational state, many rotational states are populated, only some of which have available to them pathways for MPA to the quasicontinuum. Thus, molecules originally in some rotational states are excited, forming the hot ensemble, while others remain cold.[16] Since the depleted levels cannot be repopulated fast enough during pumping, a so-called "rotational bottleneck" develops. It can be

overcome either by using short, high intensity pulses so that all molecules can be excited or by increasing the gas pressure.[2] The collisions occurring at these higher pressures allow for rotational relaxation which puts the cold molecules into rotational states from which MPA can occur. For example, a 100-fold increase in the dissociation yield of CDF_3 (at a CO_2 laser fluence of 10 J/cm^2) is observed on addition of 20 Torr of Argon buffer gas to 65 mTorr of CDF_3.[19] Eventually, at a certain pressure, all the molecules are excited and any further pressure increase actually lowers the dissociation yield because of V-V, and V-T,R relaxation. This allows the fraction of molecules (q) to be determined as the ratio of the dissociation yield under the given conditions (β) to the maximum yield at high pressure (β_{max}).[2]

Because of the presence of these two ensembles, one must define two terms to describe the average absorbed energy - $\bar{n}$, the average number of photons absorbed per molecule, and $\bar{n}_q$, the average number of photons absorbed per "hot" molecule. Thus, $\bar{n}$ is the product of $\bar{n}_q$ and q. Studies on the dependence of $\bar{n}_q$ and q on excitation wavelength have been particularly revealing. As the excitation wavelength is shifted to the red, q decreases (less molecules reach the quasicontinuum), but $\bar{n}_q$

increases (the absorption cross-section increases in the quasicontinuum). Therefore, it has been concluded that the overall resonant character of MPA is determined by the fraction of molecules, q, reaching the quasicontinuum.[2]

As previously mentioned, theoretical models of the excitation through the lower levels are semi-quantitative in nature. The difficulty in describing the process is due to the anharmonicity. Each successive vibrational transition is lower in energy than the previous one and thus the excitation source does not remain in resonance with the vibrational manifold. To compensate for this anharmonicity, various schemes have been proposed including power broadening, rotational compensation, anharmonic splitting of excited degenerate modes, and the breakdown of selection rules allowing "forbidden" transitions to occur.[3]

The vibrational energy levels, E_v, of a polyatomic are given by the following equation:[3]

$$E_v/hc = \sum \nu_i v_i + \sum X_{ii} v_i (v_i - 1) + \sum\sum X_{ij} v_i v_j \quad \ldots(1.1)$$

where ν_i are the fundamental frequencies, and X_{ii} and X_{ij} are the anharmonic diagonal and cross terms. From this equation, it is apparent that the mismatch of energy between the v-th level and the energy of v photons

increases with $v^{2.3}$.

This anharmonicity can possibly be overcome in part by power broadening of the rovibrational levels in the presence of the intense IR field. However, this power broadening is proportional to the square root of v and thus is likely only of any importance for the first couple of steps.[3]

As discussed by Fuss and Kompa,[3] numerous rotational energy levels are present in each vibrational level. Thus, it is possible that the presence of this rotational energy may in part correct for the anharmonicity.

A second type of rotational compensation was proposed by Bagratishvili et al.,[2] who considered three consecutive vibrational transitions in which the first is a P-transition ($J \longrightarrow J-1$), the second is a Q-transition ($J-1 \longrightarrow J-1$) and the third an R-transition ($J-1 \longrightarrow J$). In this manner, for certain J, the anharmonicity may be exactly cancelled out by the change in rotational energy. However, this is only possible for a very select few rotational levels. Furthermore, in SF_6, it has been shown that the positions of the peaks in the MPA spectrum do not coincide with the expected positions of these PQR-type resonances, and it can be concluded that they are of

limited importance.[3] Similar schemes involving successive PQQR and PPRR transitions have also been proposed.[20]

A third type of rotational compensation, suggested by Platonenko,[21] involves emission from v=n to a rotational sublevel of v=n-1 which was not previously populated by laser excitation. This newly populated level may then be capable of undergoing MPA.

Often in IRMPD, a degenerate mode is being pumped. For example, spherical tops, such as SF_6 and SiF_4, have triply degenerate modes. However, anharmonic terms in the Hamiltonian not only red-shift these modes on excitation, but also cause splitting of the degeneracy. In general, this splitting can be close to, or of the same magnitude as the anharmonic shift. Combined with the above-mentioned rotational compensation schemes, this splitting of degeneracies can support the MPA process.[3]

The final scheme proposed to allow for the MPA of molecules through the first few levels takes into account the involvement of transitions normally thought of as being forbidden in linear spectroscopy. However, it is possible that some of these forbidden transitions become allowed in the presence of an intense infrared laser field. Examples include transitions with $J > 1$ and, in spherical tops, transitions with ΔR and Δn not equal to zero.[3]

In general, these theories are capable of predicting at least the major features of the MPA process through the first few levels, the wavelength and intensity dependence of the MPA and the formation of hot and cold molecular ensembles on excitation.

The next stage in the IRMPA process involves excitation of the molecule through the so-called quasicontinuum. In a very simple sense, this portion of the MPA process can be understood by considering that the density of vibrational states is very large and a transition in resonance with the laser field is virtually assured. Absorption in the quasicontinuum is generally characterized in terms of the cross-section, σ, which is a function of the IR field frequency, λ, and the vibrational energy content of the molecule, E_{vib}.

In order to properly study absorption in the quasicontinuum, one must separate it from absorption in the lower levels. This is accomplished by a two-frequency excitation scheme, in which the first resonant pulse promotes the molecule to the quasicontinuum and the second pulse (detuned to the red) excites the molecules through the quasicontinuum. The energies absorbed from each of these pulses (e_1 and e_2) are measured separately, and then the absorption is measured with both lasers operating

(e_{1+2}). The difference, $(e_{1+2}) - (e_1 + e_2)$, gives the absorption in the quasicontinuum, e_{qc}. The quasicontinuum absorption spectrum shows very wide, smooth bands around each IR active vibrational mode of the molecule, these bands being red-shifted and broadened compared to the one-photon spectrum.[2] An important observation is that the width of these peaks exceeds the bandwidth, indicating the non-resonant character of absorption in the quasicontinuum. The absorption cross-section is also found to increase with increasing e_{vib}, due to an increase in the vibrational amplitude of the highly excited molecule.[2] The absorption cross-section can be adequately described by the Lorentzian model given below:[22]

$$\sigma_{qc}(\lambda, E_{vib}) = [\sigma_{int}/\pi][\delta/((\lambda-\nu_{max})^2+\delta^2] \qquad ....(1.2)$$

Here, ν_{max} (the central frequency) shifts to the red with increasing e_{vib}, δ(the half-width) increases with e_{vib}, and σ_{int} (the integral absorption cross-section) also increases with e_{vib}.

Because of the non-resonant character of the absorption in the quasicontinuum, the cross-section is mainly fluence, not intensity, dependent. For example, a change in intensity of four orders of magnitude led to an increase of only 1.5 orders in the amount of absorbed

energy.[2] Recent experiments have shown some intensity dependences, indicating that the process is not completely non-resonant in nature.[23]

The intermolecular energy distribution of molecules excited to the quasicontinuum has also been established. As mentioned previously, a hot and cold ensemble is created initially. However, studies solely on the hot ensemble have shown that these molecules are not distributed in a Boltzmann fashion. The energy distribution of IRMP excited molecules has a steeper high energy tail and a narrower distribution than a Boltzmann. Therefore, calculations based on the Boltzmann distribution tend to overestimate the dissociation yield at low excitations and underestimate it at higher excitation energy.

Perhaps the most important feature of excitation in the quasicontinuum is the nature of the intramolecular energy distribution. This has been measured using two techniques, time-resolved IR emission[17] and anti-Stokes Raman scattering.[16] The signals obtained in these experiments are proportional to the vibrational energy in the particular mode being observed. For example, in the cases of SF_6 and CF_3I, the anti-Stokes Raman signal has been observed in all of the modes probed, not just the

mode being excited. The strength of the signal was independent of decay time, from approximately the end of the CO_2 laser pulse to a few microseconds after the pulse.[16] Thus, it is apparent that stochastization (randomization of the vibrational energy among all modes) has occurred during the course of the interaction with the IR laser field without the aid of any collisions. While the rate of stochastization naturally varies with molecular structure, anharmonic forces between modes, and the vibrational frequencies of the molecule, it is apparent from calculations that it probably occurs on a picosecond time scale. Therefore, it is not surprising that stochastization occurs with the CO_2 laser pulse durations normally employed (ns).[2]

The presence of stochastization in IRMPA is very important in determining the properties of the dissociation process. Because randomization of energy occurs in the quasicontinuum (before the dissociation limit is reached), the dissociation can be perfectly described by existing theories for describing thermal unimolecular reactions (RRKM theory).[24]

This theory is based on the assumption that some of the energy possessed by a molecule (called the non-fixed energy) can be freely redistributed between the various internal degrees of freedom of the molecule, and

that any deviation from an equilibrium distribution is purely statistical. The theory postulates that any molecule containing a non-fixed energy greater than the dissociation energy of the lowest reaction pathway has a non-zero probability of reaction, and that the rate of reaction will be proportional to the probability that sufficient energy becomes localized in the vibrational mode corresponding to the reaction coordinate.[24]

The conversion of the excited molecule to products is divided into two steps, in which a distinction is made between an energized molecule (A^*) and an activated complex (A^+):[24]

$$A^* \xrightarrow{k_a(E)} A^+ \xrightarrow{k^+} \text{Products} \qquad \ldots.(1.3)$$

Here, $k_a(E)$ is the rate constant for conversion of A^* having non-fixed energy E to A^+, and k^+ is the absolute rate at which the activated complexes proceed to products. Using statistical mechanics, $k_a(E)$ is determined as follows:[24]

$$k_a(E) = (L^+ \sum P(E_{vr}))/(hN^*(E^*)) \qquad \ldots.(1.4)$$

where L^+ is a statistical factor, $\sum P(E_{vr})$ is the total

number of rovibrational states of A^+ with energy less than or equal to E^+ $(=E^* - E_{diss})$, and $N^*(E^*)$ is the total density of states of A^*.

RRKM theory is capable of making numerous predictions regarding the dissociation process. Firstly, it predicts that the dissociation mechanism corresponding to the lowest activation energy will be favored. This prediction is borne out experimentally in all known cases. For example, CF_2Cl_2, when irradiated at either the CF or CCl stretching frequency, yields the same products (consistent with the low energy CCl bond rupture).[25] Thus, even though energy is being initially deposited in the CF_2 portion of the molecule, reaction was occurring in the CCl modes, indicating energy randomization prior to reaction. Similar conclusions were drawn from a study on CH_2FCH_2Br,[26] which can dissociate to yield either HF or HBr. Even though irradiation was performed at the CF stretching frequency, the observed yield (HBr:HF=10:1) is as predicted by RRKM theory.

RRKM theory is also capable of predicting the rate of dissociation of the excited molecule, and from this its expected lifetime can be obtained. For example, the lifetime of $C_6F_{13}I$ was measured using a short pulse CO_2 laser for photolysis and multiphoton ionization for time-resolved detection of the product iodine atoms.[27] The

observed dissociation lifetime (around 6 ns) corresponds (from RRKM theory) to the absorption of 54 photons/molecule. The actual number of photons absorbed was estimated to be 54 - 59 photons/molecule in close agreement with the RRKM prediction.

That dissociative lifetimes on the order of a few nanoseconds have been obtained in IRMPD experiments is not surprising since, for a typical CO_2 laser pulse, the rate of pumping is about 5×10^8 s^{-1}.[7] Thus, when the molecule is excited to an energy level where the dissociation rate exceeds the pumping rate, up-pumping can no longer compete and reaction will occur before the molecule can be further excited. This allows the use of RRKM theory to predict the number of excess photons that will be absorbed by a particular molecule prior to its dissociation. The theory predicts that k_a will increase very rapidly with the number of photons absorbed for smaller molecules and less rapidly for larger molecules. Thus, it would be expected that smaller molecules would absorb fewer excess photons prior to dissociation than larger molecules.[7] This prediction is consistent with experiment as CF_3I absorbs 2 or 3 excess photons,[28] SF_6 8 or 9 excess photons,[29] and $(CF_3)_3CBr$ can be excited to an energy at least twice the dissociation limit.[2] This excess energy

in the large molecules usually manifests itself as vibrational energy in the product fragments, and explains the common observation of secondary dissociation.

IRMPD experiments and RRKM predictions can also be compared by measuring the translational energy distribution of the product fragments of an IRMPD experiment in a molecular beam. Intuitively, if energy randomization did not occur, then it would be expected that upon absorption of the final photon before dissociation, the molecule would dissociate explosively with the fragments produced acquiring non-zero translational energy. If, however, the energy acquired by absorption of the last photon is first redistributed over the entire molecule, the molecule would be expected to "fall apart", with little or none of the excess energy appearing as product translation.[3]

Molecular beam studies have been conducted by a group at Berkeley[28-30] on a wide variety of molecules which can be divided into two groups, those whose dissociation involves a simple bond rupture and those which involve a 3- or 4- center elimination reaction. The experiment, in general terms, is conducted as follows: firstly, an experimental velocity distribution is measured from the molecular beam studies; secondly, a translational energy distribution is determined which matches this

velocity distribution; finally, translational energy distributions at different reactant energy levels are obtained from RRKM calculations, and compared to the experimentally determined one.

The most studied of the simple bond-rupture cases is SF_6.[29] The product translational energy distributions were found to peak at zero, ruling out a mode-controlled explosive dissociation mechanism. Furthermore, the theoretically obtained distribution (for excitation of 8 or 9 photons in excess of the dissociation limit) corresponds very well with the experimental distribution, lending credence to the validity of the energy redistribution model of collisionless IRMPD. The results obtained for the other bond-rupture cases are very similar.[28] The cases of 3- or 4- center elimination studied at Berkeley all involve HCl elimination.[30] Their analysis in relation to RRKM theory is more complicated, owing to the presence of a barrier to back reaction. Thus, in addition to the energy in excess of the dissociation limit, the potential energy of the exit barrier is also available for distribution among the product fragments. It was assumed that all this excess energy appears as product translational energy, and the experimentally determined translational energy

distributions were compared to the now adjusted RRKM distribution. For example, in CF_2HCl (with a back reaction barrier of 6 kcal/mol), it was found that the experimental and theoretical distributions both peaked at about 6 kcal/mol, but that the theoretical distribution was narrower. This discrepancy was considered to be due to the fact that fragment interaction along the exit channel has been neglected. Thus, while comparison of experimental results to RRKM predictions are more difficult in reactions containing a barrier to back reaction, the two distributions are quite similar if it is assumed that most of the energy due to the back reaction barrier appears as fragment translational energy.

Thus, the statistical RRKM theory, which is based on the rapid redistribution of the non-fixed energy in a highly excited molecule relative to its reaction rate, is successful in quantitatively predicting the products, the branching ratios, the dissociative lifetimes, the number of photons absorbed, and the product translational energy distributions obtained in IRMPD experiments.

IRMPD has found numerous applications in the laboratory. Firstly, it provides an excellent method for the preparation of highly vibrationally excited molecules, whose spectroscopy can then be studied.[3] Also, numerous unimolecular reactions (dissociations and isomerizations)

can be triggered in this fashion, allowing for their study and comparison to theory.[2] The technique provides a convenient method for the controlled study of many radicals. IRMPD produces relatively cold radicals which can then be reacted with substrates at room temperature, something that cannot be accomplished in typical pyrolysis studies.[2] A great deal of the initial excitement in the study of IRMPD arose from the demonstration that the process could be made isotopically selective by the proper selection of photolysis frequency. In this fashion, a number of isotopic selectivity schemes have been demonstrated on a laboratory scale, with elements as small as hydrogen[10] and as large as uranium[31] being enriched. (The area of hydrogen isotope separation will be discussed in more detail later as it pertains to the results obtained in the $CDCl_3/CHCl_3$ system.) IRMPD has also found some use in chemical synthesis. For example,[32] the IRMPD of BCl_3 in the presence of H_2 produces $BHCl_2$ in a very clean reaction, whereas the $BHCl_2$ yield in the corresponding thermal reaction is only a few percent. Synthesis of isotopically enriched compounds, again making use of the isotopic selectivity of IRMPD, has also been demonstrated.[2]

1.3 THEORY OF INFRARED ABSORPTION

In this thesis, detection and quantification of the products of IRMPD are performed by monitoring their absorptions in the infrared. Thus, the theory required to obtain quantitative information from infrared absorption spectra will now be presented.

The basic starting point for any discussion of quantitative absorption measurements is the Beer-Lambert Law:

$$I(\nu)=I_o(\nu)\ \exp(-\alpha(\nu)L) \qquad \ldots.(1.6)$$

where I and I_o are the transmitted and incident beam intensities, and L is the pathlength. The fractional absorption per unit pathlength, $\alpha(\nu)$, is defined as follows:[33]

$$\alpha(\nu)= S\ (P_a/760)\ \Phi(\nu-\nu_o) \qquad \ldots.(1.7)$$

where S is the linestrength (in cm molecule^{-1}), and P_a is the sample pressure in Torr.

The lineshape function $\Phi(\nu-\nu_o)$ is determined by three different types of line broadening. Natural broadening is directly related to the Heisenberg

uncertainty principle. The second effect is collisional broadening, which is dependent on the collisional diameters of the colliding species, their pressures, and their masses. The third effect is Doppler broadening which occurs because the absorbing molecule has an appreciable velocity. Thus, the frequency of light absorbed or emitted by molecules with non-zero velocity in the line of sight is slightly altered. The half-widths ($\Delta\nu_N$, $\Delta\nu_C$, and $\Delta\nu_D$) of the absorption line for these three phenomena can be shown to be of the following form:[33]

$$\Delta\nu_N = 1/4\pi c(\gamma_u + \gamma_l) \qquad \ldots.(1.8a)$$

where $\gamma_{u,l}$ are inverse half-lives of the upper and lower states;

$$\Delta\nu_C = 1/4\pi c(2Z_u + 2Z_l) \qquad \ldots.(1.8b)$$

where $Z_{u,l}$ are the collision frequencies for the upper and lower states;

$$\Delta\nu_D = (2kT \ln 2/mc^2)^{1/2} \nu_{l,u} \qquad \ldots.(1.8c)$$

where ν_{lu} is the transition frequency.

If the three effects are combined, the following expression is obtained for the absorption coefficient:[33]

$$\alpha(\nu)=s(P_A/760\Delta\nu_D)(\ln 2/\pi)^{1/2}(a/\pi)\int_{-\infty}^{\infty}\frac{\exp(-y^2)dy}{a^2+(x-y)^2} \quad ....(1.9)$$

where $a=(\ln 2)^{1/2}(\Delta\nu_N+\Delta\nu_C)/\Delta\nu_D$, $x=(\nu-\nu_o)(\ln 2)^{1/2}/\Delta\nu_D$, and $y=(\nu'-\nu_o/\nu_o)(mc^2/2kT)^{1/2}$.

Experimentally, the most easily measured parameter is α_o, the absorption at linecenter. Thus, in the above equation, $x=0$. The equation can also be simplified by considering different pressure regimes. At low pressure (usually less than 1 Torr), the collisional broadening is negligible and equation (1.9) takes the following form:[33]

$$\alpha_o = (s/\Delta\nu_D)(\ln 2/\pi)^{1/2}(P_A/760) \quad ....(1.10)$$

At intermediate pressures, where collisional and Doppler broadening are of similar magnitudes,[33]

$$\alpha_o=(s/\pi^{1/2})(a/\Delta\nu_D)(1-\mathrm{erf}(a))\exp(a^2)P_A/760 \quad ....(1.11)$$

where erf(a) is the error function. At high pressure, where $\Delta\nu_C$ is much greater than $\Delta\nu_D$,[33]

$$\alpha_o = (s/\pi\Delta\nu_C)(P_A/760) \qquad \ldots.(1.12)$$

These equations for α_o can then be used in two different ways. In cases where linestrength data are available in the literature (for example, HCl) measurement of α_o in the lab allows the determination of the partial pressure of the species of interest. In other cases, the linestrength is not known (for example, in the cases of the transient species such as CF_2 and CF_3). However, a knowledge of the partial pressure of the species (from the stoichiometry of a dissociation reaction) and a measurement of α_o leads to a determination of the previously unknown linestrength.

Once a linestrength has been determined in the manner described above, it is also possible to estimate the infrared bandstrength. In general, the linestrength can be expressed as follows:[33]

$$s=(8\pi^3\nu/3hcp)(Ng_{NK}/Q_vQ_r)R_v^2R_r^2\exp(-E(N,K)/kT)$$
$$[1-\exp(hc\nu/kT)] \qquad \ldots.(1.13)$$

where ν is the frequency of the transition, Q_v and Q_r are the vibrational and rotational partition functions, R_v^2 is the vibrational transition moment, R_r^2 is the Honl-London

factor, g is the degeneracy, and E(N,K) is the rotational energy of the lower state. To obtain the bandstrength, A, a summation over all rotational states is performed:[33]

$$A=(8\pi^3\nu_o/3hcp)(N/Q_v)R_v^2[1-\exp(hc\nu_o/kT)] \quad ....(1.14)$$

Combining the two above equations, the bandstrength can then be determined from the rotational partition function of the molecule in question, as well as the Honl-London factor and Boltzmann factor for the transition for which the linestrength has been measured:

$$A=(\nu_o/\nu)(sQ_r/g_{NK}R_r^2)(1/\exp(-E(N,K)/kT)) \quad ....(1.15)$$

1.4 SUMMARY

In this thesis, the IRMPD of various halocarbons is studied using a time-resolved tunable diode laser absorption technique. This introductory chapter has provided a detailed description of the IRMPD process in three stages - the resonant absorption of the first few photons, the absorption of photons through the vibrational quasicontinuum, and the excitation and dissociation of the molecule in the continuum above the dissociation limit.

It has also provided the background theory required in the quantitative analysis by IR absorption of the products (both stable and transient) of an IRMPD experiment.

CHAPTER 2

EXPERIMENTAL

2.1 INTRODUCTION

In this chapter, a description of the experimental methods and techniques used in this thesis will be presented, including a discussion of gas handling and irradiation techniques, as well as Fourier Transform (FT) and tunable diode laser (TDL) infrared detection techniques. A full discussion of the TDL technique for transient detection will follow.

2.2 GASES AND GAS HANDLING TECHNIQUES

All gases were handled on a conventional grease-free vacuum line equipped with an Edwards E2M2 two stage mechanical pump and an Edwards EO40X55 vapor diffusion pump, capable of achieving a background pressure of 10^{-6} Torr. Background pressures were measured on an Edwards Penning gauge, while sample pressures were measured on an MKS Instruments Baratron (10 Torr) gauge. Gas mixtures were made in cells or bulbs equipped with cold fingers,

which could be isolated from the cell with a stopcock.

The following gases were obtained from Matheson Gas Products (with stated purities in parentheses): CF_2HCl (99.9%), $(CF_3)_2CO$ (99.9%), NO (99%), N_2 (98%), C_2H_4 (99.5%), Ar (99.9995%). With the exception of C_2F_4 (obtained from P.C.R. Inc.), the remaining gases were obtained from Canada Liquid Air: O_2 (99.9%), CH_4 (99.5%), c-C_3H_6 (research grade), HCl (99.9995%), H_2 (99.9999%). All laser gases were also obtained from Canada Liquid Air: N_2 (high purity, 99.998%), CO_2 (bone dry, 99.8%), He (H.P., 99.9995%), and air (dry). The remaining chemicals used were as follows: $CDCl_3$ (99.8% atom D, MSD Isotopes), $CHCl_3$ (analytical reagent grade, BDH), C_2Cl_4 (reagent grade, Baker), and CCl_4 (reagent grade, Caledon). All gases were purified by bulb-to-bulb distillation before use and their purity was checked by FT-IR and, where applicable, by TDL spectroscopy.

2.3 PHOTOLYSIS AND STABLE PRODUCT ANALYSIS TECHNIQUES

All static sample photolyses were conducted as shown in Figure 2.1. The irradiations were performed with a low repetition rate, high energy Lumonics K-922S TEA CO_2 laser, operated at 0.5 Hz. About 50% of the energy of

FIGURE 2.1: Experimental design for static sample photolyses. The CO_2 laser beam is focussed by means of a 25 cm BaF_2 lens into the cell. Polyethylene sheets are used as necessary to obtain the desired CO_2 laser pulse energy.

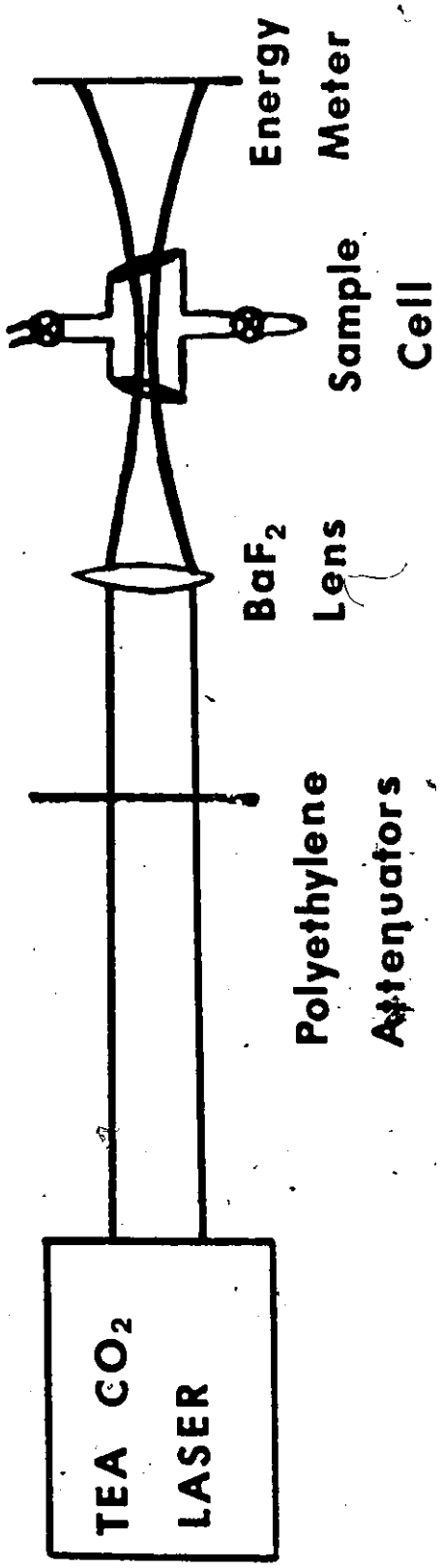
Energy Meter
Sample Cell
BaF_2 Lens
Polyethylene Attenuators
TEA CO_2 LASER

each laser pulse was contained in the first 200 ns with the remainder in a tail lasting for about 1 μs. The output of the CO_2 laser was focussed using a BaF_2 lens (usually 25 cm focal length) such that the focal point was at the midpoint of the gas cell. The energy of the beam was measured with a Gentec joulemeter (Model ED-500), and the beam size was measured by determining the size of a beam spot on thermal paper. The beam was attenuated using an NH_3 absorber cell and polyethylene sheets as required to achieve the desired laser fluence (energy per unit area).

The cylindrical cells used for irradiation were constructed of either Monel or Pyrex, and were 10 cm in length and 2.5 cm in diameter. They were equipped with 2.5 cm diameter plane NaCl or KCl windows obtained from Janos Optical Corporation. The windows were tilted slightly off perpendicular. This eliminates feedback of CO_2 laser radiation which can cause damage to laser optics and also eliminates feedback in TDL detection which can cause instability of the TDL output wavelength and mode structure.

Stable product analysis was accomplished either by FT-IR or TDL absorption spectroscopy. The FT-IR spectra were obtained on a Nicolet 7199 FT-IR spectrometer. Unless otherwise stated, spectra were recorded with a 2

cm^{-1} resolution.

The tunable diode lasers used in these experiments were obtained from Spectra Physics, and cooled by a CTI - Cryogenics helium compressor system. The cryogenic temperature stablizer (CTS) and laser control module (LCM) were obtained from Laser Analytics, Inc. The output wavelength of the TDL is first roughly controlled by adjusting the temperature of the diode (between 14 and 85K) using the CTS unit. Fine tuning of the output wavelength is then accomplished by changing the applied current to the diode (using the LCM). The output wavelength is determined using a 0.5 m monochromator, which was calibrated using the various orders of a HeNe laser. (Linear interpolation was used to determine wavelengths between orders).

TDLs, in general, operate multi-mode. That is, they simultaneously emit at more than one wavelength. By subtle adjustments of temperature and current, regions of near single mode operation can be found. (For all measurements in this thesis, greater than 75% of the diode power was contained in a single mode). For purposes of quantification, all calculations were done using only the TDL power in the mode being absorbed, not the total TDL power.

Periodically, the TDLs had to be warmed to room temperature for removal of condensed water from the cold head, purging of the high pressure He lines used for cooling, or refurbishing of piston components. This warming and re-cooling of the TDLs lead to changes in the TDL output characteristics, and total recalibration of the diode is often necessary after each temperature cycle.

The experimental design for TDL stable product analysis is shown in Figure 2.2. The TDL beam is chopped by a mechanical chopper and focussed through the cell onto a Hg-Cd-Te detector (Model HCT-100, Infrared Associates Inc.) with a response time of 400 ns. The detector signal is fed into a lock-in amplifier (Princeton Applied Research, Model 126) whose phase is set to match that of the chopper so that phase sensitive detection is achieved. The output of the lock-in amplifier is used to drive the Y scale of a Hewlett-Packard 7004B XY-recorder. The X-scale (frequency scale) of the XY-recorder is driven by the "recorder out" function of the LCM. A spectrum is recorded by applying a dc ramp to the TDL, resulting in a scan of transmitted TDL power versus wavelength. For absorptions of less than about 1%, second harmonic detection was used to improve the signal to noise ratio. This detection technique is performed by superimposing a small ac current onto the dc ramp, resulting in a small

FIGURE 2.2: Schematic diagram of TDL stable product analysis apparatus. The TDL beam is focussed into the cell by means of L_1, and then focussed onto the IR detector using L_2. The TDL beam is chopped by the mechanical chopper. Detection is done using a lock-in amplifier whose phase matches that of the chopper.

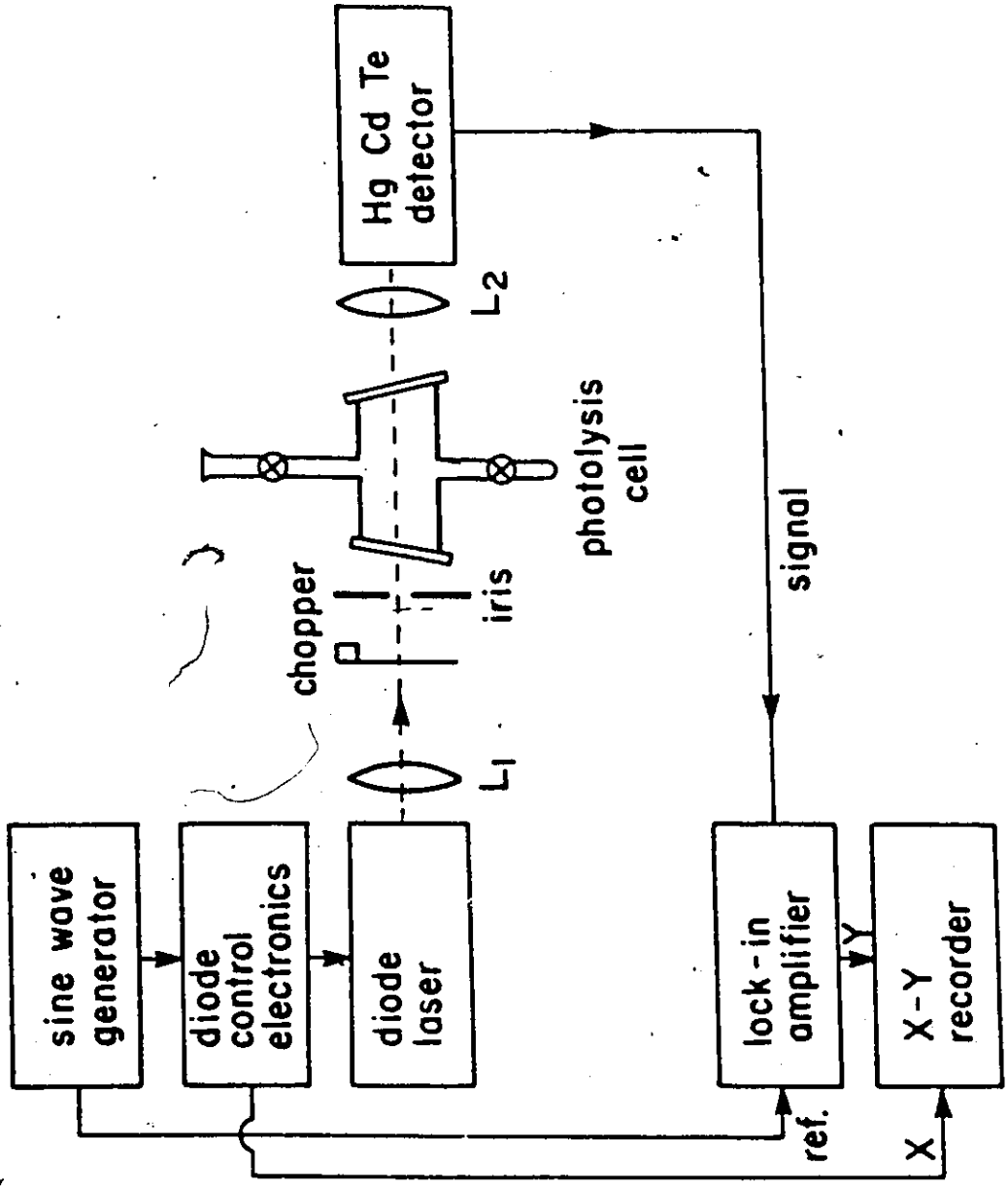
Hg Cd Te detector
L2
photolysis cell
signal
chopper
iris
L1
sine wave generator
diode control electronics
diode laser
lock-in amplifier
X-Y recorder
Y
ref.
X

frequency modulation of the TDL output. The TDL power transmitted through the sample cell is then detected synchronously at twice the frequency of the modulation. (Synchronization is achieved by matching the phase of the function generator with that of the lock-in amplifier.) If the frequency excursion caused by the ac modulation is small compared to the width of the absorption feature, this procedure effectively yields the second derivative of the signal. A full discussion of the second harmonic detection technique is presented in reference 34.

The important experimental parameter in obtaining quantitative information is the absorption coefficient per cm, α_o, which is proportional to concentration ($I = I_o \exp(-\alpha_o l)$, see Chapter 1). The parameters I and I_o for an isolated absorption feature are defined in Figure 2.3. In the case of second harmonic detection, the height of the second derivative signal is proportional to the absorption strength in a direct absorption experiment.

Quantification can then be obtained in two ways. In the case of a stable substance (for example, C_2F_4), a standard Beer's Law plot of α_o versus pressure is created using samples of known pressure. In cases of more reactive species, such as HCl, quantification is accomplished using known linestrength data, using equation

FIGURE 2.3: Calibration plots for CO and CO-$CHCl_3$ mixtures. Line A, showing detection of pure CO, gives a linestrength for R(8) in agreement with the literature. Line B shows the effects of pressure broadening on the CO absorption coefficient. The data are consistent with a pressure-broadening coefficient of 8.0×10^{-5} cm^{-1} $Torr^{-1}$, as measured in our lab. Line C, with detection done on R(6), shows that the measured absorption coefficient (by either direct or second harmonic detection) is linear over a range of CO pressures of greater than three orders of magnitude. The inset defines the parameters I and I_o, used in the measurement of α_o.

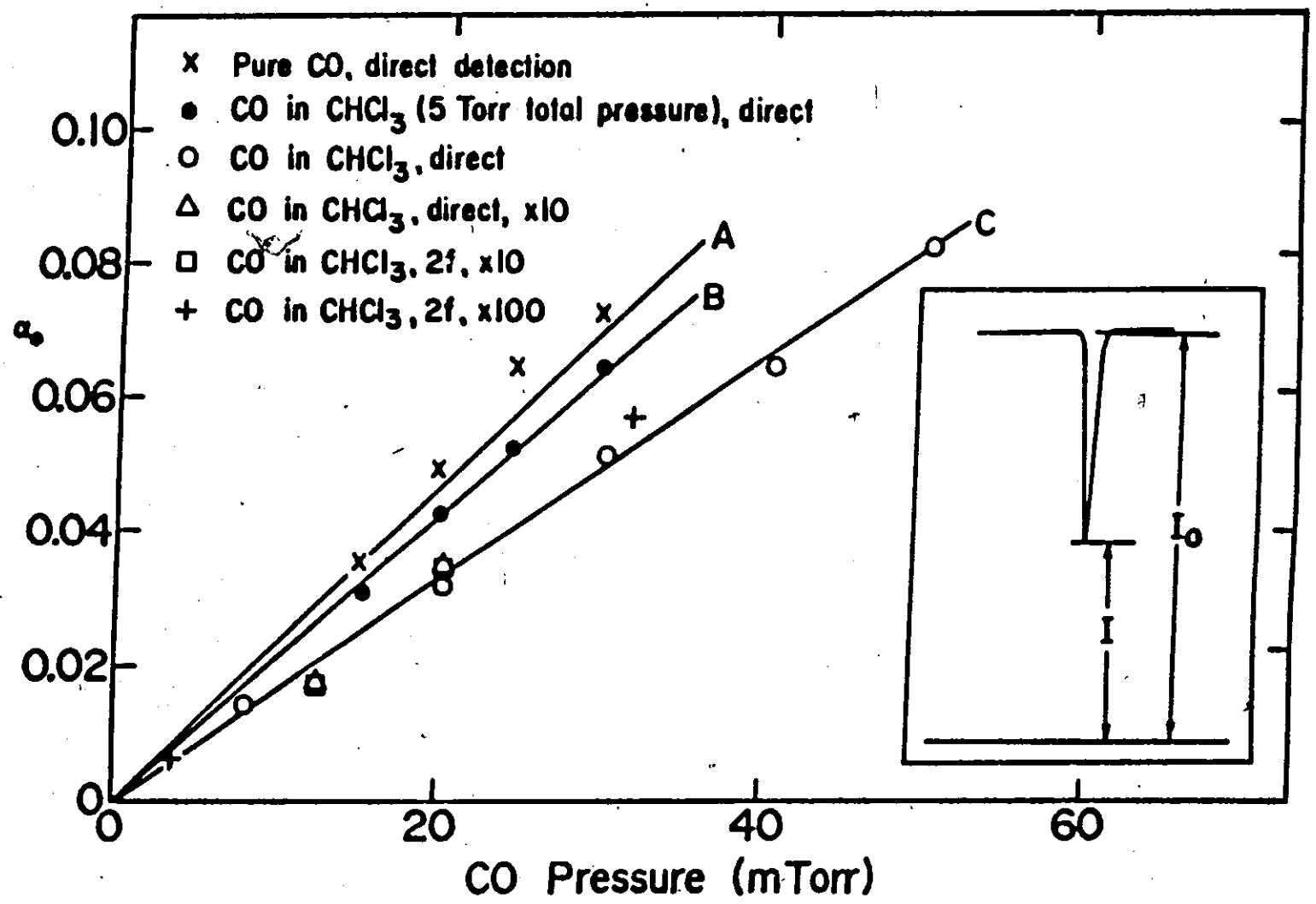
× Pure CO, direct detection
• CO in $CHCl_3$ (5 Torr total pressure), direct
○ CO in $CHCl_3$, direct
△ CO in $CHCl_3$, direct, x10
□ CO in $CHCl_3$, 2f, x10
+ CO in $CHCl_3$, 2f, x100
A
B
C
α_0
0.10
0.08
0.06
0.04
0.02
0
0
20
40
60
CO Pressure (mTorr)
I_0
I

(1.10):

$$\alpha_o = (\ln 2 / \pi)^{1/2} (P/760) (s/\Delta\nu_D) \quad ....(2.1)$$

where s is the linestrength, $\Delta\nu_D$ is the Doppler width of the transition, and P is the sample pressure in Torr.

The validity of this approach to quantification has been demonstrated for CO (see Figure 2.3). Line A shows a plot of α_o versus CO pressure, with CO detection done on R(8). The slope of this plot is related to the linestrength as can readily be seen from the above equation (2.1). The linestrength obtained from this plot, $(4.0\pm0.3) \times 10^{-19}$ cm molecule^{-1}, is in agreement with the literature value of 4.2×10^{-19} cm molecule^{-1}.[35]

The effect of pressure broadening is noted in line B. Again, CO absorption coefficients are measured on R(8), but this time the CO is diluted in $CHCl_3$ (such that the total pressure is 5 Torr). Collisional broadening now becomes significant, and a Voigt profile is obtained (see equation (1.11)). The data obtained is consistent with a value of $\Delta\nu_C$ of 4×10^{-4} cm^{-1}, as measured in our laboratory by Paul Beckwith.

Finally, the linearity of α_o versus pressure over a wide pressure range is demonstrated. Here, CO is monitored on R(6), and CO samples (ranging in pressure

from .04 mTorr to 50 mTorr) are again diluted in $CHCl_3$ to a total pressure of 5 Torr. Line C shows that the plot is indeed linear over the entire CO pressure range (more than three orders of magnitude), regardless of whether CO is monitored by direct absorption or by second harmonic detection.

2.4 TIME-RESOLVED DETECTION OF TRANSIENTS WITH TDLs

In addition to the detection of stable products by TDL spectroscopy, a novel TDL technique for the time-resolved detection of transient products of IRMPD has been developed in our lab (in collaboration with Carl Brown and Paul Beckwith). To date, the technique has been applied to the detection of two short-lived species, CF_2 and CF_3. In addition, short timescale detection of the stable molecules CF_4, C_2F_4, C_2F_6, CO, HCl, DCl, COF_2, and DF, has been achieved to eliminate the effects of wall or secondary reactions. The salient features of the technique, described in detail in reference 36, will be summarized here.

The experimental set-up for transient detection with TDLs is shown in Figure 2.4. Photolysis is achieved with a high repetition rate Lumonics TEA-801A CO_2 laser.

FIGURE 2.4: Schematic of TDL transient detection apparatus. Lens L_1 is used to focus the TDL beam, while lens L_2 collimates the CO_2 laser beam. The two beams are combined on beamsplitter M_1 and focussed on L_3 into the capillary cell. The two beams are then separated on a diffraction grating, with the TDL beam then being focussed onto the infrared detector, and the CO_2 laser beam being focussed onto an energy meter.

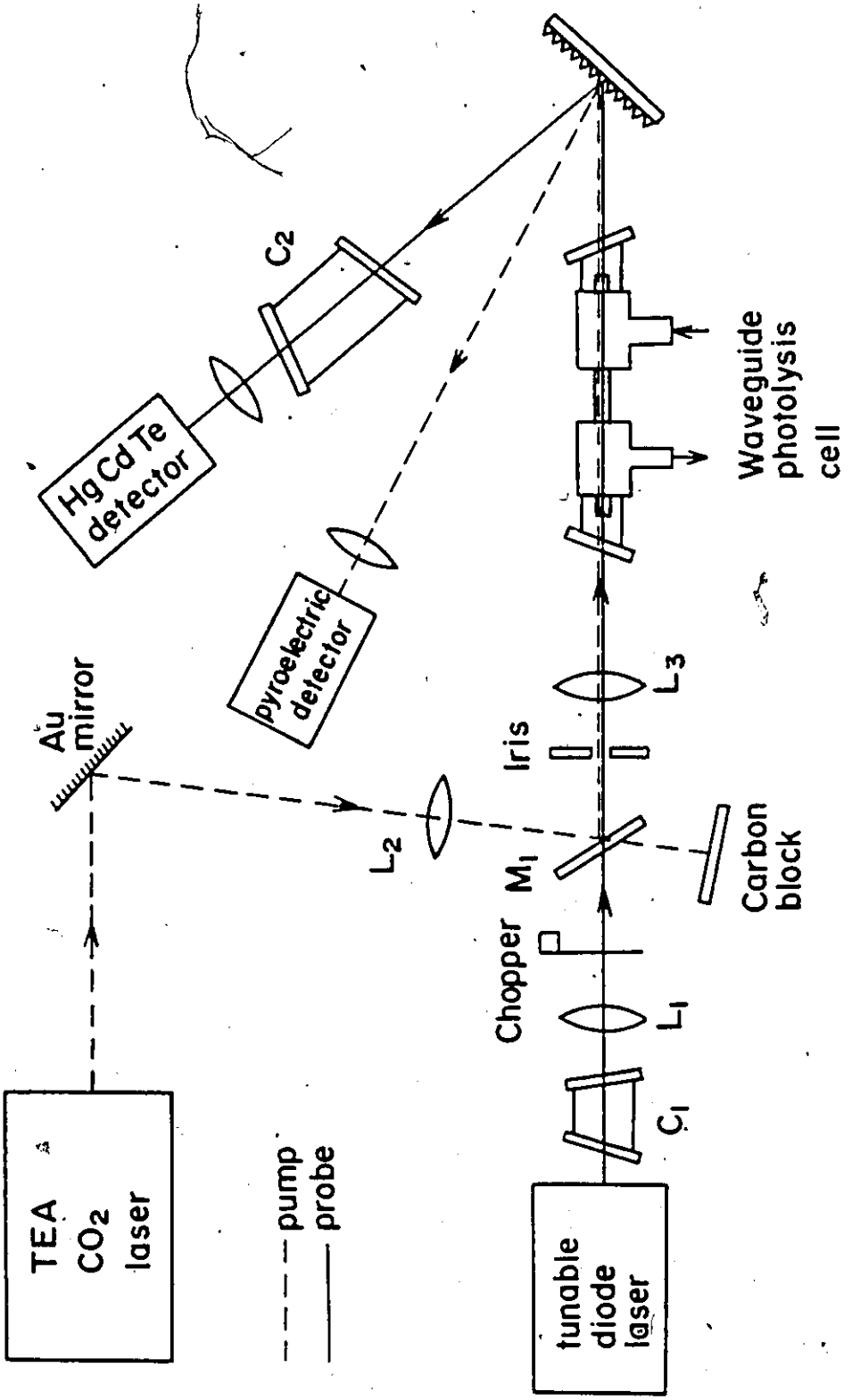
TEA
CO_2
laser
pump
probe
tunable
diode
laser
C_1
L_1
Chopper
M_1
L_2
Carbon
block
Au
mirror
Iris
L_3
pyroelectric
detector
Hg Cd Te
detector
C_2
Waveguide
photolysis
cell

The output of this CO_2 laser and the TDL laser are combined on a ZnSe beamsplitter, and both beams are focussed through a capillary waveguide cell using a BaF_2 lens with a focal length of 25 cm. The cell consists of a 15 cm long, 1 mm diameter quartz capillary housed in a 25 cm Pyrex cell equipped with angled NaCl plane windows (2.5 cm diameter) at each end. The cell can contain either a static fill of the desired precursor gas or the gas can be flowed through the cell if desired. The two beams traverse the capillary cell, and are then separated on a diffraction grating. The TDL beam is then focussed onto the infrared detector (400 ns response time) using a Ge f/2 lens. Two absorber cells are also included in the experimental set-up, one in front of the IR detector and the other at the TDL output. These cells contain a gas which absorbs at the output frequency of the CO_2 laser. Without these cells, stray CO_2 radiation either reaches the detector, causing interference, or feeds back into the TDL causing a slight frequency shift in its output.

The techniques described above offer two major advantages, the first being the use of the capillary cell. In addition to providing for a high CO_2 laser fluence over an increased interaction length, the capillary cell is invaluable in confining the TDL probe beam which otherwise is subject to deflection due to passage of the intense CO_2

laser pulse through the cell. This latter effect arises from transient changes in the refractive index of the gas or the various optics due to the heating caused by the passage of the CO_2 laser pulse. Without the use of a capillary cell, it is very difficult to distinguish between probe beam deflection and true absorption as can be seen in early work in our lab[36] and other published work.[37]

The other main advantage is that our work makes use of the tunability of the TDL laser. A high frequency sinusoidal current is applied to the TDL (using a Hewlett Packard 3311A Function Generator), which leads to both wavelength and amplitude modulation of the TDL beam. A trigger pulse from the function generator, stepped down in frequency, is used to trigger the firing of the CO_2 laser pulse so that the CO_2 laser pulse is synchronized with the TDL detection. An idealized schematic of the detector output in a transient detection experiment is illustrated in Figure 2.5. Note that in each modulation cycle, the transient absorption is sampled twice, once in each direction. Using a digital storage oscilloscope (Tektronix 468), it is a simple matter to record and average a number of scans to improve the signal to noise ratio. Background scans can also be collected with the

FIGURE 2.5: Idealized schematic of the detector output in a transient detection experiment. In each modulation cycle, the absorption feature is sampled twice, once in each direction.

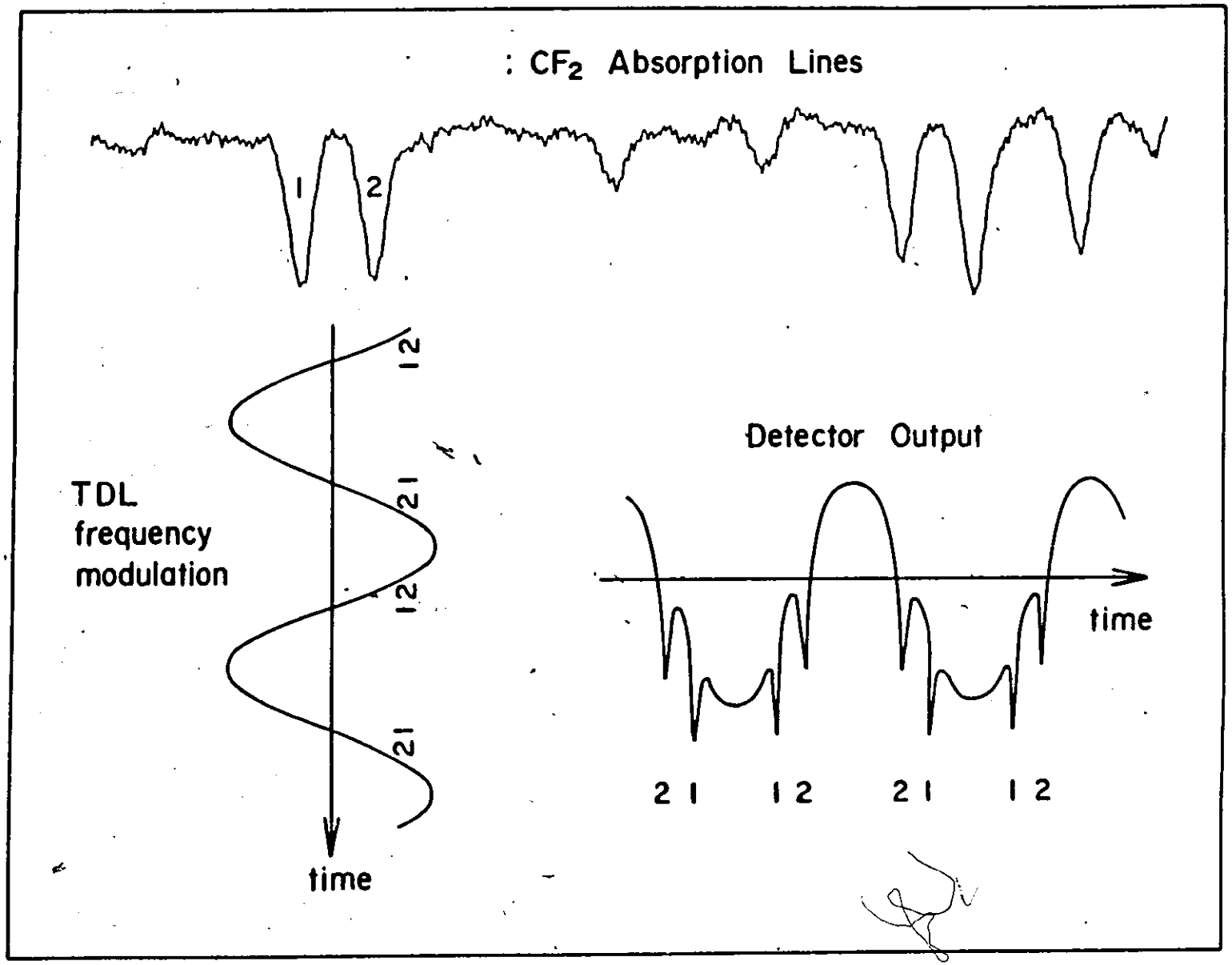
: CF_2 Absorption Lines
1
2
TDL
frequency
modulation
12
21
12
21
time
Detector Output
time
2 1
1 2
2 1
1 2

CO_2 laser blocked. Subtraction of this background signal on an IBM-PC is done to eliminate the majority of the AM signal and any precursor absorptions that may be present, as shown in Figure 2.6.

At present, the TDL can be modulated at frequencies as high as 250 kHz, allowing for a time resolution of a few microseconds. However, due to electrical interference from the CO_2 laser pulse, transient absorption detection is only possible after about 20 microseconds, sufficient for the detection and monitoring of even the shortest lived transients encountered in this work.

The sensitivity of the transient technique has been shown[36] to be strictly detector noise limited. With the addition of an analog subtraction scheme to eliminate the majority of the AM component of the signal before digital subtraction, absorbances of 3×10^{-5} have been achieved for an isolated N_2O absorption feature.

It remains to discuss the method used in the identification of the transient absorption features. For stable species, such as HCl, DCl, or CO, identification of absorption features could be done using prepared samples of these gases. With the aid of a monochromator, the output wavelength of the TDL could be obtained to within about 0.1 cm^{-1}, so that identification of the particular

FIGURE 2.6: Demonstration of the advantages of background subtraction in TDL transient spectroscopy. Note that the subtraction removes the precursor absorptions and enhances the CF_2 signal. The CF_2 is produced by photolysis of 1.5 Torr of C_2F_3Cl, and both the signal and background represent the average of 50 scans.

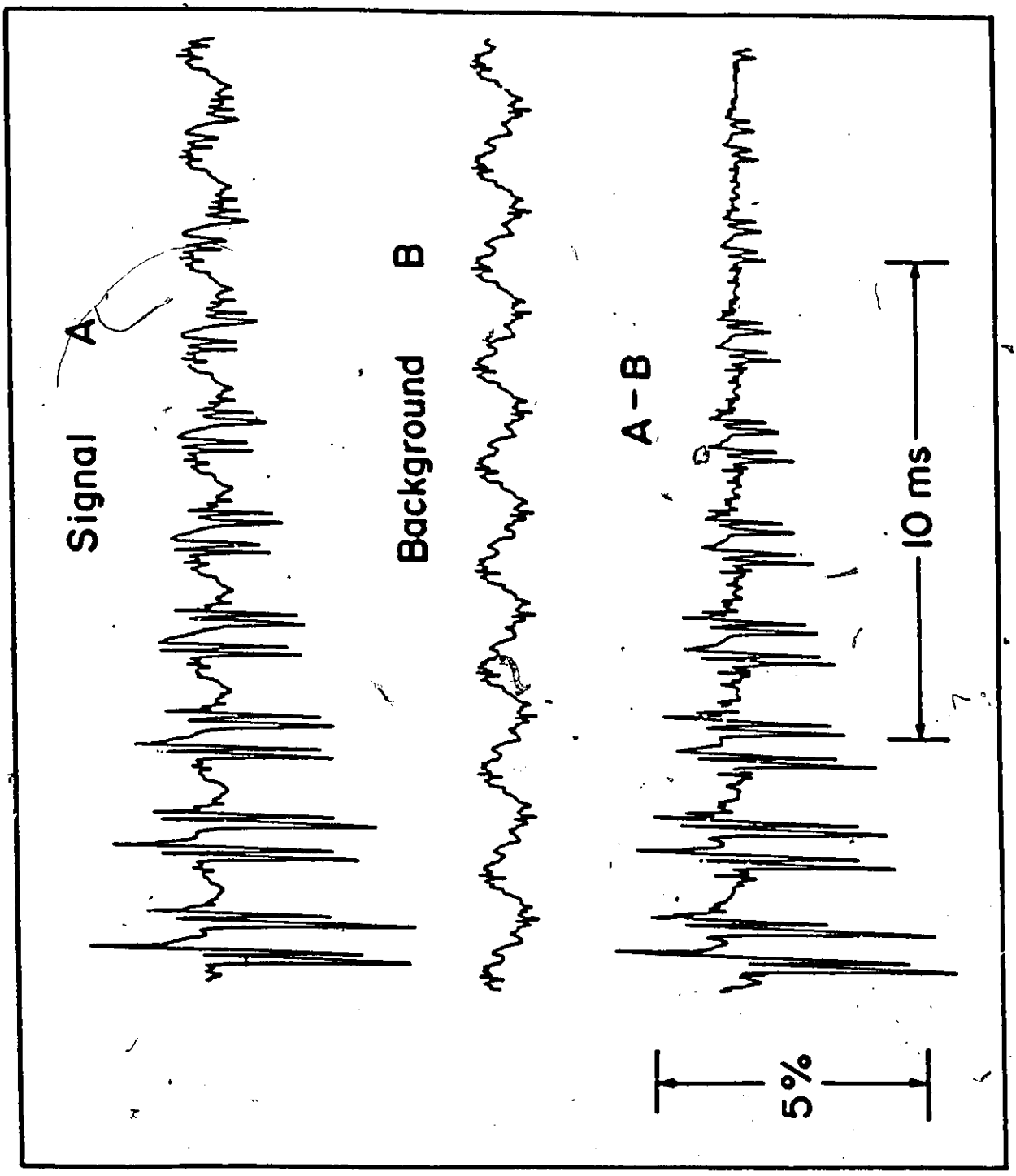
Signal
A
Background
B
A-B
10 ms
5%

transition is routine.

The detection of the transient species CF_2 and CF_3 was done with the aid of the spectroscopic studies of Davies et al.[38] for CF_2 and Yamada and Hirota[39] for CF_3. A full discussion of the technique employed is deferred to the results chapters (Chapter 3 for CF_2 and Chapter 4 for CF_3).

2.5 SUMMARY

In this chapter, the experimental procedures used in this work have been described. These include a discussion of the techniques used in gas handling and purification, sample preparation, sample irradiation, FT-IR and TDL infrared spectroscopic analysis, and time-resolved TDL analysis.

The work of C.E. Brown and P.H. Beckwith in the development of the time-resolved TDL absorption technique is gratefully acknowledged.

CHAPTER 3

IRMPD OF CF_2HCl

3.1 INTRODUCTION

This chapter describes the results obtained from the infrared multiphoton dissociation of CF_2HCl. Included among these results are a confirmation of the photolysis mechanism, the measurement of an infrared absorption linestrength for CF_2, a calculation of the ν_1 bandstrength of CF_2 (from the measured linestrength), and a measurement of the rate constant for combination of two CF_2 molecules to form C_2F_4. All of these results were obtained by monitoring the time-resolved production of CF_2, HCl, and C_2F_4 with TDLs following the IRMPD of CF_2HCl.

3.2 EXPERIMENTAL

The general techniques used for photolysis and for analysis of stable and transient products are described in Chapter 2. Only the details specific to the IRMPD of CF_2HCl will be presented here.

An FT-IR spectrum of 2 Torr CF_2HCl, recorded in a

10 cm long Pyrex cell, is shown in Figure 3.1. Photolysis of the CF_2HCl is accomplished using the 9R(26) CO_2 laser line at 1082.29 cm^{-1}. Stable product analyses are performed as described in Chapter 2.

The experimental design for transient detection of CF_2 and HCl is as in Figure 2.5 (Chapter 2). Typically, the capillary cell is filled with 800 mTorr of CF_2HCl. Since the reaction time of CF_2 is comparable to the flow time through the cell, the CF_2HCl could not be flowed in this experiment. Thus, all measurements were made after one pulse, with no signal averaging. Background subtraction was performed as described in Chapter 2.

For this work, HCl was monitored on P(9) at 2677.732 cm^{-1} (over a 5 ms timescale to eliminate wall reactions) as shown in Figure 3.2, while C_2F_4 was monitored near 1175 cm^{-1}. C_2F_4 calibrations were done by measuring α_o as a function of pressure for standard samples of known pressure.

It remains to discuss the procedure for the detection of CF_2. The IR spectroscopy of the ν_1 band of CF_2 has been studied using TDLs by Davies et al.[38], who produced CF_2 in a microwave discharge of CF_2CFCl. The microwave discharge experiment of Davies et al. was reproduced in our lab,[36] and a series of lines (the $^rQ_3$

FIGURE 3.1: FT-IR spectrum of 2 Torr of CF_2HCl. The pathlength is 10 cm, while the FT-IR resolution is set at 2 cm^{-1}.

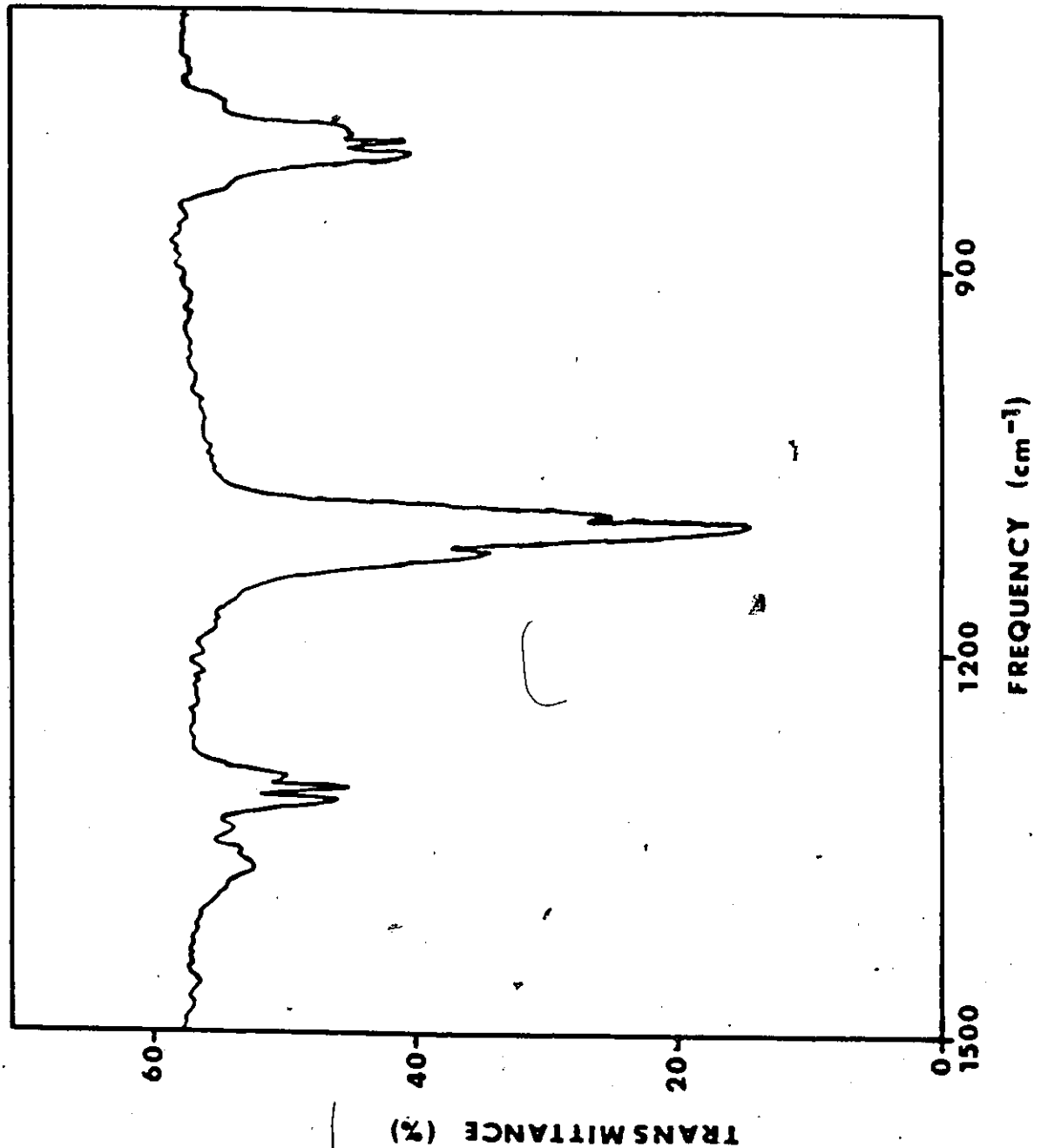
TRANSMITTANCE (%)
60
40
20
0
1500
1200
900
FREQUENCY (cm⁻¹)

FIGURE 3.2: Transient TDL absorption by HCl. The absorption feature monitored is P(9) at 2677.732 cm^{-1}. The HCl is produced by photolysis of 800 mTorr of CF_2HCl.

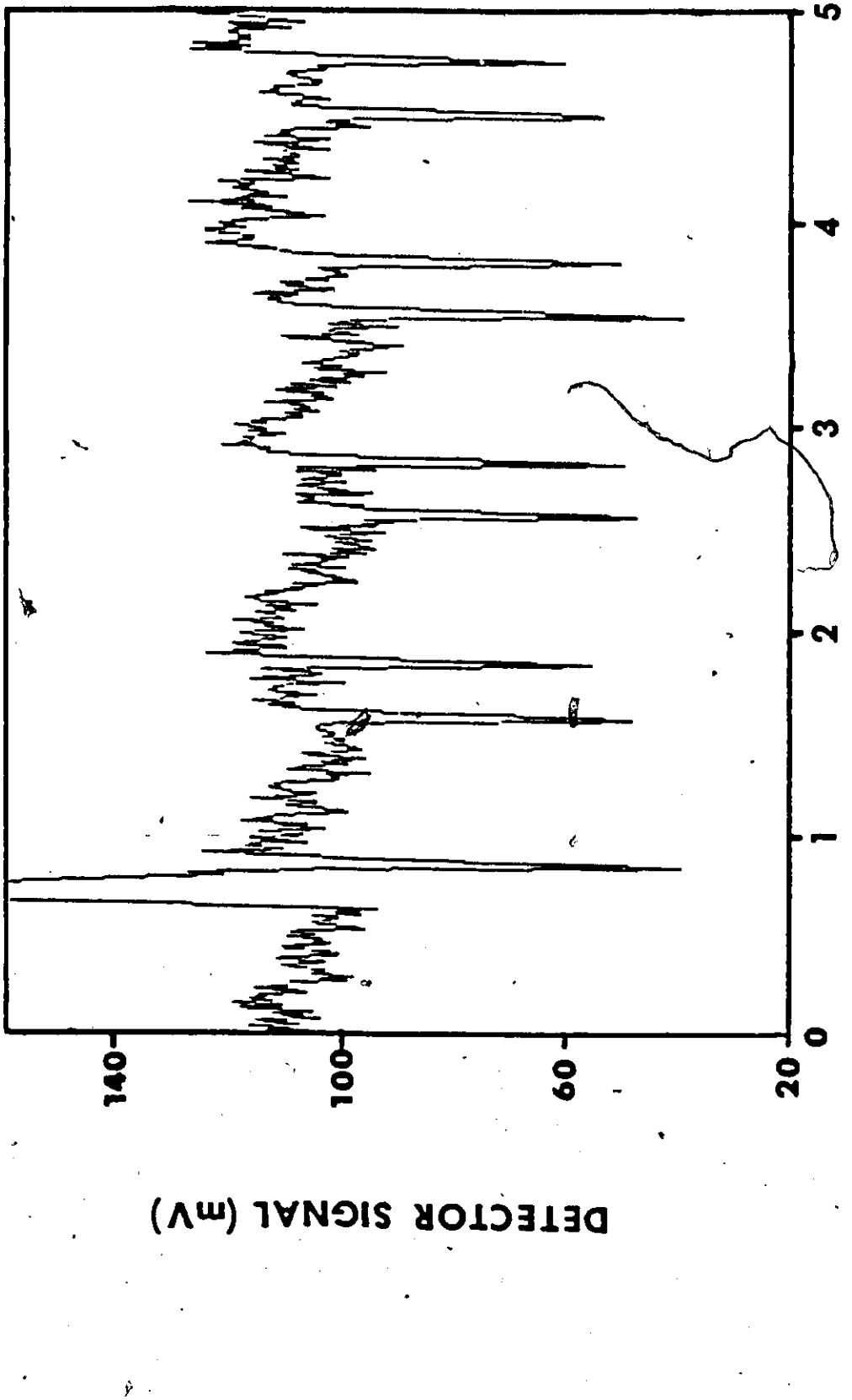
DETECTOR SIGNAL (mV)
140
100
60
20
0
1
2
3
4
5
TIME (ms)

sub-branch) of CF_2 near 1243 cm^{-1} was identified with the aid of a monochromator. Figure 3.3 shows both our spectrum in this region and that of Davies for comparison. By using the same TDL temperature and current settings in the transient set-up, CF_2 was easily identified in the IRMPD of CF_2CFCl and C_3F_6. In particular, a set of three closely spaced lines in the $^rQ_3$ sub-branch (at 1243.0015 cm^{-1}, 1243.0082 cm^{-1}, and 1243.0185 cm^{-1}) were easy to locate and were used to confirm the presence of CF_2 (see Figure 3.4). The measurements on CF_2 linestrengths and kinetics are made on the highest frequency line of this triplet ($^rQ_3(9)$ at 1243.0185 cm^{-1}).

3.3 PHOTOLYSIS MECHANISM

The IRMPD of CF_2HCl has been well studied.[30,34,40-44] King and Stephenson,[40] using state-selective laser induced fluorescence (LIF) detection of CF_2, first determined that the primary IRMPD mechanism for CF_2HCl was as follows:

$$CF_2HCl \rightarrow CF_2 + HCl \quad \ldots.(3.1)$$

This reaction would be followed by recombination of the CF_2 to form C_2F_4:

FIGURE 3.3: TDL spectrum of CF_2 in the region of 1243 cm^{-1}. The figure shows the absorption lines created in a microwave discharge by Davies et al.[38], and in our lab for comparison. The lower trace shows an expanded view of a portion of the spectrum.

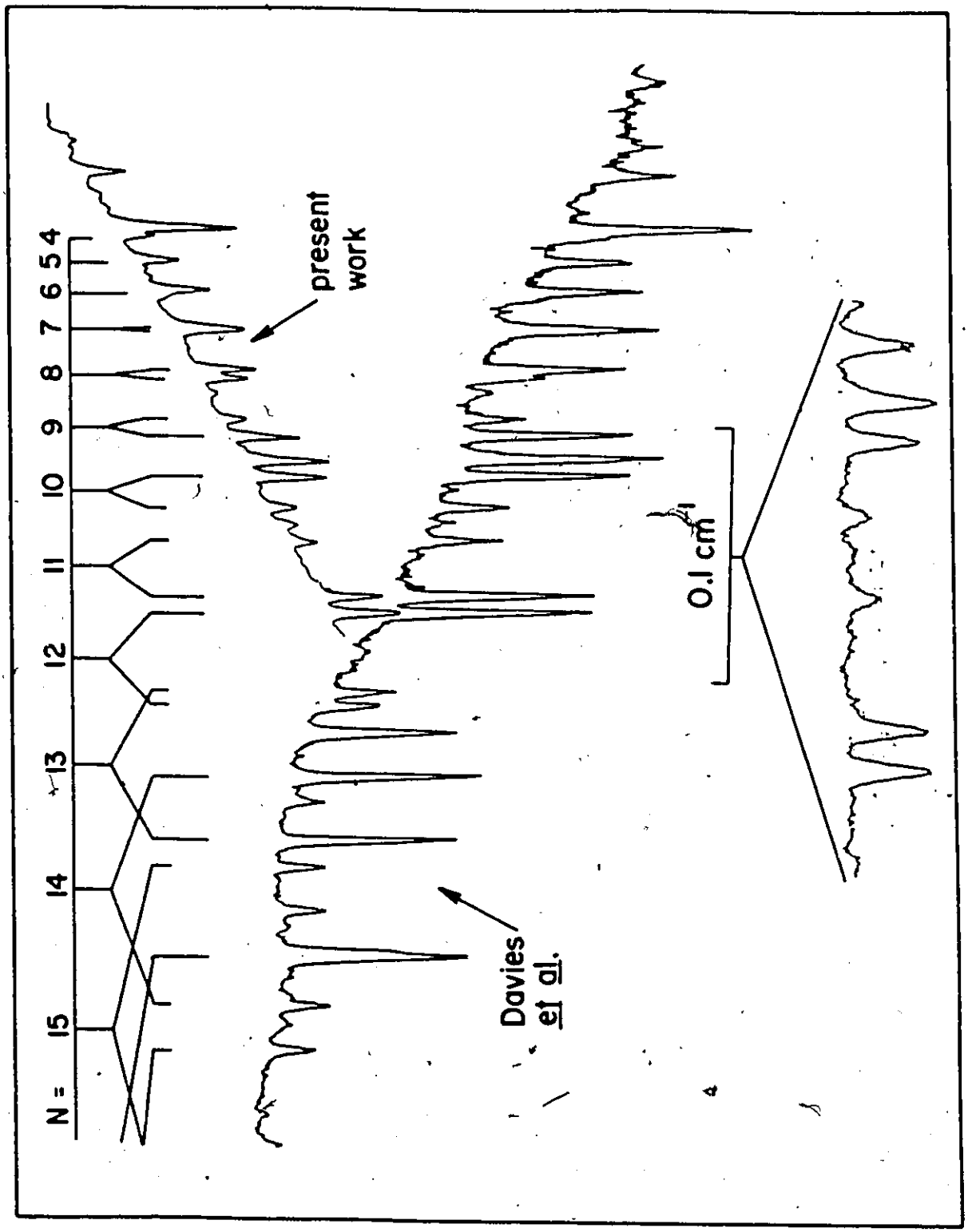
N = 15 14 13 12 11 10 9 8 7 6 5 4
present work
Davies et al.
0.1 cm⁻¹

$$2\ CF_2 \rightarrow C_2F_4 \quad \ldots(3.2)$$

These workers were able to measure the vibrational, rotational, and translational temperatures (1160K, 2000K, and 2300K, respectively) of the nascent CF_2 product.

The dissociation mechanism, equation (3.1), was confirmed in a molecular beam experiment by Sudbo et al.[37] who detected the photolysis products by time-of-flight mass spectrometry. Further studies involving LIF detection of CF_2[41,42] and infrared emission from HCl[41] followed.

Evidence for three minor CF_2HCl dissociation channels was presented by Martinez and Herron[43] using mass spectrometric detection:

$$CF_2HCl \rightarrow CFCl + HF \quad \ldots(3.3a)$$

$$\rightarrow CHCl + F_2 \quad \ldots(3.3b)$$

$$\rightarrow CHF + ClF \quad \ldots(3.3c)$$

However, these authors concluded that these minor channels accounted for less than 1% of the total CF_2HCl dissociated.

A more recent report[44] suggests that at lower

fluences (2.5 J cm^{-2}), another dissociation channel competes with equation (3.1). The authors suggest that a new product, "a halogenated derivative of butane", is obtained. Inspection of the infrared spectra presented in this report led us to conclude that this new product was, in fact, COF_2 which likely results from reaction of CF_2 with the Pyrex photolysis cell, or possibly with O_2. Our own studies in a conventional Pyrex cell (10 cm in length, and 2.5 cm in diameter) using a focussed CO_2 beam the peak fluence of which was varied from 2.5 J cm^{-2} to 20 J cm^{-2}, revealed only C_2F_4 and HCl when analyzed by Fourier Transform IR spectroscopy. In our capillary cell, where wall reactions are more significant, trace amounts of COF_2 can be detected with a TDL.

3.4 RESULTS AND DISCUSSION

3.4.1 CF_2 and HCl VIBRATIONAL RELAXATION

It is apparent from the above discussion that the dissociation of CF_2HCl occurs almost exclusively via equation (3.1). This leads to the important conclusion that the concentration of CF_2 and HCl immediately following the passage of a CO_2 laser pulse are equal. (Even though some of the dissociation may occur via the

minor channels described in equation (3.3), none of these channels leads to the formation of either CF_2 or HCl.) Thus, quantification of the HCl produced by a CO_2 laser pulse (using known linestrength data) makes possible the determination of the absolute CF_2 concentration following the pulse. That is, an infrared linestrength for CF_2 can be obtained.

Before proper quantification can be accomplished, it is important that both the CF_2 and the HCl have rotationally and vibrationally relaxed, since both are formed in excited states and detection occurs in the vibrational ground state. The HCl signal was found to be constant over a timescale ranging from about 25 μs to at least 10 ms, which indicates that the HCl has had sufficient time for rotational and vibrational relaxation, but not sufficient time for any wall reactions to have occurred (even though diffusion to the walls has occurred over this time period). Typical rate constants for HCl vibrational relaxation in collisions with halogenated methanes[45] indicate that relaxation should occur over a timescale of tens of microseconds at the pressures employed in this work. Thus, it appears that quantifying the HCl (v=0) at a time of 1 or 2 ms after the CO_2 laser pulse yields an accurate measure of the total HCl produced

in the pulse.

Evidence for rotational relaxation in CF_2 can be observed in Figure 3.4, as the ratio of the signal intensity of the three lines is not constant with time. The middle line of the triplet, arising from a state with higher rotational excitation, is more intense at early times relative to the outside lines. As time progresses, the intensity of the outside lines increases relative to the central line until thermal equilibrium occurs after about 150 μs. The overall growth of the CF_2 signal over this time period is attributed to vibrational relaxation (CF_2 has a vibrational level in coincidence with a vibrational level of the parent CF_2HCl). Addition of other molecules with vibrational coincidences with CF_2 (CF_4 and N_2O) had no effect on the kinetics of CF_2 decay or on its peak yield. Thus, it appears that the CF_2 has relaxed to the vibrational ground state after about 150 μs. Since at this time the amount of CF_2 lost due to reaction is negligible, it is possible to make an accurate determination of the amount of CF_2 produced in the laser pulse.

In addition, the temperature of the gas after passage of a CO_2 laser pulse is important, since absorption strengths are temperature dependent. To measure this temperature, a trace of N_2O was added to the

FIGURE 3.4: TDL transient absorption spectrum showing the presence of the CF_2 triplet near 1243 cm^{-1}. CF_2 is produced by irradiation of 800 mTorr of CF_2HCl. The TDL sweeps over three CF_2 lines at a modulation frequency of 40 kHz. The strongest absorption line corresponds to about 20% absorption. The growth of the two outer lines relative to the central line of the triplet is attributed to rotational relaxation. The overall growth of the triplet is attributed to cascading of vibrationally excited CF_2 into the vibrational ground state.

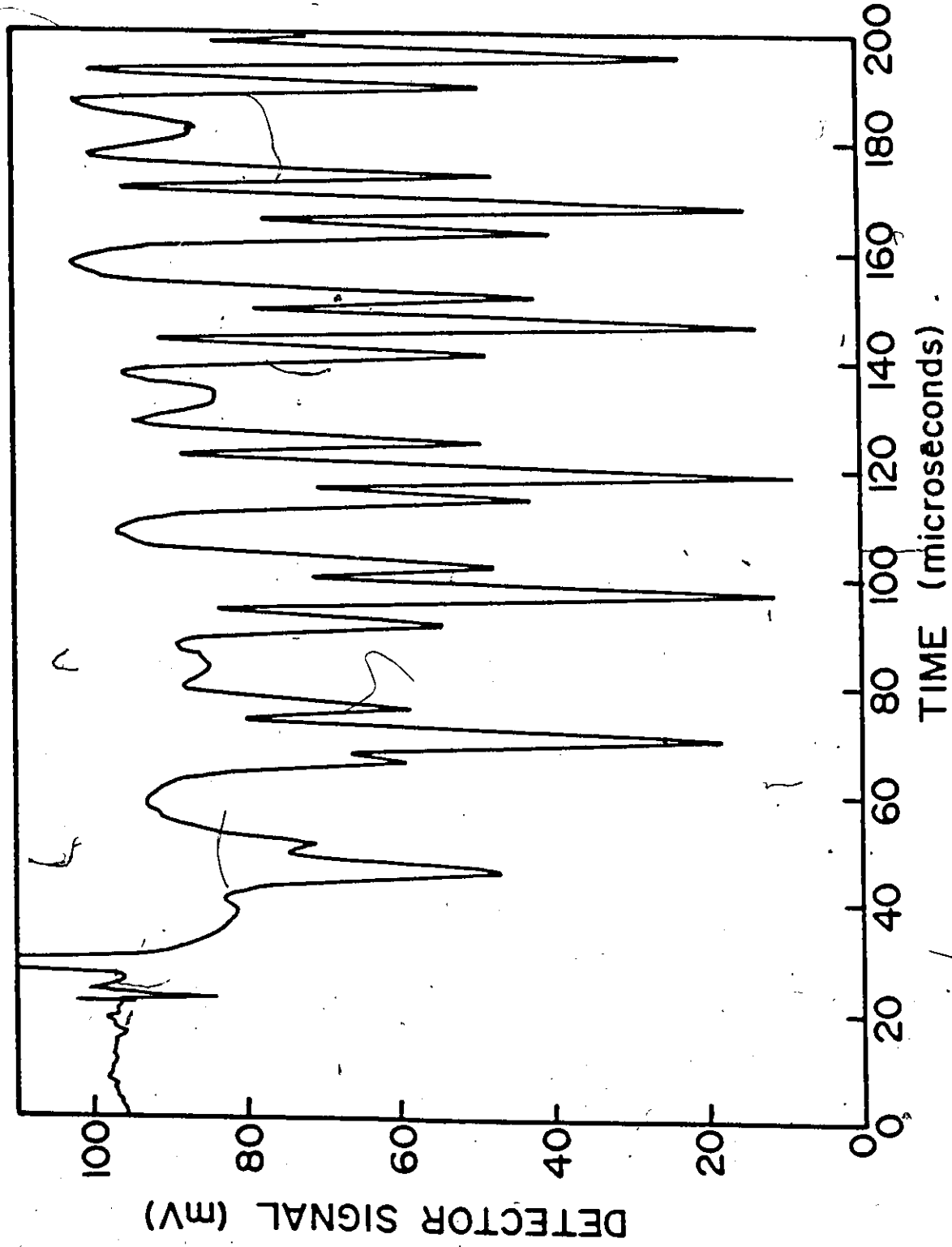
DETECTOR SIGNAL (mV)
100
80
60
40
20
0
0
20
40
60
80
100
120
140
160
180
200
TIME (microseconds)

photolysis mixture and the time-resolved absorption of N_2O on a temperature-sensitive transition (P(45) at 1243.795 cm^{-1}) was performed. After passage of a CO_2 laser pulse, no measureable increase in N_2O absorption (to within 10%) was noted over 20 ms, indicating no significant temperature change. (A 10% increase in N_2O absorption on P(45) would correspond to a temperature change of less than 10 K.)

3.4.2 LINESTRENGTH AND BANDSTRENGTH CALCULATIONS

In order to quantify the product HCl (and thus the CF_2), a number of independent data sets from the IRMPD of CF_2HCl over a range of conditions was required. Thus, the peak transient CF_2 signal (at about 200 μs) and the peak HCl signal (at about 1 ms) were measured as a function of CO_2 laser fluence. Absolute quantification is accomplished using known linestrength data (2.68×10^{-20} cm molecule^{-1} for HCl P(9))[46] as follows:[33]

$$\alpha_o = (\ln 2/\pi)^{1/2} (P/760) (s/\Delta\nu_D) \quad \ldots.(3.4)$$

where α_o is the absorption per cm at line center, s is the linestrength, P is the pressure in Torr, and $\Delta\nu_D$ is the

Doppler limited linewidth. It should be noted that equation (3.4) represents pure Doppler broadening, and ignores the effects of pressure broadening. However, in equation (3.5), only the ratio of $\alpha_o(CF_2)$ to $\alpha_o(HCl)$ is required in the calculation. Since the effect of pressure broadening will be similar in both cases, it can be neglected without producing any significant change in the results.

Thus, the ratio of linestrengths of CF_2 and HCl is given by:

$$s(CF_2)/s(HCl) = [\alpha_o(CF_2)/\alpha_o(HCl)]\ [\Delta\nu_D(CF_2)/\Delta\nu_D(HCl)] \quad \text{— ....(3.5)}$$

The ratio of $\alpha_o(CF_2)$: $\alpha_o(HCl)$ is found from Figure 3.5 to be (0.8 ± 0.2) for all fluences studied, since both products display the same fluence exponent, 1.7. (The error represents $\pm1\sigma$.) The variation in this ratio is predominantly a reproducibility error, caused by random changes in beam geometry, sample pressure, CO_2 laser fluence, etc. The ratio of the Doppler widths, as calculated from equation (1.8c) is 0.40. Thus, the CF_2 linestrength is determined to be $(9\pm2) \times 10^{-21}$ cm molecule^{-1} for the $^rQ_3(9)$ line at 1243.0185 cm^{-1}.

As a final check of the CF_2 linestrength

FIGURE 3.5: CF_2 and HCl yields (in terms of the absorption per cm, α_o) as a function of the average CO_2 laser fluence. The CF_2HCl pressure is 800 mTorr.

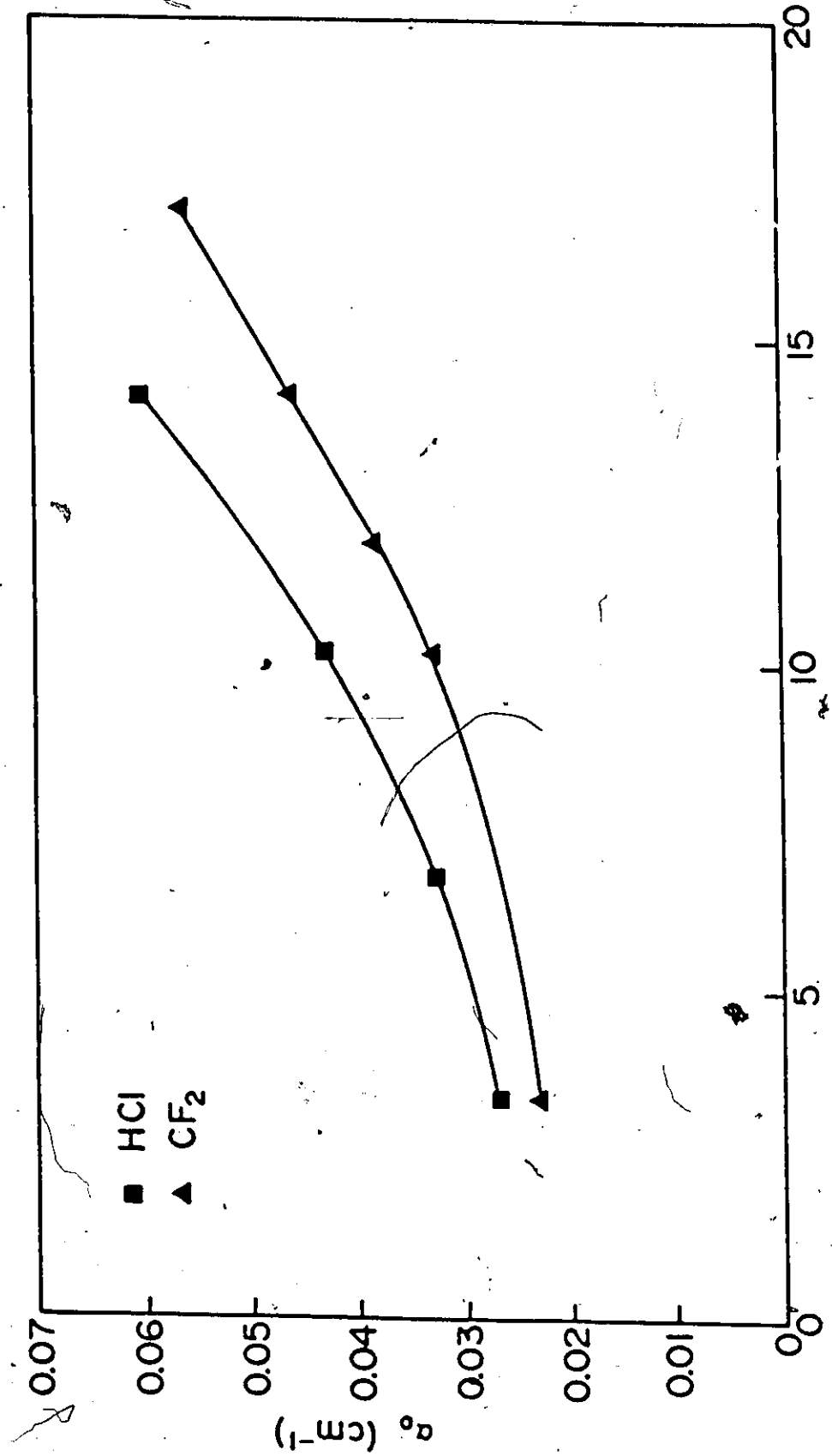
0.07
0.06
0.05
0.04
0.03
0.02
0.01
0
α_o (cm^{-1})
0
5
10
15
20
PEAK CO_2 LASER FLUENCE (J cm^{-2})
HCl
CF_2

measurement, CF_2 decay and C_2F_4 growth were monitored (in separate experiments under identical conditions). C_2F_4 pressures were obtained from a Beer's Law calibration plot, while CF_2 pressures were calculated using the linestrength determined above. Figure 3.6 shows that the C_2F_4 growth accounts for (75±25)% of the CF_2 lost. The error in this measurement is largely due to the uncertainty in the measured CF_2 linestrength. Since minor amounts of CF_2 are lost to COF_2 by wall reactions, this stoichiometry serves as an independent confirmation of the linestrength determined above. (COF_2 is difficult to quantify due to the small amounts produced and calibration difficulties due to the instability of the molecule.)

From the linestrength of the one transition measured here, it is possible to calculate the linestrength for any transition in the ν_1 band as well as the overall bandstrength for ν_1.

CF_2 is described in spectroscopic terms as a near prolate symmetric top. That is, the spectroscopic constant A is greater than B and C, the latter two being approximately equal. The parameter, κ, which is -1 for a true prolate symmetric top, 0 for a totally asymmetric top, and +1 for a true oblate symmetric top, is found to be -0.97 for CF_2 using the values of A, B, and C quoted by

FIGURE 3.6: Partial pressure of CF_2 and C_2F_4 as a function of time following photolysis of 800 mTorr of CF_2HCl at an average CO_2 laser fluence of 17 J cm^{-2}.

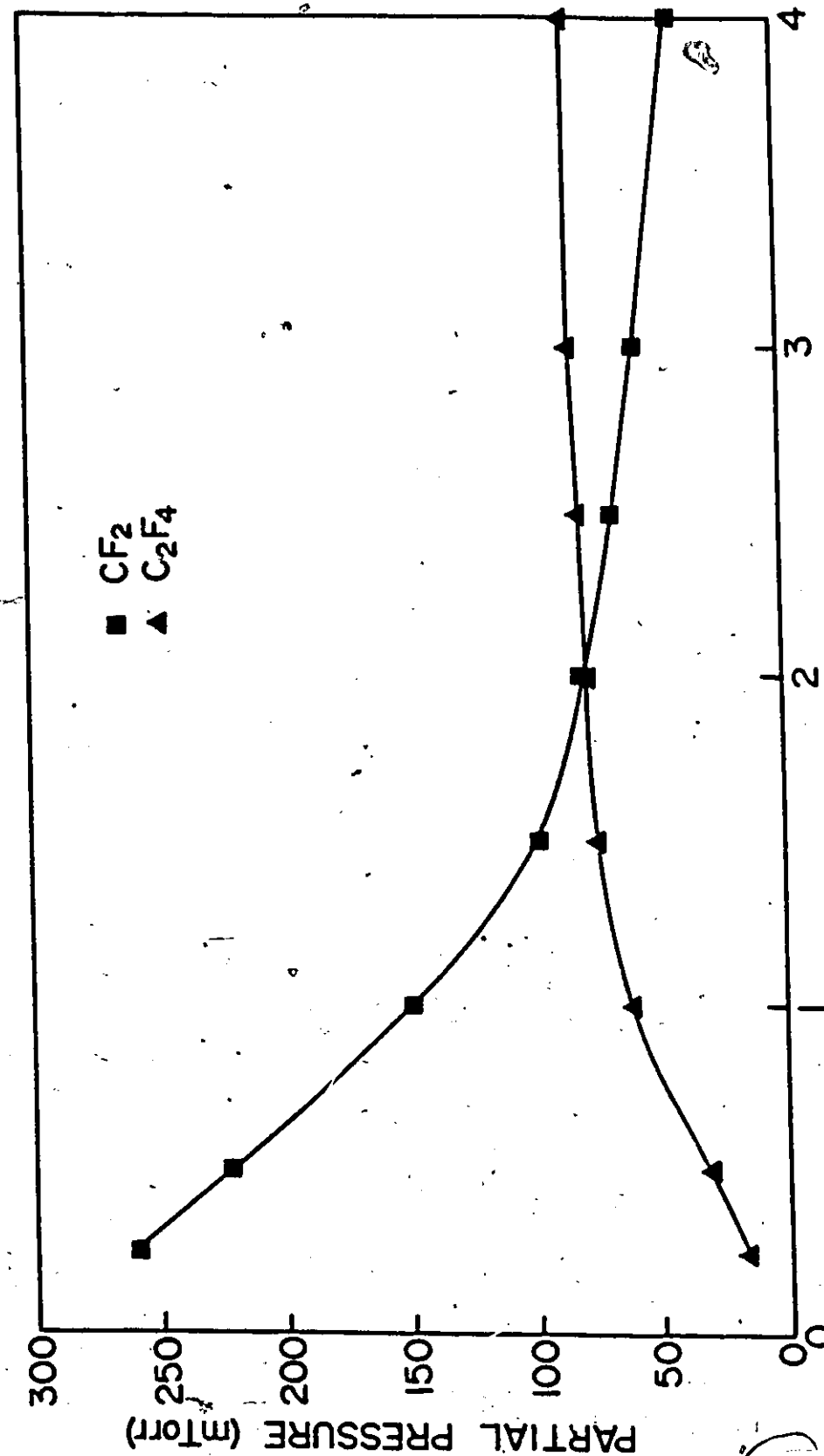
PARTIAL PRESSURE (mTorr)
300
250
200
150
100
50
0
TIME (milliseconds)
0
1
2
3
4
CF_2
C_2F_4

Davies et al.[38] However, some asymmetric doubling is observed in the CF_2 ν_1 spectrum for values of $K \leq 5$ or $N \geq 14$.[38] Indeed, the $^rQ_3(9)$ line is split into one line at 1243.0185 cm^{-1} (for which the linestrength has been measured) and another line (three times as weak) at 1243.0253 cm^{-1}.[38] Since the splitting is not too severe and is statistical in nature (3:1 ratio of the two linestrengths), for the purposes of calculation it is acceptable to treat the two $^rQ_3(9)$ lines as one line, with a strength 4/3 times that of the strongest line and then to treat CF_2 as a prolate symmetric top. Therefore, the overall linestrength of the $^rQ_3(9)$ lines is 4/3 X (9±2) X 10^{-21} = (1.2±0.3) X 10^{-20} cm molecule^{-1}.

To calculate another linestrength from the linestrength measured above, one begins with the general formula for the linestrength, s, given as follows:[33]

$$s=(8\pi^3\nu)/3hcp)\ (Ng_{NK}/Q_vQ_r)\ (R_v^2)(R_r^2)\ \exp(-E(N,K)/kT)\ [1-\exp(-hc\nu/kT)] \quad ....(3.6)$$

where ν is the transition frequency in cm^{-1}, Q_v and Q_r are the vibrational and rotational partition functions, R_v^2 is the vibrational transition moment, R_r^2 is the Honl-London factor, g_{NK} is the degeneracy of the rotational level, and E(N,K) is the energy of the lower state

rotational level.

In order to determine the linestrength of another transition from the one measured above, only the transition frequency, ν, the Honl-London factor, the degeneracy, and the Boltzmann factor need be considered, since all other terms are independent of the particular ν_1 transition being considered.

The overall bandstrength, A, obtained as the sum of s over all allowable N and K, can be approximated as follows:[33]

$$A=(8\pi^3\nu_o/3hcp)(N/Q_v)(R_v^2)[1-\exp(hc\nu/kT)] \quad ....(3.7)$$

Division of (3.6) by (3.7) and rearrangement yields:

$$A=(\nu_o/\nu)\ (s/g_{NK}\ R_r^2)\ (Q_r/\exp(-E(N,K)/kT)) \quad ....(3.8)$$

Using our measured linestrength, the Honl-London factor, the degeneracy, and the Boltzmann factor for $^rQ_3(9)$ and the rotational partition function for CF_2, the ν_1 bandstrength for CF_2 is calculated to be $(3.4\pm0.8) \times 10^{-18}$ cm molecule^{-1}.

3.4.3 CF_2 KINETICS

Quantification of the CF_2 in the manner described above allows one to know the absolute concentration of CF_2 present at any time after the laser pulse, and thus allows a study of the decay kinetics of CF_2. To observe its decay, the CF_2 signal was monitored on a longer timescale (10 ms). Since decay of CF_2 is expected to occur via combination of two CF_2 molecules to form C_2F_4, the CF_2 decay follows second order kinetics (see Appendix A):

$$d(CF_2)/dt = 2\, k_{(3.2)}\, (CF_2)^2 \qquad ....(3.9a)$$

$$(CF_2)^{-1} = -2\, k_{(3.2)}\, t \qquad ....(3.9b)$$

where $k_{(3.2)}$ is the second order rate constant for CF_2 recombination.

Thus, a plot of $(CF_2)^{-1}$ versus time should yield a straight line with slope $-2k_{(3.2)}$. From such a plot, shown in Figure 3.7, the recombination rate constant is found to be $(2.3\pm0.7) \times 10^{-14}$ cm^3 molecule^{-1} s^{-1} for 800 mTorr of CF_2HCl near room temperature. This may be compared with a pressure independent value of $(3.7\pm0.3) \times 10^{-14}$ cm^3 molecule^{-1} s^{-1} at 300K measured by Tyerman.[47] There may be some error attached to our rate coefficient

FIGURE 3.7: Second order plot (the inverse of the CF_2 linecenter absorption coefficient, α_o, versus time) showing the decay of CF_2 via recombination. The data were obtained by photolysis of 800 mTorr of CF_2HCl with a peak CO_2 laser fluence of 17 J cm^{-2}.

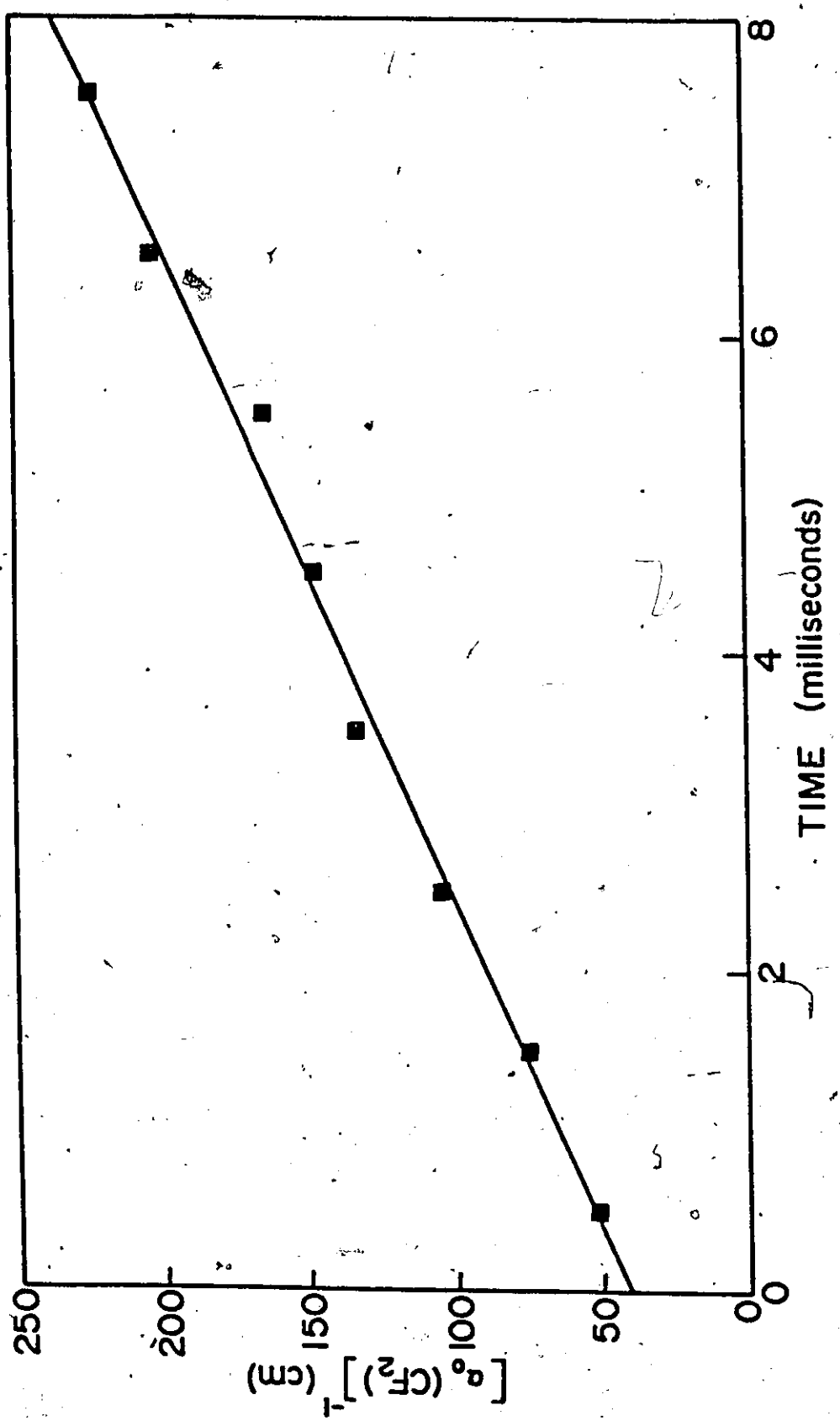
250
200
150
100
50
0
2
4
6
8
TIME (milliseconds)
$[a_o(CF_2)]^{-1}$ (cm)

determination due to inhomogeneous kinetics. That is, the radial profile of the CO_2 laser as it is transmitted through the capillary is Gaussian, and thus the CF_2 partial pressure could be somewhat higher in the center of the capillary than near the walls. However, this effect will be eliminated by diffusion in a few milliseconds. Also, some small amount of the CF_2 apparently reacts with the capillary walls to produce COF_2.[48]

3.5 SUMMARY

In this chapter, the time-resolved detection of CF_2, C_2F_4, and HCl following the IRMPD of CF_2HCl has been accomplished using tunable diode lasers. The growth of the observed CF_2 signal over short timescales (between 50 and 200 μs) shows evidence for vibrational and rotational relaxation. Studies over longer timescales (as long as 20 ms) show that CF_2 decay is second order, with a rate constant for recombination of $(2.3\pm0.7) \times 10^{-14}$ cm^3 $molecule^{-1}$ s^{-1} at 800 mTorr and room temperature, in reasonable agreement with the literature. Finally, determination of the HCl and C_2F_4 produced at a variety of fluences led to the direct quantification of the CF_2 produced and hence, the measurement of a linestrength for

CF_2: $(9\pm2) \times 10^{-21}$ cm molecule^{-1} for the $^rQ_3(9)$ line at 1243.0185 cm^{-1}. This linestrength was then used to calculate the overall bandstrength for ν_1 of CF_2 which was estimated to be $(3.4\pm0.8) \times 10^{-18}$ cm molecule^{-1}.

The majority of the work described here has been accepted for publication in Chemical Physics Letters (authors Orlando, Reid, and Smith). The work of C.E. Brown and P.H. Beckwith in establishing the detection of CF_2 with TDLs, as described in reference 36, is gratefully acknowledged.

CHAPTER 4

IRMPD OF HEXAFLUOROACETONE

4.1 INTRODUCTION

In this chapter, the results obtained in the IRMPD of hexafluoroacetone are discussed. The detection of CF_3 using the transient TDL absorption technique is established; and time-resolved detection of CF_2, GF_4, CO, COF_2, and C_2F_6 following single-pulse photolysis of hexafluoroacetone is achieved. The photolysis mechanism is elucidated, and quantification of the CO and C_2F_6 produced per pulse allows for a calculation of a CF_3 linestrength and CF_3 ν_3 bandstrength. Kinetic studies of CF_3 decay are also made. A rate constant for CF_3 recombination is obtained, and rate constants for the reaction of CF_3 with added NO and O_2 are also determined.

4.2 EXPERIMENTAL

Only the experimental details specific to the results of this chapter will be described here. An FT-IR spectrum of 0.5 Torr of hexafluoroacetone, recorded in a

10 cm long Pyrex cell; is presented in Figure 4.1. Hexafluoroacetone photolysis is done with the 10R(10) CO_2 laser line at 969.15 cm^{-1}. Stable product analysis is accomplished by FT-IR and TDL absorption spectroscopy, as detailed in Chapter 2.

Transient detection of CF_3, CF_2, CF_4, COF_2, C_2F_6, and CO following one-pulse photolysis of hexafluoroacetone was accomplished, using the experimental design presented in Figure 2.4. In this case, 600 mTorr of hexafluoroacetone is flowed through the capillary cell since the flow time through the cell was very slow compared to the CF_3 reaction rate. For this work, CO was detected on P(23) at 2046.277 cm^{-1} and quantified using known linestrength data.[35] C_2F_6 (near 1263 cm^{-1}), CF_4 (near 1269 cm^{-1}), and COF_2 (near 1263 cm^{-1}) absorption features were identified by comparison with standard samples and quantified from standard Beer's Law plots of α_o versus the concentration of the standard samples. (COF_2 calibrations yield only upper limits since COF_2 is unstable, and significant decay to CO occurs over a period of minutes.)

Obviously, the most difficult molecule to detect is the transient species, CF_3. Yamada and Hirota[39] have studied the ν_3 band of CF_3, by producing CF_3 in a 60 Hz discharge of CF_3I. With the aid of Zeeman modulation (to

FIGURE 4.1: FT-IR spectrum of 0.5 Torr of hexafluoroacetone. The spectrum is recorded at a resolution of 2 cm^{-1} over a pathlength of 10 cm.

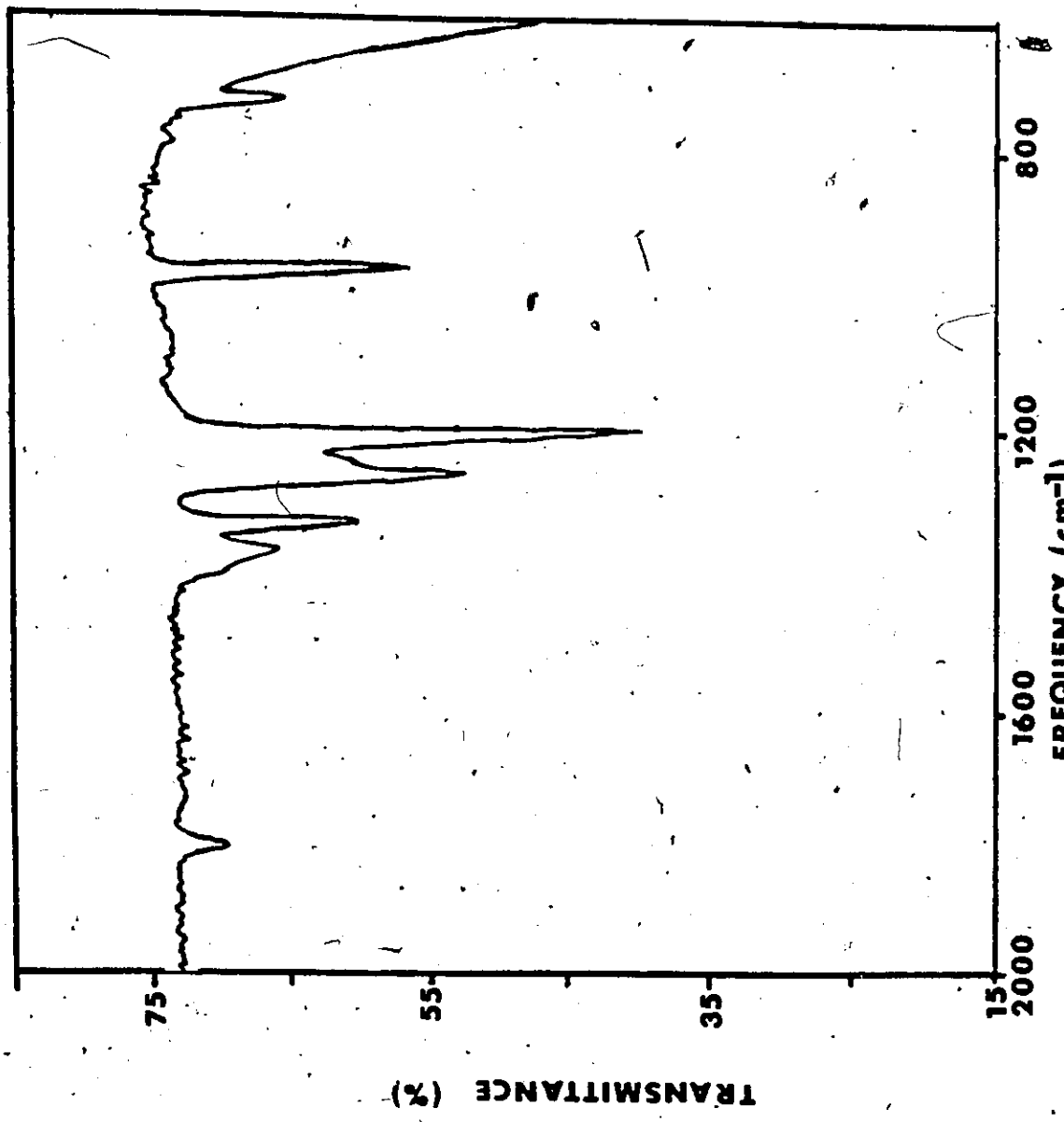
TRANSMITTANCE (%)
75
55
35
15
2000
1600
1200
800
FREQUENCY (cm⁻¹)

differentiate between the paramagnetic CF_3 absorptions and the diamagnetic stable product absorptions), they were able to identify and assign several hundred ν_3 absorption features. Attempts in our lab to produce CF_3 in a 2450 MHz discharge of CF_3I or C_2F_6 led to the detection by TDL of only CF_4 absorptions. Thus, the exact TDL temperature and current settings to find CF_3 lines were not known prior to commencement of the transient experiments. However, IRMPD of CF_3I and CF_3Br (known sources of CF_3) led to the identification of around 75 transient absorptions in the neighborhood of 1263 cm^{-1}. With the use of a monochromator and with the known absorptions of CH_4 and N_2O in this region to aid in frequency calibration, the frequencies of about 50 of these transitions could be matched (to within ± 0.001 cm^{-1}) with the frequencies reported by Yamada and Hirota. The remaining absorptions that we observe occur in a region where their TDL appears to mode hop. Therefore, the assignment of our observed transient absorptions to CF_3 is almost certain.

4.3 PREVIOUS WORK

The IRMPD of hexafluoroacetone was first realized

in the late 1970's,[49] and subsequent studies showed that the process could be made isotopically selective for ^{13}C and ^{18}O.[50-52] However, while other reports[53,54] on IRMPD of hexafluoroacetone have appeared in the literature, the primary photolysis mechanism has not been firmly established.

There appears to be only one report in the literature regarding the thermolysis of hexafluoroacetone.[55] In that work, the authors report two primary photolysis mechanisms:

$$(CF_3)_2CO \rightarrow CF_3COF + CF_2 \quad ....(4.1)$$

$$\rightarrow C_2F_6 + CO \quad ....(4.2)$$

with the first reaction dominating at high temperature (above 850K) and the second dominating at lower temperatures. The low pre-exponential factor ($10^{9.6}$) determined for $k_{(4.2)}$ led to the conclusion that reaction (4.2) proceeded via direct elimination of C_2F_6 rather than via the sequential production of two CF_3 molecules (equation (4.3)), which then combine to form C_2F_6 (equation (4.4)):

$$(CF_3)_2CO \rightarrow CF_3CO + CF_3 \quad \ldots.(4.3a)$$

$$CF_3CO \rightarrow CF_3 + CO \quad \ldots.(4.3b)$$

$$2\ CF_3 \rightarrow C_2F_6 \quad \ldots.(4.4)$$

In contrast, the photolysis of $(CF_3)_2CO$ in both the near UV[56] and the vacuum UV[57] has been shown to occur via the reaction pathways (4.3) and (4.4). To the best of our knowledge, none of the IRMPD studies conducted to date[49-54] has confirmed whether the dissociation occurs via direct production of C_2F_6 or via successive elimination of two CF_3 molecules. Thus, the first step in our study was to determine the IRMPD mechanism.

4.4 RESULTS AND DISCUSSION

4.4.1. PHOTOLYSIS MECHANISM

Irradiations of 1 Torr of hexafluoroacetone were conducted in standard photolysis cells at peak CO_2 laser fluences (at the focus) ranging from 3 J cm^{-2} to 16 J cm^{-2}. FT-IR analysis showed the presence of C_2F_6, CO, and an absorption feature at 1896 cm^{-1} assigned to CF_3COF. TDL absorption spectroscopy confirmed the presence of CO and C_2F_6, and also showed evidence for some C_2F_4. The yield of C_2F_4 relative to C_2F_6 was always less than 10%

over the fluence range studied, and did not seem to indicate any trend with fluence. These observations led to the conclusion that the main dissociation channel involved (as expected) the formation of C_2F_6 via reaction (4.2) and/or (4.3) while a minor channel led to the production of CF_2 and CF_3COF (reaction (4.1)). Addition of H_2 to the photolysis mixture led to the production of small amounts of CHF_3 (detected by FT-IR), suggesting that CF_3 production was occurring.

To distinguish conclusively between reaction (4.2) and (4.3), we set out to detect CF_3 using time resolved TDL absorption spectroscopy. Figure 4.2 shows that CF_3 is indeed formed following the IRMPD of hexafluoroacetone. Detection is done on $^rR_{16}(20)$ at 1264.739 cm^{-1}. Kinetic analysis (see Section 4.4.5) showed the CF_3 decay to be second order, consistent with reaction (4.4). Further, it was shown (see Figure 4.3) that no C_2F_6 is present immediately following the pulse, but that the concentration of C_2F_6 increases with time following the pulse. (The time dependence of C_2F_6 growth is difficult to measure quantitatively because of the interference of CF_3 absorption at early time as seen in Figure 4.3). Thus, it seems certain that the IRMPD of hexafluoroacetone involves the initial production of CF_3 (reaction (4.3)),

FIGURE 4.2: Transient tunable diode laser absorption signal from CF_3 created in the IRMPD of hexafluoroacetone. The detection is done on the $^rR_{16}(20)$ CF_3 absorption line at 1264.739 cm^{-1}.

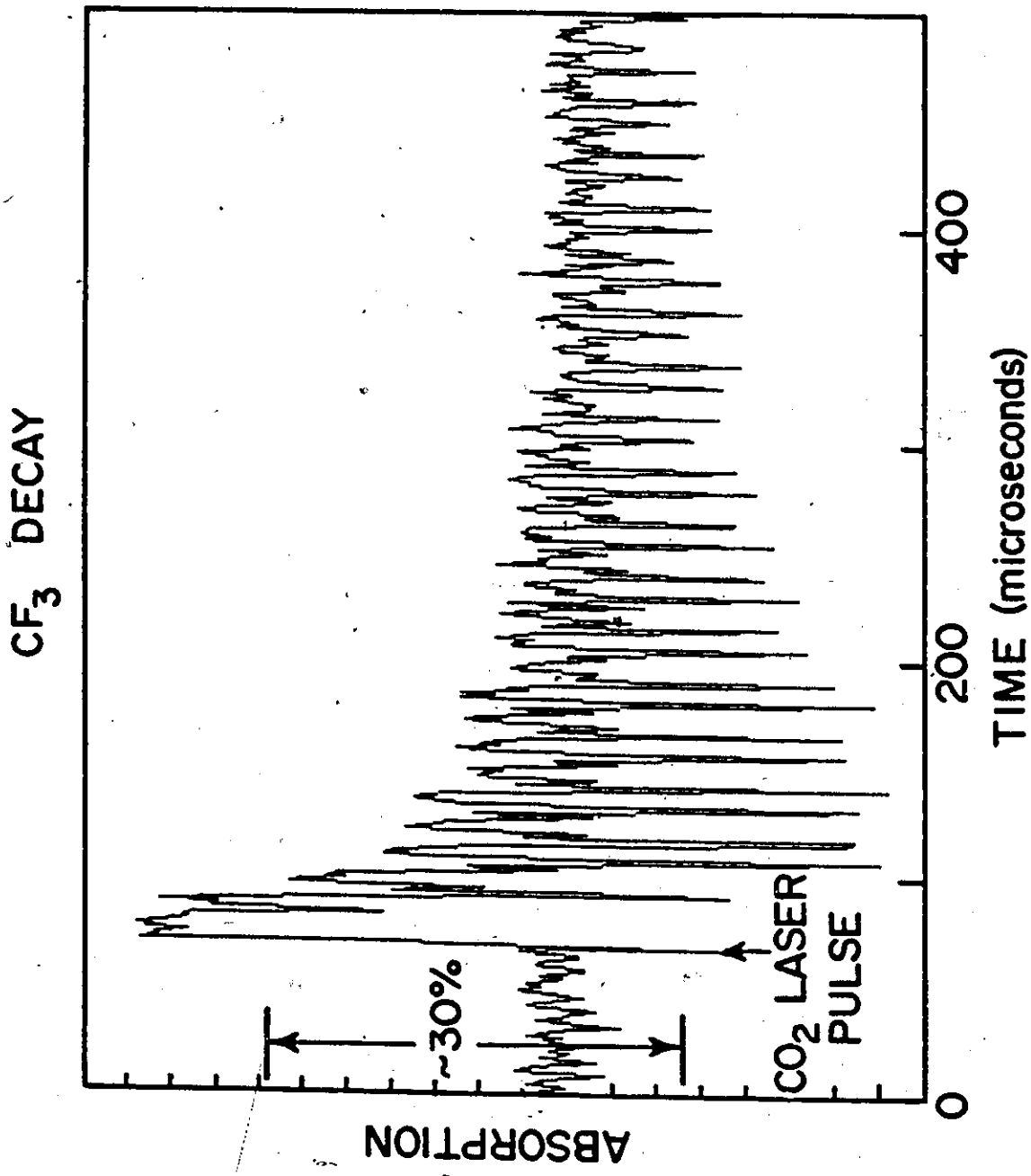
CF_3 DECAY
ABSORPTION
~30%
CO_2 LASER PULSE
0
200
400
TIME (microseconds)

FIGURE 4.3: Transient absorption near 1263 cm^{-1}, showing CF_3 decay immediately following the CO_2 laser pulse, and the growth of C_2F_6 at later times.

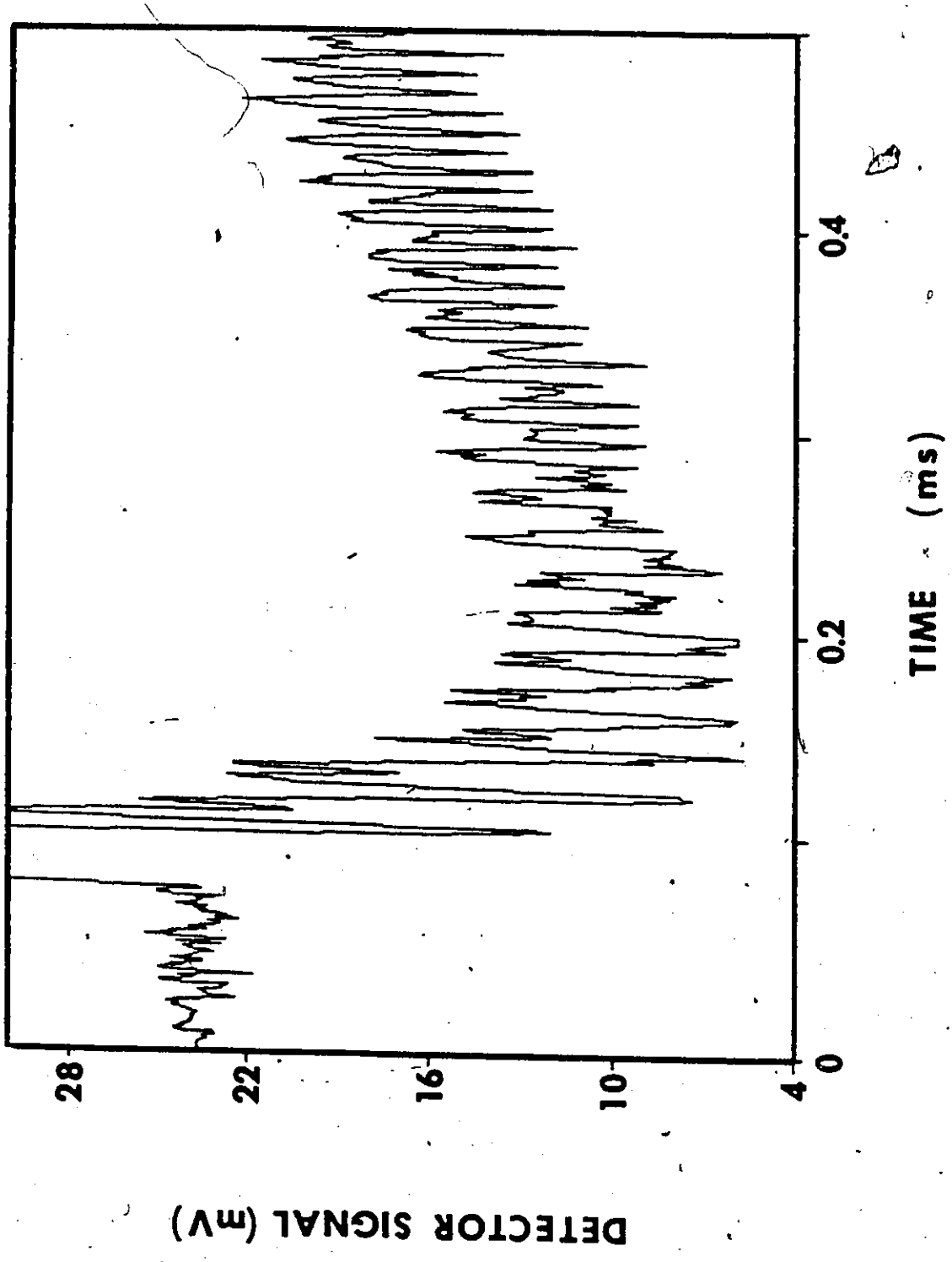
DETECTOR SIGNAL (mV)
28
22
16
10
4
0
0.2
0.4
TIME (ms)

which is followed by combination of CF_3 to form C_2F_6 (reaction (4.4)).

A search was also made for CF_2, CF_4, and COF_2 using the transient TDL technique. No evidence for CF_2 or CF_4 was found, indicating that less than 2 mTorr of each of these species was formed after a CO_2 pulse, even at the highest fluences used. This would indicate that secondary dissociation of CF_3 radicals to CF_2 and disproportionation of two CF_3 radicals to form CF_2 and CF_4 are unimportant mechanisms for CF_3 decay under the conditions employed in this study. Trace amounts of COF_2 (less than 5 mTorr per pulse) were noted, probably the result of CF_3 reactions with the Pyrex walls of the cell.

From the stoichiometry of reactions (4.3) and (4.4), it is apparent that each dissociation of hexafluoroacetone produces one molecule of CO, and two molecules of CF_3 which combine (over a timescale of about 400 μs) to form one molecule of C_2F_6. Thus, from a measurement of the initial CO yield and C_2F_6 yield 400 μs after the one-pulse photolysis of hexafluoroacetone it is possible to quantify the CF_3 and thus obtain its infrared absorption linestrength and bandstrength.

4.4.2 Vibrational Relaxation of CF_3

It is important that the CF_3 be vibrationally and rotationally thermalized following photolysis, since detection is done in the vibrational ground state. The increase in the CF_3 absorption signal over the first 50 μs following the CO_2 laser pulse (see Figure 4.2) is attributed to cascading from vibrational excited states. Since CF_3 has a vibrational energy level coincidence with the parent hexafluoroacetone (near 1280 cm^{-1}), the rate of CF_3 relaxation should be fairly rapid. Addition of N_2O (which also has a vibrational energy level coincidence with CF_3) to the photolysis mixture had no effect on either the risetime of the CF_3 signal or its peak yield. Thus, it is likely that CF_3 vibrational relaxation is near completion after about 50 μs.

4.4.3 Product Yield as a Function of Fluence

To properly quantify the C_2F_6 and CO (and thus the CF_3) obtained in the IRMPD of hexafluoroacetone, a number of independent data sets over a range of conditions was required. Thus, these yields were monitored over a range of fluences. A plot of C_2F_6 yield (after CF_3

recombination is complete) and CO yield (measured 100 μs after the pulse) versus fluence is given in Figure 4.4. As expected, the CO and C_2F_6 yields are equal within experimental error. From the stoichiometry of the dissociation, the initial CF_3 yield is twice the C_2F_6 and CO yield. Thus, the CF_3 absorption at linecenter, α_o, can be related to twice the C_2F_6 or CO yield at each fluence studied (see Figure 4.5).

4.4.4 CF_3 LINESTRENGTH AND BANDSTRENGTH CALCULATIONS

Before quantification can be done, it is important that the gas temperature immediately following photolysis be known since absorption linestrengths are temperature dependent. To measure this temperature, a small amount of N_2O was added to the photolysis mixture and transient absorption measurements on the P(45) N_2O line at 1243.795 cm^{-1} were performed. No noticeable increase in N_2O absorption (within 10%) was noted over a timescale of 20 ms, indicating no detectable temperature rise (less than 10K) following the passage of the CO_2 laser pulse.

The linestrength can then be obtained using equation (1.10):[33]

$$\alpha_o = (\ln 2/\pi)^{1/2} (s/\Delta\nu_D) (P/760) \qquad ....(4.5)$$

FIGURE 4.4: CO(+) and C_2F_6(□) yields from IRMPD of 600 mTorr hexafluoroacetone as a function of the average incident CO_2 laser fluence. The irradiations are done with the 10R(10) CO_2 laser line.

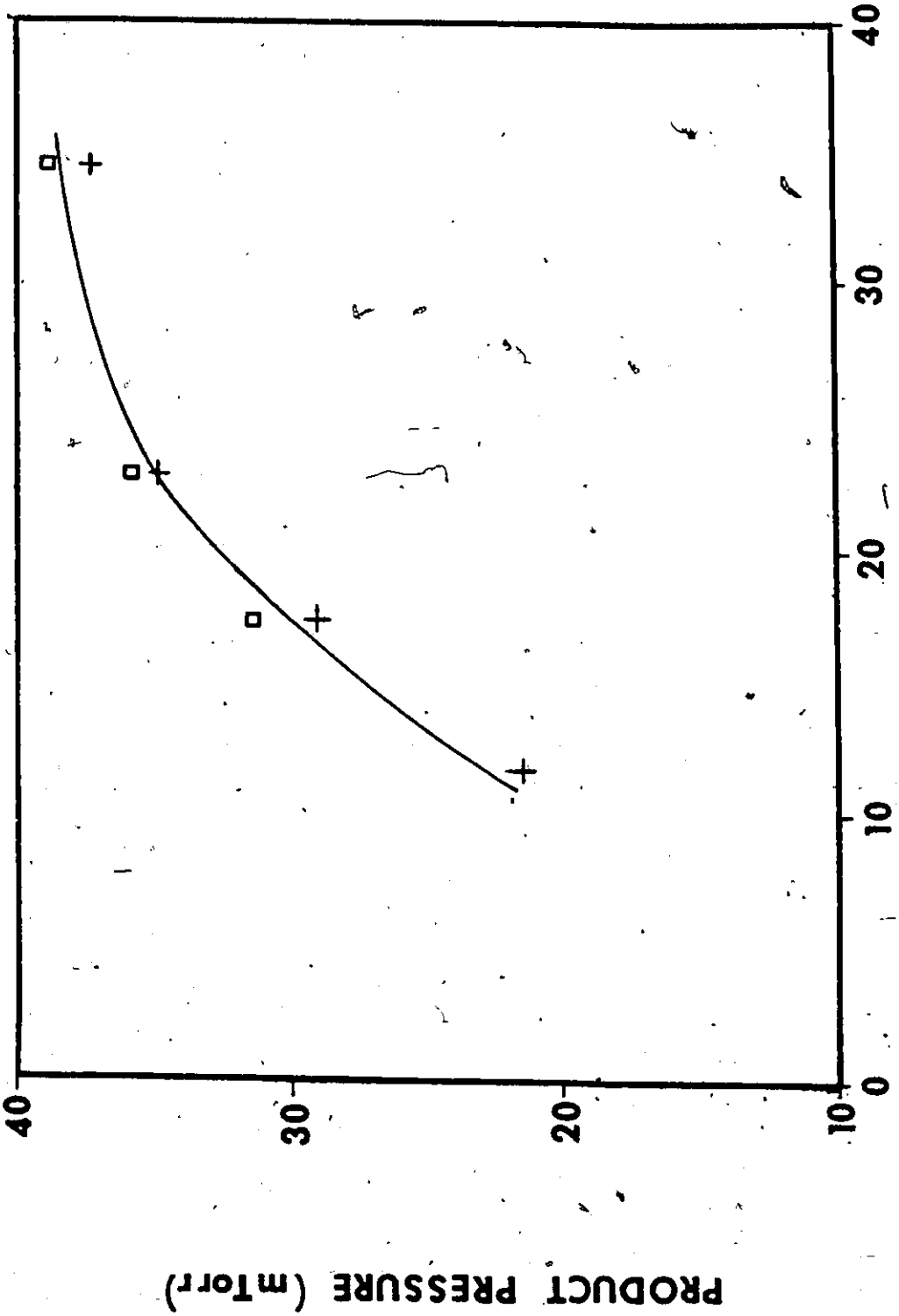
PRODUCT PRESSURE (mTorr)
40
30
20
10
0
10
20
30
40
CO_2 LASER FLUENCE (J cm^{-2})

FIGURE 4.5: Plot of CF_3 absorption per cm at linecenter, α_o, as a function of CF_3 pressure. α_o for CF_3 is measured at a variety of CO_2 laser fluences, and the CF_3 pressure is obtained from the CO and C_2F_6 yields measured at each of these fluences and a knowledge of the dissociation stoichiometry.

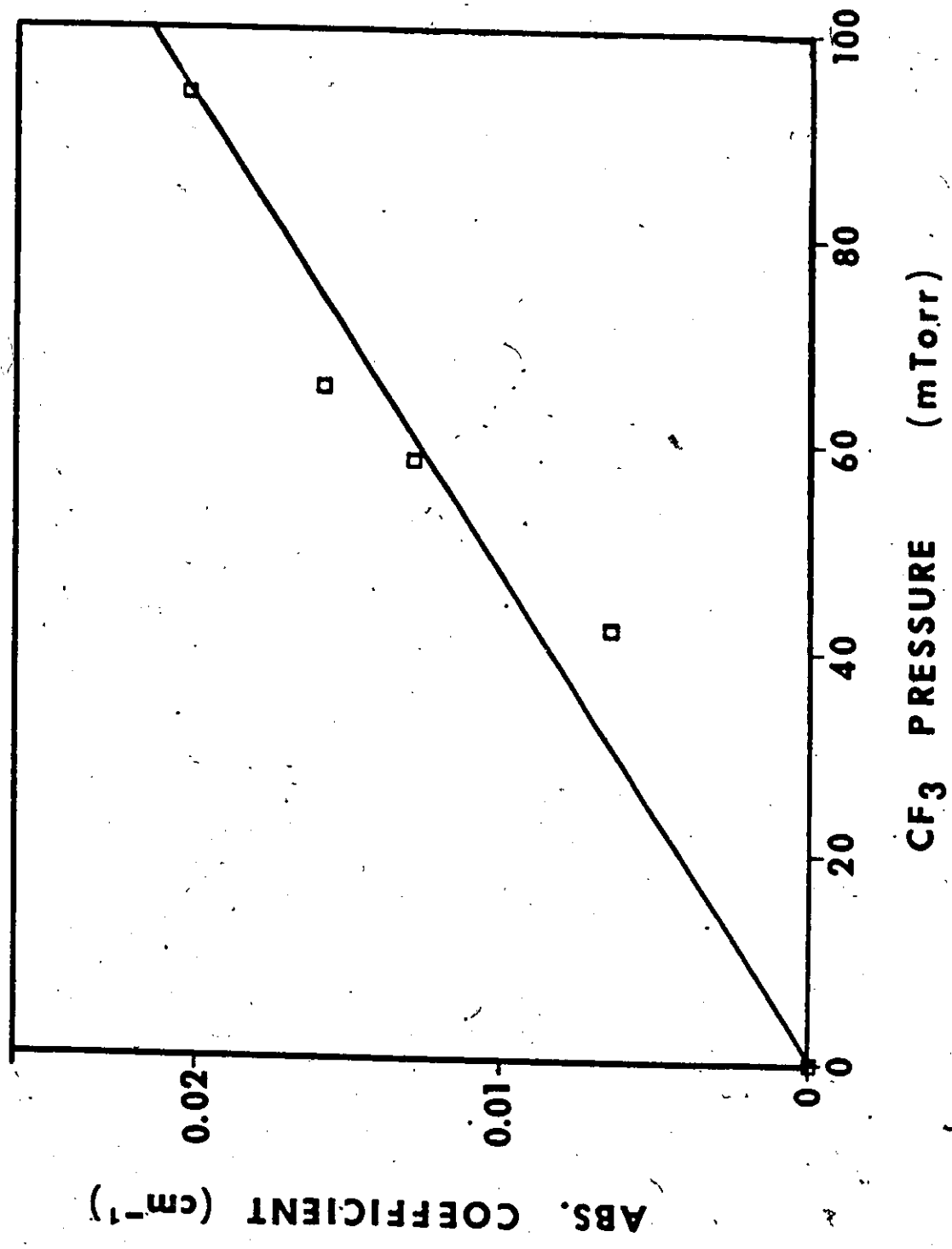
ABS. COEFFICIENT (cm⁻¹)
0.02
0.01
0
0
20
40
60
80
100
CF3 PRESSURE (mTorr)

where s is the linestrength, P is the pressure in Torr, and $\Delta\nu_D$ is the Doppler width. Thus, the slope of the α_o versus P plot (Figure 4.5) is $(\ln 2/\pi)^{.5}(s/\Delta\nu_D)$. $\Delta\nu_D$ for CF_3, from equation (1.8c), is 9.44×10^{-4} cm^{-1} and thus the linestrength for $^rR_{16}(20)$ of CF_3 (1264.739 cm^{-1}) is found to be $(1.4\pm0.3) \times 10^{-20}$ cm $molecule^{-1}$. The error in the linestrength arises from the reproducibility error in the CO and C_2F_6 yields (about $\pm10\%$ for each, $\pm1\sigma$).

As in the case of CF_2, the measurement of this single CF_3 ν_3 linestrength allows the calculation of all other ν_3 linestrengths as well as an estimate of the ν_3 bandstrength. CF_3 can be described in spectroscopic terms as an oblate symmetric top. That is, the spectroscopic constants A and B are equal and are greater than C, while $\kappa = 1$. In order to calculate another linestrength from the one measured here, only the transition frequency, ν, the Honl-London factor, the degeneracy and the Boltzmann factor for the new line need be calculated, since all other terms are independent of the particular ν_3 transition under consideration.

The bandstrength, A, can then be calculated from the degeneracy, Boltzmann factor, and measured linestrength for $^rR_{16}(20)$ and Q_r for CF_3, using equation (1.15):

$$A = [s(Q_r)]/[R_r^2(g_{NK})\exp(-E(N,K)/kT)] \quad \ldots.(4.6)$$

The CF_3 ν_3 bandstrength is determined in this manner to be (8 ± 2) X 10^{-18} cm molecule^{-1}. This ν_3 bandstrength is about a factor of two or three larger than our previously measured value for CF_2 ν_1, and is about a factor of 25 smaller than that of CF_4 ν_3, one of the strongest infrared absorption bands recorded.

4.4.5 CF_3 KINETIC STUDIES

Calculation of the CF_3 linestrength and bandstrength as detailed above allows for a determination of its absolute concentration at any time following the CO_2 laser pulse. In Figure 4.2, a peak CF_3 absorption of about 35% is obtained. This absorption corresponds to a concentration of about 3 X 10^{15} molecules cm^{-3}. While no attempt was made to achieve maximum sensitivity in the present work, fractional absorptions of 3 X 10^{-5} have been obtained in related experiments.[36] This sensitivity corresponds to a minimum detectable CF_3 concentration of 3 X 10^{11} molecules cm^{-3}.

Knowledge of the CF_3 concentration as a function of time allows a study of its kinetics. In the case of pure hexafluoroacetone photolysis, the only decay of CF_3

should be via recombination (equation (4.4)). Thus,

$$d/dt\ (CF_3) = -2\ k_{(4.4)}\ (CF_3)^2 \qquad ....(4.7)$$

and CF_3 decay should be second order (see Appendix A). For second order kinetics, the initial half-life should vary as the inverse of the initial CF_3 yield:

$$t_{1/2} = 1/(k_{(4.4)}\ X\ (CF_3)_o) \qquad ....(4.8)$$

where $(CF_3)_o$ is the initial CF_3 concentration and $t_{1/2}$ is the time at which $(CF_3)=1/2\ (CF_3)_o$. To test that equation (4.8) is indeed valid, the initial CF_3 yield was varied by a factor of five (from 50 mTorr to 250 mTorr) by varying both the CO_2 laser fluence and the initial hexafluoroacetone pressure. In fifteen separate trials (see Table 4.1), the product of $t_{1/2}$ and $(CF_3)_o$ was constant to within $\pm$ 10%. This observation, coupled with the fact that all CF_3 appears to be converted to C_2F_6 (the CO and C_2F_6 yields are equal), leads us to conclude that we are indeed measuring a recombination rate and not a CF_3 reaction with the cell walls, even though wall collisions must be occurring.

CF_3 recombination has most recently been studied

TABLE 4.1: Initial half-life of CF_3 decay at various initial CF_3 concentrations, $(CF_3)_o$, formed by the IRMPD of hexafluoroacetone. The rate constant, k, for CF_3 recombination is reported for each trial in units of cm^3 $molecule^{-1}$ s^{-1}. The half-lives are estimated to within ± 5 μs, while $(CF_3)_o$ is estimated to within $\pm$ 10%. Each entry in the table is the average of three separate trials, recorded under identical conditions.

TABLE 4.1

HFA Pressure	$kX10^{12}$	$(CF_3)_o$ (mTorr)	1^{st} Half Life (μs)	$(t_{1/2})X(CF_3)_o$ (mTorr.μs)
600	2.2	52	130	6760
400	2.3	57	120	6840
600	2.0	71	110	7810
800	2.1	82	85	6970
600	2.2	229	30	6870

by Selamoglu et al.[58], who obtained a value of (3.0±0.4) X 10^{-12} cm^3 $molecule^{-1}$ s^{-1} for the rate constant of reaction (4.4) near room temperature at a pressure of about 10 mTorr. Detailed RRKM calculations for reaction (4.4) were also performed in reference 58. In these calculations, a hindered Gorin model for the transition state was employed. That is, the vibrations corresponding to the bending of a CF_3 group relative to the C-C bond are replaced by two hindered CF_3 rotations in the transition state, each with axes normal to the C-C bond axis. The degree of hindrance is given by a parameter, η, which reduces the effective moment of inertia by an amount (100-η)/100. This model, with η=92%, was found to give a good fit to experimental results for $k_{(4.4)}$ at a variety of pressures and temperatures. From these calculations, the authors conclude that their value for $k_{(4.4)}$ (measured at 10 mTorr) represents approximately 75% of the high pressure limited value, while extrapolation of their calculations to the pressures employed in our study indicate that our results should be at or very near the high pressure limit. Indeed, we see no variation in our measured rate constant, $k_{(4.4)}$, upon variation of the hexafluoroacetone pressure from 380 mTorr to 800 mTorr, or upon addition of 1 Torr Ar to the photolysis sample. The average rate constant obtained in this work is (2.2±0.5) X

10^{-12} cm^3 $molecule^{-1}$ s^{-1}, in good agreement with reference 58. (The error is largely due to the error in the CF_3 linestrength). An example of a second order decay plot (the inverse of α_o versus time) is presented in Figure 4.6.

In addition, the decay of CF_3 has been monitored in the presence of added NO and O_2. For these cases, CF_3 decay can also occur via:

$$CF_3 + 2\ X \rightarrow CF_3X + X \quad \ldots.(4.9)$$

$$CF_3 + X + M \rightarrow CF_3X + M \quad \ldots.(4.10)$$

where X = O_2 or NO.

Since the recombination rate cannot be neglected relative to reaction with the added gas, the analysis of Laguna and Baughcum was used:[59]

$$\ln 2/t_{1/2} = k_{(4.9)}(X)^2 + k_{(4.10)}(X)(M) + (k_{(4.4)}/\ln 2)(CF_3)_o \quad \ldots.(4.11)$$

where $(CF_3)_o$ is the initial CF_3 concentration and $t_{1/2}$ is the time at which $(CF_3) = 1/2\ (CF_3)_o$. Figure 4.7 shows a plot of $1/t_{1/2}$ versus (O_2) or (NO). (The hexafluoroacetone pressure is constant at 600 mTorr). In

FIGURE 4.6: Second order decay plot (the inverse of the absorption coefficient per cm versus time) for the recombination of CF_3. CF_3 is created from the IRMPD of 600 mTorr of hexafluoroacetone. The 10R(14) laser line, with a fluence of 34 J cm^{-2}, is employed.

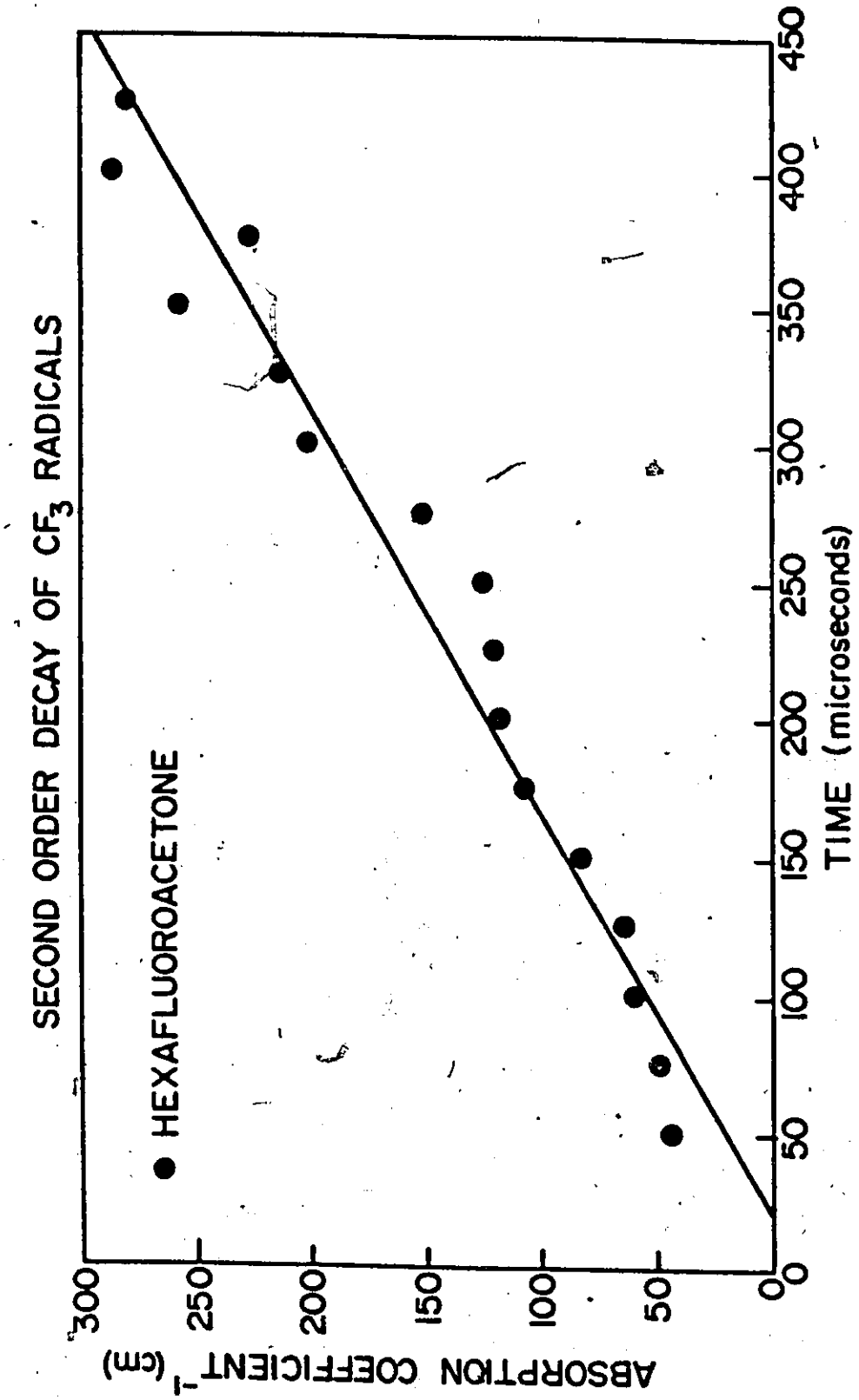
SECOND ORDER DECAY OF CF_3 RADICALS
HEXAFLUOROACETONE
ABSORPTION COEFFICIENT^{-1} (cm)
TIME (microseconds)
0
50
100
150
200
250
300
350
400
450

FIGURE 4.7: Plot of the inverse CF_3 half-life (ms^{-1}) versus the concentration of added O_2 or NO (Torr). CF_3 is created by the IRMPD of 600 mTorr of hexafluoroacetone at a CO_2 laser fluence of 34 J cm^{-2} (on 10R(10)).

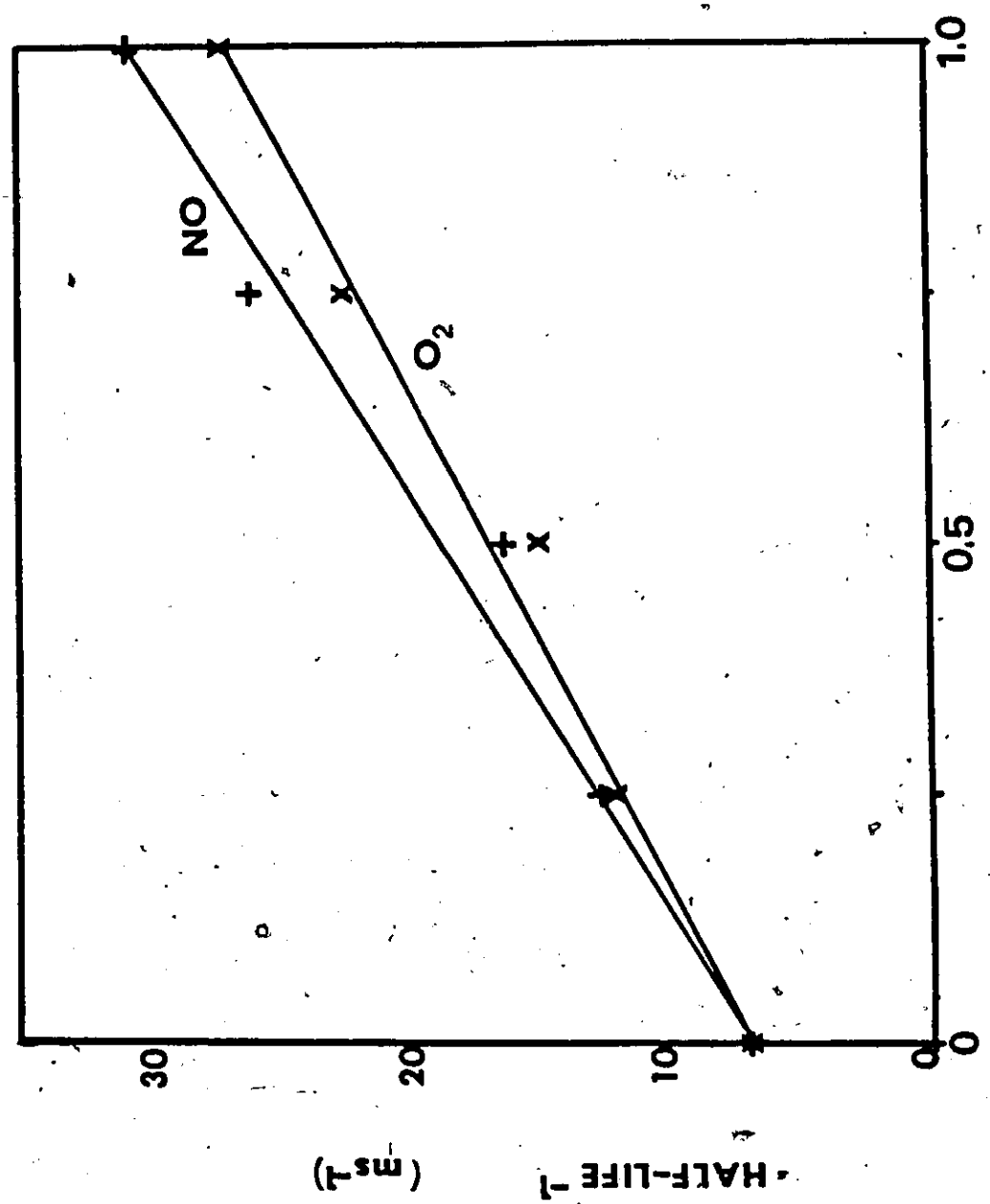
NO
O_2
0
10
20
30
0.5
1.0
GAS PRESSURE (Torr)
HALF-LIFE $^{-1}$ (ms^{-1})

both cases, this plot gives a good straight line, whereas a plot versus $(O_2)^2$ or $(NO)^2$ is curved. This is interpreted as meaning that hexafluoroacetone is a much better third body than O_2 or NO, and reaction (4.10) dominates over reaction (4.9). The slopes of these plots yield the rate constants for reaction (4.10), $(2.1\pm0.5) \times 10^{-29}$ and $(2.8\pm0.7) \times 10^{-29}$ cm^6 $molecule^{-2}$ s^{-1} for X = O_2 and NO, respectively, where the quoted errors in the slopes are $\pm1\sigma$. The rate constant for CF_3 with O_2 (M=N_2) has recently been reported as $(1.9\pm0.2) \times 10^{-29}$ cm^6 $molecule^{-2}$ s^{-1},[60] in excellent agreement with our value. To the best of our knowledge, the only published rate constant for the reaction of CF_3 and NO is a high pressure limited value of 1.6×10^{-11} cm^3 $molecule^{-1}$ s^{-1}, measured at total pressures greater than 20 Torr.[61]

4.5 SUMMARY

In this chapter, the IRMPD of hexafluoroacetone has been investigated, using a time-resolved TDL absorption technique to identify and measure absolute yields of transient and stable products of the photolysis. It was found that the major dissociation pathway led to the production of CO and two CF_3 radicals, which then combine to form C_2F_6. The lack of measureable yields of

CF_2) or CF_4 eliminates the possibility of secondary dissociation or disproportionation of CF_3 as significant processes for its removal under the conditions employed here. Evidence for a second channel of dissociation, forming CF_3COF and CF_2, was found in many-pulse photolyses. The quantification of the C_2F_6 and CO formed in a single pulse allowed for the quantification of the CF_3 and thus a measure of a CF_3 linestrength, $(1.4\pm0.3) \times 10^{-20}$ cm molecule^{-1} for $^rR_{16}(20)$, and the CF_3 ν_3 bandstrength, $(8\pm2) \times 10^{-18}$ cm molecule^{-1}. In addition, the kinetics of CF_3 decay have been studied. The room temperature rate constant for recombination of CF_3 to form C_2F_6 was measured to be $(2.2\pm0.5) \times 10^{-12}$ cm^3 molecule^{-1} s^{-1} at or near the high pressure limit, while the room temperature rate constants for CF_3 reacting with O_2 and NO were found to be $(2.1\pm0.5) \times 10^{-29}$ and $(2.8\pm0.7) \times 10^{-29}$ cm^6 molecule^{-2} s^{-1}, respectively.

The time-resolved TDL detection of CF_3 and the determination of the CF_3 recombination rate constant are described in a paper accepted for publication in Chemical Physics Letters (authors Brown, Orlando, Reid, and Smith). The remainder of the work has been submitted for publication to the Journal of Physical Chemistry (authors Orlando and Smith). In particular, acknowledgement is due

to C.E. Brown for the attempts to identify CF_3 in the microwave discharge, and for collaboration in the establishment of the CF_3 TDL detection and the measurement of the CF_3 recombination rate constant.

CHAPTER 5

IRMPD OF $CDCl_3/CHCl_3$: HYDROGEN ISOTOPE SEPARATION

5.1 INTRODUCTION

In this chapter, the use of TDL absorption spectroscopy in studies of isotope separation by IRMPD is examined. Quantitative analysis of HCl and DCl following IRMPD of chloroform ($CDCl_3$ and $CHCl_3$) is performed, and DCl detection following IRMPD of natural abundance $CDCl_3$ in $CHCl_3$ is achieved. However, it is shown that quantitative measurements of HCl and DCl on a timescale of minutes following IRMPD are complicated by the presence of isotope exchange reactions and wall adsorption and desorption effects. To overcome these complications, short timescale HCl/DCl detection (~ 25 μs) using TDL absorption spectroscopy is developed. This technique, in conjunction with stable product FT-IR analyses, provides information on the isotopic selectivity of $CDCl_3/CHCl_3$ IRMPD and on the post-photolysis mechanism.

5.2 EXPERIMENTAL

Only the details specific to $CDCl_3/CHCl_3$ IRMPD experiments will be presented here, with the general techniques described in Chapter 2.

An FT-IR spectrum of a mixture of 2.5 Torr $CDCl_3$ and 2.5 Torr $CHCl_3$ (recorded in a 10 cm long Pyrex cell) is shown in Figure 5.1. The spectrum was recorded with a 4 cm^{-1} resolution. Selective absorption by $CDCl_3$ can be achieved near 900 cm^{-1}, where $CHCl_3$ does not absorb. CO_2 laser irradiation is done using the 10P(48) CO_2 laser line in the case of stable product analyses, and 10P(38) in the case of transient DCl/HCl detection unless otherwise stated. (10P(38) was used for the transient DCl/HCl measurements rather than the more efficient 10P(48) because the high repetition rate TEA 801-A laser did not provide sufficient energy on 10P(48)).

For TDL spectroscopy, DCl was detected on R(7) at 2168.962 cm^{-1}, R(8) at 2177.605 cm^{-1} or P(2) at 2068.272 cm^{-1}, while HCl was detected on P(11) at 2625.726 cm^{-1} or on P(9) at 2677.732 cm^{-1}. Linestrength data for DCl were obtained from Benedict *et al.*[62], while HCl linestrength data were obtained from Pine *et al.*[46] FT-IR detection of CCl_4 was done at 793 cm^{-1}. Quantitative analysis was

FIGURE 5.1: An FT-IR spectrum of a mixture of 2.5 Torr $CDCl_3$ and 2.5 Torr $CHCl_3$, recorded in a 10 cm long Pyrex with a resolution of 4 cm^{-1}.

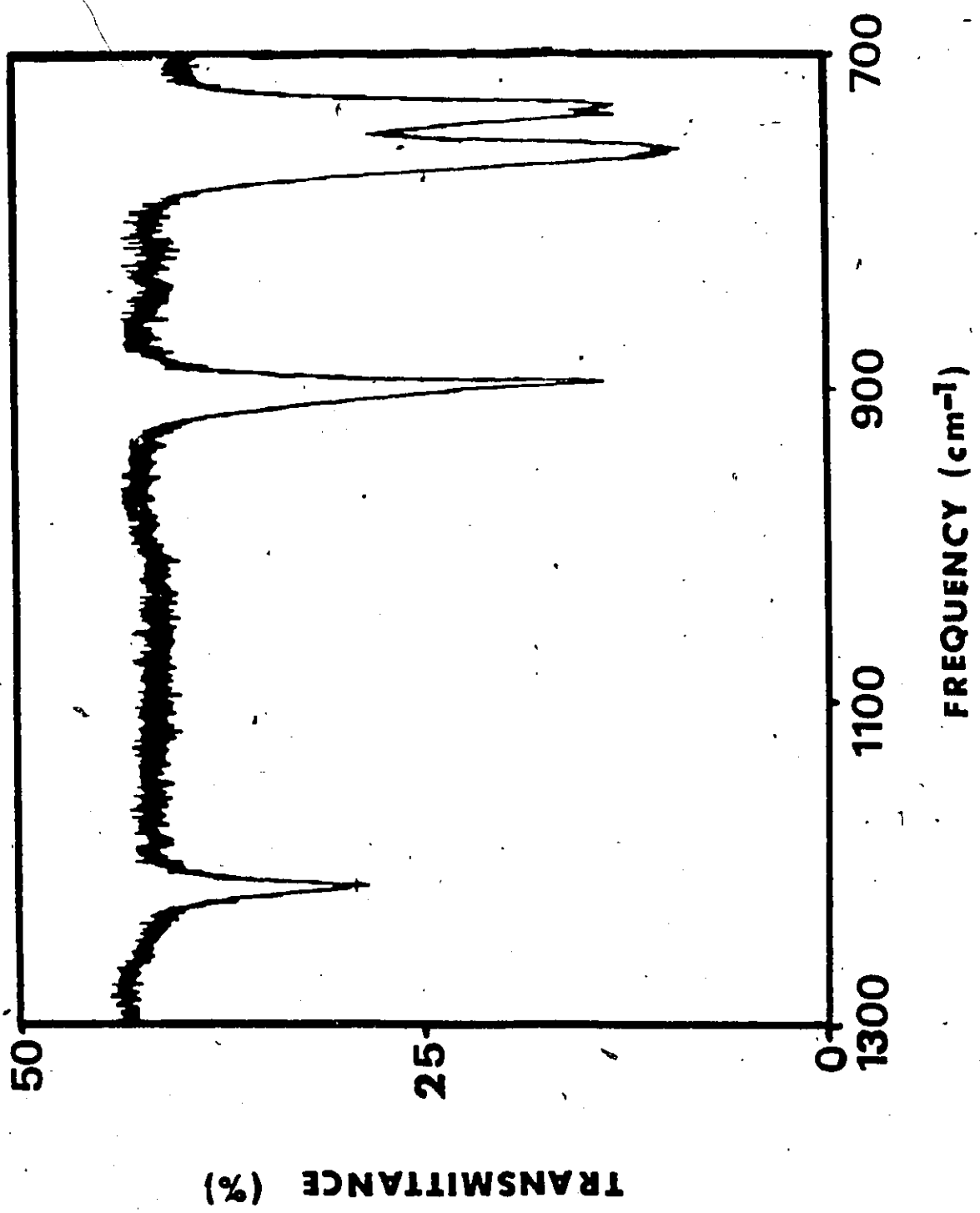
50
25
0
TRANSMITTANCE (%)
700
900
1100
1300
FREQUENCY (cm⁻¹)

based on a standard Beer's Law calibration plot of α_o versus CCl_4 pressure. Similarly, $CDCl_3$ was detected at 744 cm^{-1}.

5.3 PREVIOUS WORK

The use of IRMPD for isotope separation is based on the fact that the absorption of the first few photons in the IRMPD process involves resonant transitions, as described in Chapter 1. Thus, in a gas mixture containing two different isotopic species of a molecule, one species can be made to selectively absorb CO_2 laser photons in the presence of the other by tuning the CO_2 laser to an absorption feature of the desired species. In the case of hydrogen isotope separation, the isotope shift (the difference between the positions of the absorption features of the two isotopic species) is very large - hundreds of cm^{-1} - and selective irradiation of one species is easy. In the case of heavier isotopes (eg., ^{12}C and ^{13}C), the isotope shift is considerably smaller (a few cm^{-1}) but selective IRMPD can still be achieved.

Halocarbons have attracted a great deal of attention since their strong absorption coefficients in the wavelength region of the CO_2 laser and high density of

vibrational states make them relatively easy to decompose. In particular, the haloforms have been recognized as being attractive for hydrogen isotope separation schemes.

CDF_3[10,19,63-68] was recognized as a possible deuterium from hydrogen separation candidate because the linear absorption coefficient of CDF_3 is more than 2000 times that of CHF_3 in the CO_2 laser wavelength region (10.2 to 10.3 μm).[19] The major carbon-bearing product in the IRMPD of CDF_3 is C_2F_4, and the dissociation mechanism was determined to be as follows:

$$CDF_3 \rightarrow CF_2 + DF \quad ....(5.1)$$

$$2\ CF_2 \rightarrow C_2F_4 \quad ....(5.2)$$

with other unidentified products present in less than 5% abundance.

The isotopic enrichment of these processes can be expressed in terms of two parameters: β, the isotopic selectivity, and γ, the product isotope ratio. In the case of CDF_3/CHF_3, these parameters are defined as follows:

$$\beta = \{(DF)/(HF)\} / \{(CDF_3)_o/(CHF_3)_o\} \quad ....(5.3)$$

$$\gamma = (DF)/(HF) \quad ....(5.4)$$

where $(CDF_3)_o$ and $(CHF_3)_o$ are the initial concentrations of these species, and (DF) and (HF) are the amount of these species produced in the photolysis.

Four separate laboratories have undertaken studies of the CDF_3/CHF_3 system. Herman and Marling[10] measured the amount of ^{13}C in the C_2F_4 that was produced by the irradiation of a mixture of $^{12}CDF_3$ and $^{13}CHF_3$ in order to determine isotopic selectivity. They studied the effects of laser wavelength, fluence, CDF_3/CHF_3 pressure ratio, and total pressure and found peak β values of over 20000. It was also found[19] that the addition of an inert buffer gas (argon) led to a large increase in the dissociation yield. This effect is attributed to rotational relaxation of ground state molecules into resonance with the laser (rotational hole-filling, see Chapter 1). Two-frequency IRMPD studies have also been conducted.[63] It was found that the IRMPD spectrum was broadened relative to the single frequency spectrum.

Tuccio and Hartford[64] detected vibrationally excited DF and HF by time-resolved IR fluorescence techniques and measured a dissociation selectivity of 19000. They estimate a β value of 5000 in natural fluoroform.

Evans and McAlpine[65,66] measured isotopic

selectivity by collecting the water formed by reaction of the $^{1,2}HF$ with the cell walls, heating the water over U metal to form various isotopic forms of H_2, and analyzing this H_2 gas by mass spectrometry. These authors were able to collect water enriched up to 30% in deuterium from natural fluoroform, a β value of over 2000. Their observation that the dissociation yield decreases with increasing fluence, then increases above 3 J/cm^2 is thought to be due to a bottlenecking effect which is overcome at high fluence. Their studies on the effect of collisions (by varying the total pressure and pulse length) are also consistent with the rotational hole-filling model of Herman and Marling.

Selective decomposition of CHF_3 at natural abundance has also been achieved, with the CHF_3 concentration decrease monitored by IR spectrometry.[67]

CTF_3 IRMPD has also been studied for tritium separation.[69,70] By varying pulse energy, laser wavelength, pulse length, total pressure, and temperature, selectivities as high as 10^4 have been achieved for removal of trace amounts of tritium.[69]

Hydrogen isotope separation studies involving chloroform have been less abundant. T/D isotopic enrichment factors of 165 were obtained by selective IRMPD of $CTCl_3$ at 835 cm^{-1} using a CO_2 laser-pumped NH_3 laser.[71]

Later studies[72,73] led to the achievement of T/D enrichment factors of greater than 15000. While D/H separation using chloroform has been proposed[74], no selectivity measurements have been made to date largely due to the interference of product FT-IR peaks with the starting material.

In addition to selectivity measurements, the photolysis and post-photolysis dissociation mechanism of chloroform has been studied, although some information in this area is still lacking. Herman et al.[75], in a molecular beam - time of flight mass spectrometric study, showed conclusively that the first dissociation step in the IRMPD of $CDCl_3$ (>99.1%) involves the production of DCl:

$$CDCl_3 \rightarrow CCl_2 + DCl \qquad \ldots.(5.5)$$

Further mechanistic work[72,74] can be summarized as follows:

$$2\ CCl_2 \rightarrow C_2Cl_4^* \qquad \ldots.(5.6a)$$

$$C_2Cl_4^* \xrightarrow{M} C_2Cl_4 \qquad \ldots.(5.6b)$$

$$C_2Cl_4^* \rightarrow C_2Cl_3 + Cl \qquad \ldots.(5.6c)$$

$$C_2Cl_4^* \rightarrow C_2Cl_2 + Cl_2 \quad \text{....(5.7a)}$$

$$\rightarrow C_2Cl_2 + 2\,Cl \quad \text{....(5.7b)}$$

$$CCl_2 + CDCl_3 \rightarrow C_2Cl_4 + DCl \quad \text{....(5.8)}$$

$$DCl + (H_2O) \rightarrow HCl + (HDO) \quad \text{....(5.9)}$$

where (H_2O) and (HDO) represent water adsorbed on the cell walls, and $C_2Cl_4^*$ represents vibrationally excited C_2Cl_4.

A large series of reactions involving Cl atoms was proposed in reference 72, leading to the formation of C_2Cl_6, CCl_4, and C_4Cl_6, although the occurrence and relative importance of these reactions was not confirmed:

$$Cl + CDCl_3 \rightarrow CCl_3 + DCl \quad \text{....(5.10)}$$

$$2\,CCl_3 \rightarrow C_2Cl_6 \quad \text{....(5.11a)}$$

$$\rightarrow C_2Cl_4 + Cl_2 \quad \text{....(5.11b)}$$

$$\rightarrow CCl_4 + CCl_2 \quad \text{....(5.11c)}$$

$$\rightarrow C_2Cl_5 + Cl \quad \text{....(5.11d)}$$

$$CCl_2 + CCl_3 \rightarrow C_2Cl_4 + Cl \quad \text{....(5.12)}$$

$$2\,C_2Cl_3 \rightarrow C_4Cl_6 \quad \text{....(5.13a)}$$

$$\rightarrow C_2Cl_2 + C_2Cl_4 \quad \text{....(5.13b)}$$

$$Cl + CCl_3 \rightarrow CCl_4 \quad \ldots.(5.14)$$

$$2\ Cl \rightarrow Cl_2 \quad \ldots.(5.15)$$

The efforts presented in this chapter, then, represent an attempt to apply the techniques of TDL absorption spectroscopy (in conjunction with FT-IR analysis of stable products) to the study of isotope separation. The sensitivity of TDL absorption spectroscopy for hydrogen halide molecules will be demonstrated. Measurements on the isotopic selectivity of $CDCl_3/CHCl_3$ IRMPD will be made and studies on the post-photolysis mechanism (especially with regard to the existence and extent of possible isotopically non-selective radical reactions) will be described.

5.4 RESULTS AND DISCUSSION

5.4.1 EFFECT OF ADDITIVES ON PRODUCT YIELD IN $CDCl_3$ IRMPD

A series of experiments was undertaken to measure the yield of carbon-bearing products in the IRMPD of $CDCl_3$. Particular attention is paid to the CCl_4 yield in the presence of additives and some conclusions regarding the mechanism of its formation are drawn.

Irradiation of 1 Torr $CDCl_3$ (buffered with 1 Torr Ar) yields C_2Cl_4, C_2Cl_2, and CCl_4. The yield of C_2Cl_4 is not measureable by FT-IR spectroscopy as its major peak (near 912 cm^{-1}) overlaps with a $CDCl_3$ absorption, and its other (weaker) absorption (near 780 cm^{-1}) appears as a shoulder on the $CDCl_3$ absorption in this region. Quantification of C_2Cl_2 (which absorbs at 988 cm^{-1}) is also not possible as standard samples of this explosive gas are not available for purposes of calibration. CCl_4 yields were measured from the strength of its absorption at 793 cm^{-1}. In addition, $CDCl_3$ dissociation yields were monitored at 744 cm^{-1}. Line A of Figure 5.2 shows the CCl_4 yield in the IRMPD of a mixture of 1 Torr $CDCl_3$ and 1 Torr Ar (at a peak focal fluence of 10 J cm^{-2}) to represent about 10-15% of the total carbon-bearing product. The remainder of the product is believed to be mostly C_2Cl_4 (formed by reactions (5.6) and (5.8)) and C_2Cl_2 (formed predominantly by reaction (5.7)). No evidence for C_2Cl_6 was noted.

The irradiation of 1 Torr $CDCl_3$ in the presence of 1 Torr H_2, 1 Torr C_2F_4, or 1 Torr NO greatly reduces the CCl_4 yield (indeed, no CCl_4 was detectable, line B of Figure 5.2), while having no measurable effect on the overall $CDCl_3$ dissociation yield. The most likely

FIGURE 5.2: Plot of the product yield of CCl_4 and dissociation yield of $CDCl_3$ following the photolysis of 1 Torr $CDCl_3$ in the presence of various additives. The irradiation is done on 10P(48), with a peak focal fluence of 10 J cm^{-2}. Errors are $\pm 1\sigma$.

Line A: CCl_4 yield following irradiation of 1 Torr $CDCl_3$ with 1 Torr Ar.

Line B: Upper limit of CCl_4 yield following irradiation of 1 Torr $CDCl_3$ with 1 Torr C_2F_4.

Line C: CCl_4 yield following irradiation of 1 Torr $CDCl_3$ with 1 Torr Cl_2.

Line D: CCl_4 yield following irradiation of 1 Torr $CDCl_3$ with 5 Torr Cl_2.

Line E: Average dissociation yield of $CDCl_3$ in the above experiments A through D. The difference in the dissociation yield in the four cases was not significant.

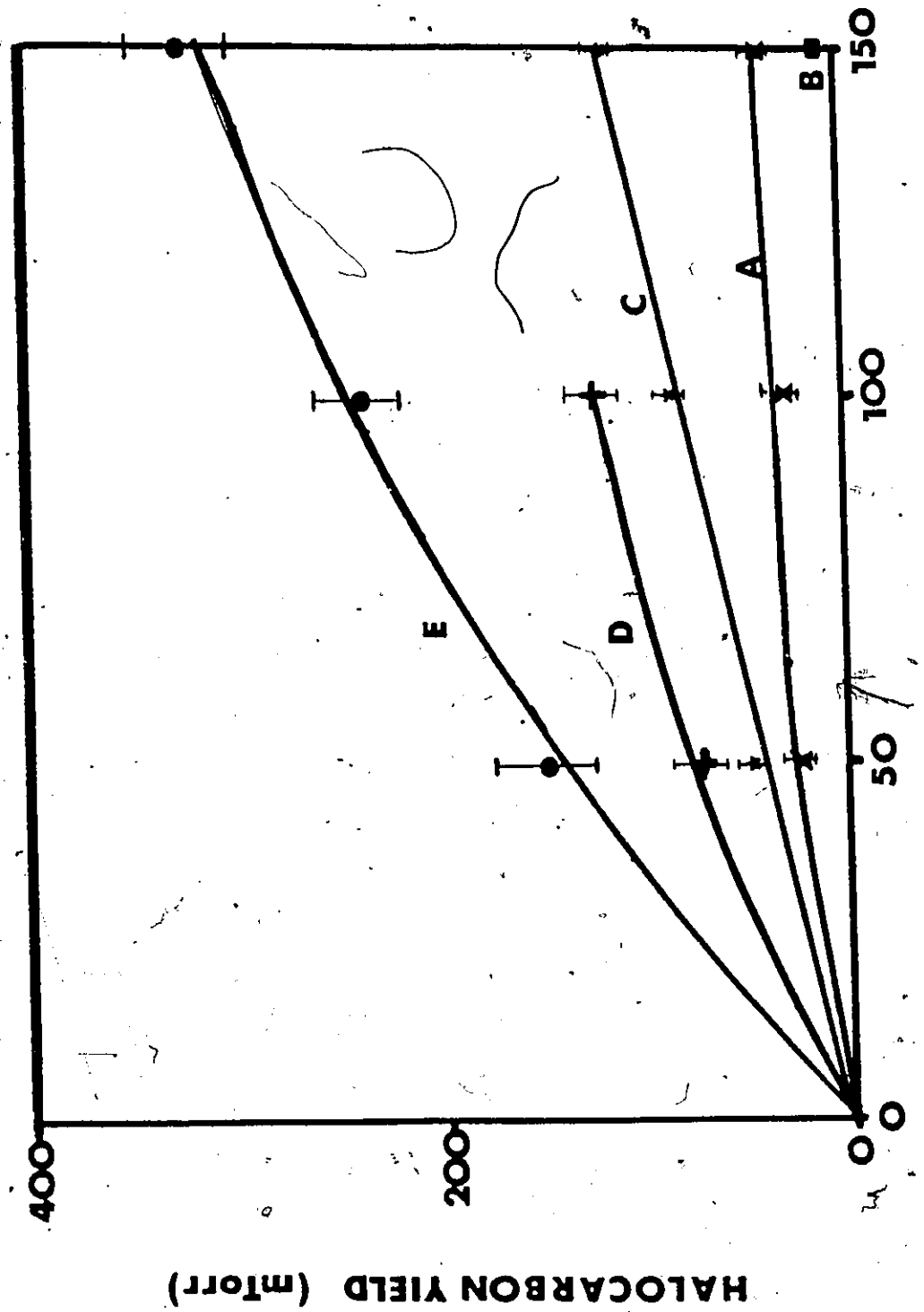
HALOCARBON YIELD (mTorr)
400
200
0
0
50
100
150
NO. OF PULSES
A
B
C
D
E

explanation for this observation is that the additives (H_2, C_2F_4, or NO) act as scavengers for chlorine atoms. Thus, reaction (5.10) does not occur, as Cl preferentially reacts with the additive rather than with $CDCl_3$. With CCl_3 no longer present and Cl atoms removed by the scavenger, reaction (5.11c) and especially reaction (5.14) no longer occur and CCl_4 is not formed.

The irradiation of 1 Torr $CDCl_3$ in the presence of 1 Torr Cl_2 or 5 Torr Cl_2 was also performed. The addition of Cl_2 increased the CCl_4 yield without having any noticeable effect on the $CDCl_3$ dissociation yield. In the presence of 1 Torr Cl_2, CCl_4 represented ~35% of the photolysis product (Line C of Figure 5.2), while in the presence of 5 Torr Cl_2 it constituted ~ 55% of the total product (Line D of Figure 5.2). The increased CCl_4 yield may be the result of two possible reactions:

$$CCl_3 + Cl_2 \rightarrow CCl_4 + Cl \qquad \ldots.(5.16)$$

or

$$CCl_2 + Cl_2 \rightarrow CCl_4 \qquad \ldots.(5.17)$$

It is likely that it is reaction (5.17) that is most important and not (5.16). Reaction (5.16) leads to the regeneration of the Cl atoms consumed in the formation of CCl_3 (reaction (5.10)). This could then lead to a

chain reaction involving Cl atoms and Cl_2 molecules:

$$Cl + CDCl_3 \rightarrow CCl_3 + DCl \quad ....(5.10)$$

$$CCl_3 + Cl_2 \rightarrow CCl_4 + Cl \quad ....(5.16)$$

However, no noticeable increase in $CDCl_3$ consumption is observed, even on the addition of 5 Torr Cl_2. Thus, such a chain mechanism cannot be operating.

Very little is known about the gas phase kinetics of CCl_2. However, from the one investigation made in this area,[76] it can be concluded that CCl_2 is more reactive than CClF and far more reactive than CF_2. For example, while the reaction of CF_2 with F_2 is very slow (less than 2×10^{-15} cm^3 $molecule^{-1}$ s^{-1}),[77] CCl_2 reacts with F_2 with a rate constant of 3×10^{-13} cm^3 $molecule^{-1}$ s^{-1}.[76] Thus, it is very possible that the increased CCl_4 yield can be attributed to the reaction of CCl_2 and Cl_2.

In summary, the addition of chlorine atom scavengers (C_2F_4, NO, H_2) serves to greatly decrease the CCl_4 yield in $CDCl_3$ IRMPD. Thus, it is likely that CCl_4 production occurs (in the absence of additives) as a result of Cl attack on $CDCl_3$:

$$Cl + CDCl_3 \rightarrow CCl_3 + DCl \quad ....(5.10)$$

followed by

$$CCl_3 + Cl \rightarrow CCl_4 \quad \text{....(5.14)}$$

or

$$CCl_3 + CCl_3 \rightarrow CCl_4 + CCl_2 \quad \text{....(5.11c)}$$

Although the possibility of a chain reaction exists in the absence of additives,

$$Cl + CDCl_3 \rightarrow CCl_3 + DCl \quad \text{....(5.10)}$$

$$CCl_3 + Cl_2 \rightarrow CCl_4 + Cl \quad \text{....(5.16)}$$

the addition of Cl_2 to the reaction mixture does not promote $CDCl_3$ dissociation. Therefore, no evidence exists for the presence of a chain mechanism and the increased CCl_4 yield on addition of Cl_2 is likely the result of reaction (5.17):

$$CCl_2 + Cl_2 \rightarrow CCl_4 \quad \text{....(5.17)}$$

It should be noted that the formation of CCl_4 may have a major bearing on the isotopic selectivity of the IRMPD of $CDCl_3/CHCl_3$, as the attack of Cl on chloroform, reaction (5.10a) and (5.10b),

$$Cl + CDCl_3 \rightarrow CCl_3 + DCl \quad \text{....(5.10a)}$$

$$Cl + CHCl_3 \rightarrow CCl_3 + HCl \quad \ldots.(5.10b)$$

would actually favor HCl formation (by about a factor of 3)[78] because of the kinetic isotope effect. Thus, this radical reaction may account for a major portion of the HCl produced in the photolysis. The ability to block this reaction with Cl atom scavengers may then lead to a great enhancement of the overall isotopic selectivity of the process.

5.4.2 DCl/HCl DETECTION FOLLOWING IRMPD OF CHLOROFORM

Tunable diode lasers seem to be ideally suited for studying isotope separation schemes of the type reviewed in Section 5.3. In the case of IRMPD of the haloforms, information on the isotopic selectivity of the process is contained directly in a hydrogen halide molecule (eg, HF, DF, HCl, or DCl). These molecules are ideal for detection by TDL absorption spectroscopy. Their infrared absorptions are generally very strong, leading to high sensitivity. Also, their absorption features are well separated and well characterized and are therefore easy to identify even in the case of molecules differing only in their isotopic make-up. (For example, the IR absorptions of DCl and HCl are separated by 500 cm^{-1}.) Further, these molecules cannot be detected by either gas chromatography

or mass spectrometry. Other advantages of TDL analysis are that it is non-destructive, and that it is a much more accurate and direct method than those previously used. Previous methods often relied upon the measurement of a very small decrease in the concentration of the off-resonant isotopic species, a measurement which carries a very large error, or involved complicated, indirect methods of analysis.

Initial experiments were conducted to test the reliability and reproducibility of TDL detection of DCl. Irradiations of 2 Torr $CDCl_3$ were carried out using the 10P(48) CO_2 laser line, with the experimental apparatus presented in Figure 2.1. The DCl yield was measured after 20, 40, and 60 pulses, and DCl production was shown to be linear. The DCl yield per pulse was reproducible to within $\pm$5% over a series of five measurements.

DCl production as a function of photolysis frequency was also studied. As shown in Figure 5.3, the DCl yield per pulse increased monotonically as the CO_2 laser frequency was moved from 10P(34) at 931.05 cm^{-1} to 10P(48) at 916.76 cm^{-1}, the limit of laser tunability. The linear absorption peak for $CDCl_3$ is at about 912 cm^{-1}, while the IRMP absorption peak has been reported to be at 901 cm^{-1}.[74]

FIGURE 5.3: Relative DCl yield as a function of photolysis frequency following IRMPD of 1 Torr $CDCl_3$ in a 10 cm Pyrex cell. The peak focal fluence is 10 J cm^{-2} in all cases. The error bar represents $\pm 1\sigma$.

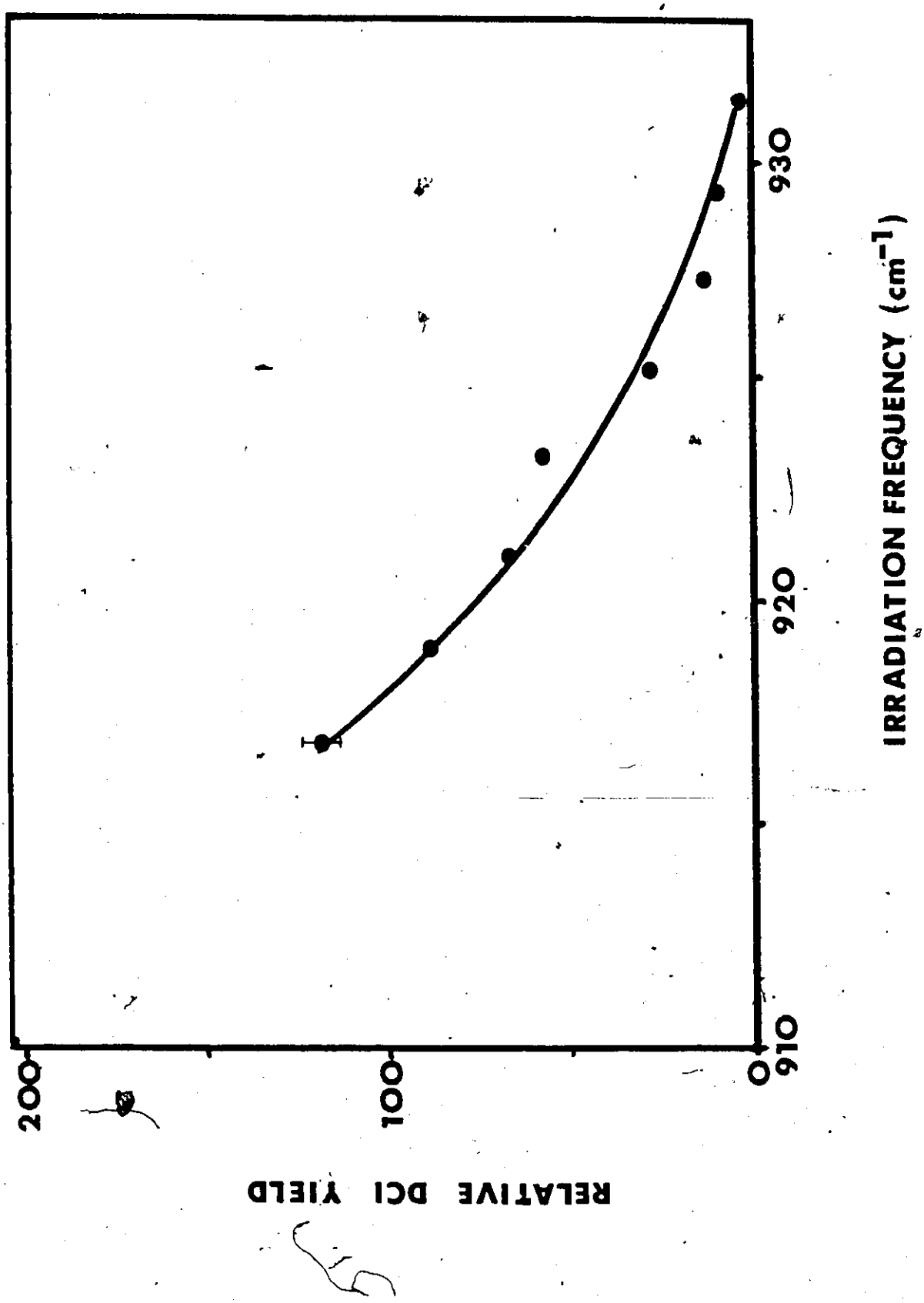
RELATIVE DCI YIELD
200
100
0
910
920
930
IRRADIATION FREQUENCY (cm⁻¹)

With the reliability of TDL detection of DCl established, an experiment designed to demonstrate the sensitivity of the technique was performed. In this experiment, DCl production from the irradiation of natural abundance $CDCl_3$ (about 140 ppm) in $CHCl_3$ was monitored using second harmonic TDL absorption spectroscopy. Figure 5.4 shows successive scans on a sample of 5 Torr $CHCl_3$. The first scan shows a background spectrum, while the second scan is a background spectrum eleven minutes later. No change in DCl concentration is noted, indicating that no wall desorption is occurring. The third scan was taken following irradiation of the $CHCl_3$ sample for 100 pulses (0.4 J/pulse) using 10P(38), while the fourth scan was taken following irradiation of the sample for 100 pulses using 10P(48). DCl (at a level of 3.5 ppm) appears only following irradiation with the more efficient 10P(48) CO_2 laser line. Thus, the appearance of DCl must be attributed to the IRMPD of the $CDCl_3$ contained in the sample, and not to thermal or shock-induced effects caused by the passage of a CO_2 laser pulse. The appearance of CO in these irradiations is thought to be due to the reaction of photolytically produced CCl_2 with the cell walls. It should be pointed out that the DCl detected in this experiment (3.5 ppm) represents only 2.5% of the original deuterium content of the sample.

FIGURE 5.4: Successive scans taken of a 5 Torr sample of natural chloroform after irradiation with 100 pulses of 10P(38) and 10P(48) radiation (about 10 J cm^{-2}). The increase in DCl concentration after irradiation with 10P(48) is attributed to IRMPD of naturally occurring $CDCl_3$ in the sample. The noise level is equivalent to about 0.8 ppm DCl.

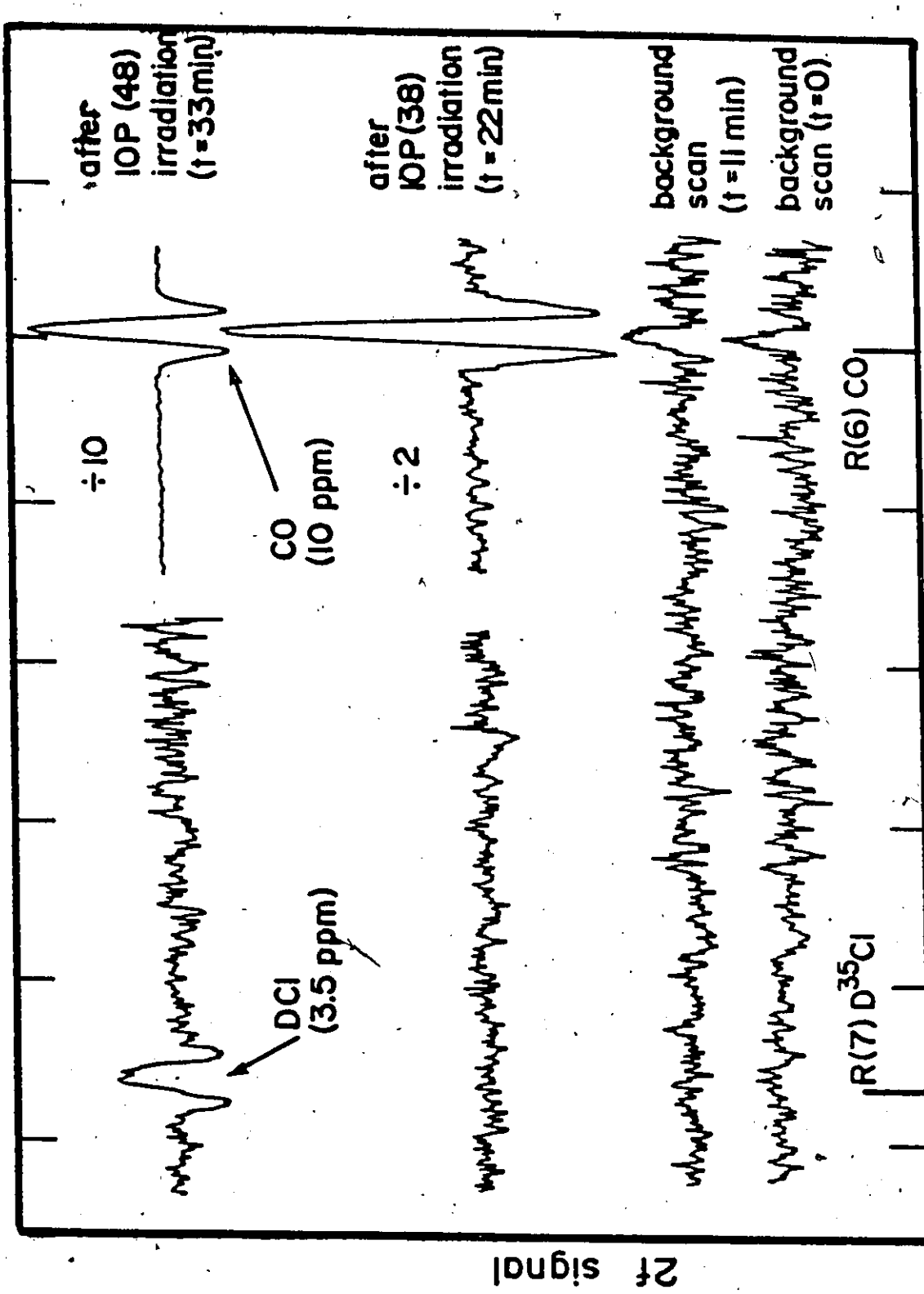
2f signal
after IOP (48) irradiation (t=33min)
÷10
CO (10 ppm)
after IOP(38) irradiation (t=22min)
÷2
DCl (3.5 ppm)
background scan (t=11 min)
background scan (t=0)
R(7) D35Cl
R(6) CO
2169.00
2169.10
2169.20
Wavenumber (cm-1)

With the demonstration of the sensitivity of TDL absorption spectroscopy for species such as DCl, it was hoped that information on the isotopic selectivity of the IRMPD of $CDCl_3/CHCl_3$ could be obtained by monitoring the production of DCl and HCl under a variety of conditions. However, such measurements are hindered by two factors. Firstly, DCl reacts with adsorbed H_2O on the cell walls, reaction (5.9), to produce HCl.[74] Thus, the irradiation of pure $CDCl_3$ actually leads to the detection of more HCl than DCl. Obviously, the measurement of only the HCl and DCl produced in a photolysis yields no isotopic information because of the presence of this scrambling mechanism.

It was thought that this problem could be overcome by also monitoring the amount of $CDCl_3$ consumed in a photolysis using TDL spectroscopy. Thus, a measure of the total (HCl + DCl) yield would give a measure of the total amount of ($CHCl_3$ + $CDCl_3$) consumed, while the loss of $CDCl_3$ would be determined independently. The difference in these two numbers would then give the amount of $CHCl_3$ decomposed, and information on the isotopic selectivity of the reaction could be obtained. To this end, a sample containing a mixture of 0.1 Torr $CDCl_3$ and 1.9 Torr $CHCl_3$ was irradiated at 10P(48) at a peak focal

FIGURE 5.5: Dissociation yield of $CDCl_3$ (lower line) and total (HCl + DCl) yield following the irradiation of a mixture of 0.1 Torr $CDCl_3$ and 1.9 Torr $CHCl_3$. The photolysis is performed at a peak focal fluence of 10 J cm^{-2} with the 10P(48) CO_2 laser line. The points labelled 1,2, and 3 represent the $CDCl_3$ dissociation yield in three separate experiments, while the points labelled a,b, and c represent the (HCl and DCl) yield in the same three experiments.

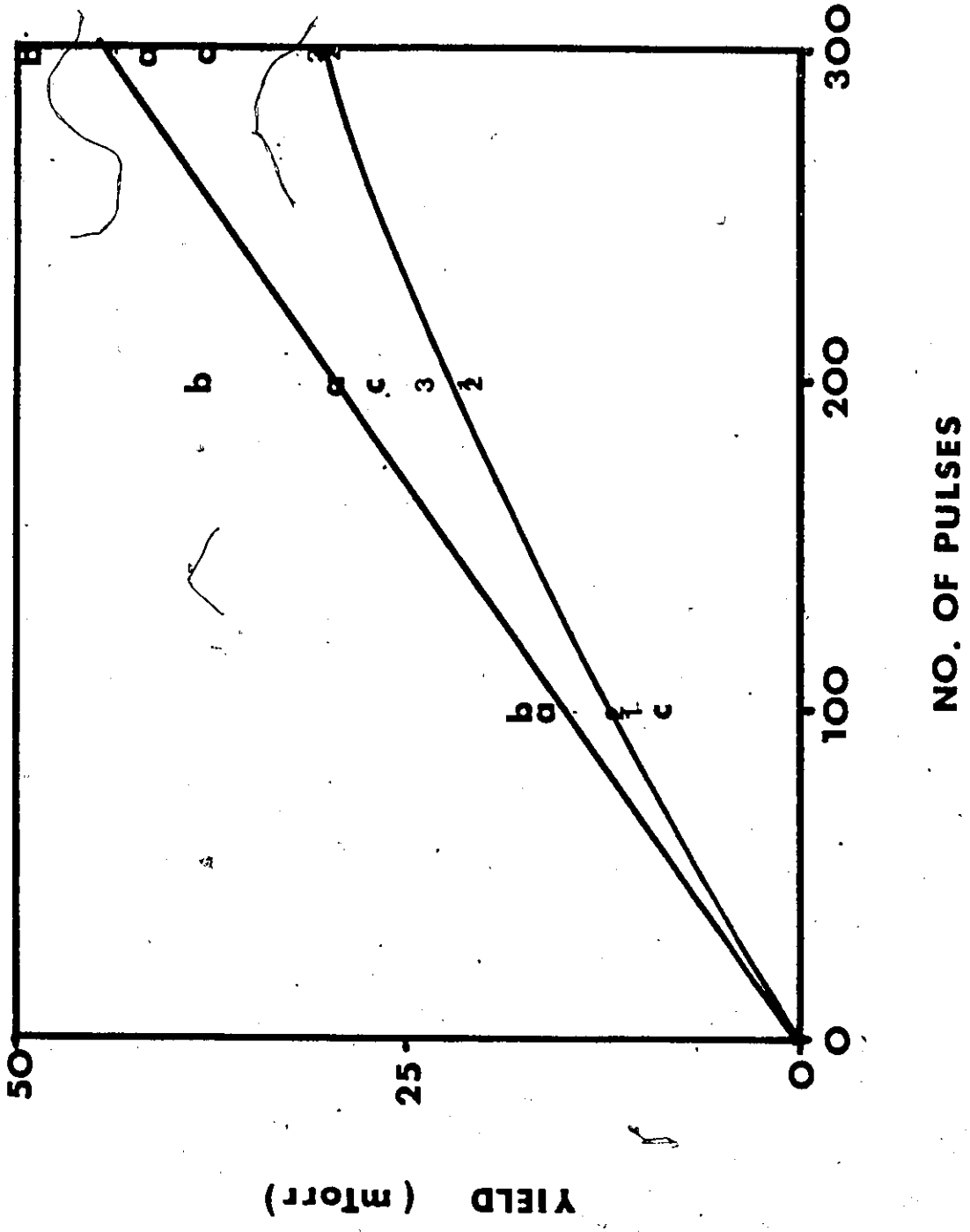
YIELD (mtorr)
50
25
0
0
100
200
300
NO. OF PULSES
a
b
c
1
2
3

fluence of 10 J cm^{-2}. Figure 5.5 shows that, in such an experiment, the amount of $CDCl_3$ lost is very reproducible but the amount of (HCl + DCl) formed is not reproducible. This effect is likely due to the wall adsorption/desorption of HCl/DCl, the magnitude of which is dependent on the prior condition of the cell walls. The importance of these adsorption/desorption effects becomes more evident when photolysis of C_2F_6 is done in a cell in which previous chloroform photolyses were performed, and significant yields of DCl and HCl are obtained. Obviously, the passage of the CO_2 laser pulse leads to removal of DCl/HCl from the cell walls, and determination of the DCl and HCl is not representative of the amount of these species produced in the photolysis.

5.4.3 TIME-RESOLVED TDL DETECTION OF DCl/HCl

It is apparent that any isotopic selectivity measurements on the chloroform system, by TDL absorption measurements of HCl and DCl, must be made without the contribution of any cell wall effects. To this end, it was decided to monitor the HCl and DCl yields on a short timescale (tens of μs), in the manner described in Figure 2.4, so that quantification is done before any wall reactions can occur and the effects of isotope exchange or

of wall adsorption/desorption processes are eliminated.

DCl analysis was performed on the P(2) transition at 2069.272 cm^{-1}, which has a linestrength (s) of 9.47 X 10^{-20} cm $molecule^{-1}$.[62] The detector limited noise level for detecting DCl is found to correspond to a fractional absorption of 2.7 X 10^{-3}. Thus, the minimum detectible DCl (under Doppler broadening conditions, and with a cell 15 cm in length) is 0.3 mTorr for a signal to noise ratio of 2. As the pressure of the sample is increased, the sensitivity decreases due to pressure broadening of the DCl absorption feature. For example, the sensitivity decreases by a factor of two at roughly 25 Torr.

Detection of HCl, using the available TDL, was not as sensitive due to the fact that detection had to be done on a weaker transition (P(9), with a linestrength of 2.68 X 10^{-20} cm $molecule^{-1}$)[46] and the fact that the diode power was much lower than in the case of DCl detection. In the HCl case, the noise level corresponds to a fractional absorption of .028, allowing for a minimum detection limit of 13 mTorr of HCl under Doppler limited conditions over a pathlength of 15 cm. Again, sensitivity decreases with pressure due to collisional broadening.

It is obvious that the experiments to be performed at this point involve the measurement of the HCl and DCl

yields from the photolysis of $CHCl_3/CDCl_3$ mixtures under a variety of experimental conditions. For example, systematic variation of the CO_2 laser wavelength and fluence, the sample pressure, $CDCl_3$ fraction, and pressure of added gas could be done. As this would constitute a large undertaking, and some experimental problems have been encountered, only preliminary measurements have been made to date.

Mixtures of $CDCl_3$:$CHCl_3$:Ar (in 1:1:1 proportions) were flowed through the capillary cell and irradiated at a fluence of ~15 J cm^{-2} with the 10P(38) CO_2 laser line. The amount of HCl formed was measured as a function of total pressure, (Line A of Figure 5.6). The HCl yield increases at greater than a linear rate with pressure. This is consistent with formation of HCl by two different mechanisms. The first mechanism involves collisional energy transfer from $CDCl_3$ (excited by the CO_2 laser photons) to $CHCl_3$ and the subsequent dissociation of the $CHCl_3$:

$$CDCl_3^* + CHCl_3 \rightarrow CHCl_3^* + CDCl_3 \quad \ldots(5.18)$$

$$CHCl_3^* \rightarrow CCl_2 + HCl \quad \ldots(5.19)$$

This process would depend on the square of the pressure. The other mechanism involves the extraction of H from

FIGURE 5.6: Transient HCl yield following the single pulse irradiation of an equimolar mixture of $CDCl_3$:$CHCl_3$:Ar (Line A) or $CDCl_3$:$CHCl_3$:C_2F_4 (Line B). The irradiation is performed with the 10P(38) CO_2 laser line at a peak focal fluence of 16 J cm^{-2}. Errors are $\pm 1\sigma$.

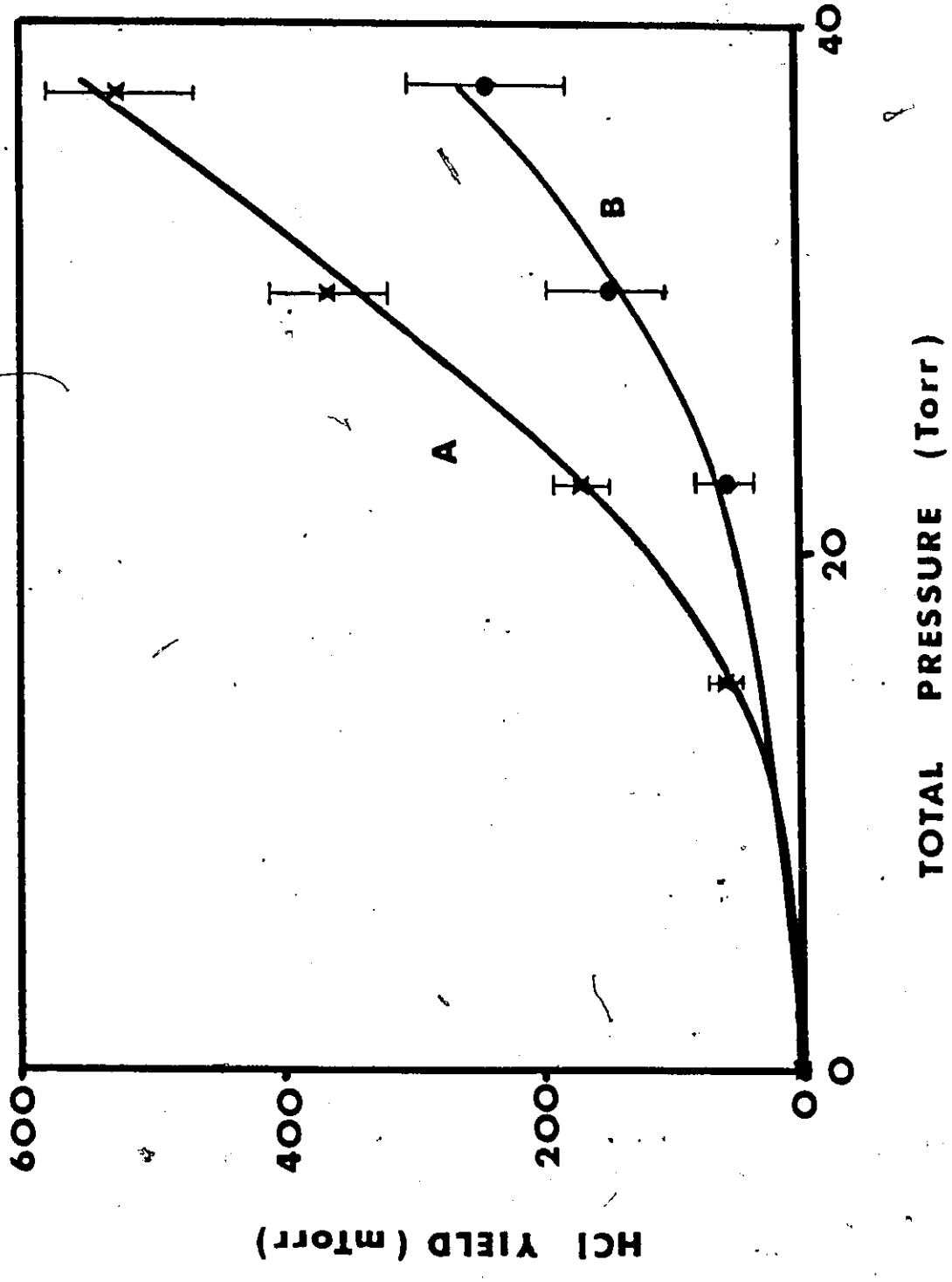
HCl YIELD (mtorr)
600
400
200
0
0
20
40
TOTAL PRESSURE (Torr)
A
B

$CHCl_3$ by Cl, reaction (5.10), which would also have a greater than linear pressure dependence.

Irradiation of mixtures of $CDCl_3$:$CHCl_3$:C_2F_4 (again in 1:1:1 proportions), under identical conditions to those described above, yields less HCl than the Ar case (see Line B of Figure 5.6). This decrease is consistent with the conclusions drawn earlier regarding the effect of C_2F_4 as a chlorine atom scavenger. The decreased yield of HCl can be attributed to the fact that Cl atoms, which in the absence of C_2F_4 react with $CHCl_3$ to produce HCl, now react preferentially with C_2F_4.

Preliminary analysis of the amount of DCl produced on irradiation of mixtures like those described above has proven difficult, as DCl yields are not reproducible. To date, no explanation for this phenomenon has been found.

5.5 SUMMARY

In this chapter, the IRMPD of $CDCl_3/CHCl_3$ has been studied. Analysis of the yield of carbon-bearing products, with and without added scavengers, leads to the conclusion that CCl_4 is produced by post-photolysis radical reactions involving chlorine atoms. No evidence for any type of chain reaction has been found.

While TDL analysis of DCl/HCl found in the IRMPD of $CDCl_3/CHCl_3$ is shown to be very sensitive (DCl is detected at the 3.5 ppm level from the irradiation of natural abundance $CDCl_3$ in $CHCl_3$), quantitative analysis of these gases over the timescale of minutes is plagued by isotope exchange reactions and adsorption/desorption processes at the cell walls.

Transient detection of DCl and HCl (on a timescale of tens of μs) shows more promise for isotopic selectivity, as measurements are made before wall processes can occur. Initial studies in this area show that a few tenths of a mTorr of DCl can be detected. Measurements of HCl yields, both with and without added C_2F_4, confirm the existence of post-photolysis radical reactions, which likely lead to the isotopically non-selective loss of chloroform and reduce the DCl/HCl product ratio.

The detection of DCl following the IRMPD of natural abundance $CHCl_3$ is published in the Journal of Photochemistry, 34, 267-279 (1986) with co-authors Beckwith, Orlando, Reid, and Smith. In particular, the collaborative work of P.H. Beckwith in setting up the TDL for DCl detection, and especially in collecting the data presented in Figure 5.4, is gratefully acknowledged.

CHAPTER 6

CONCLUSIONS

6.1 INTRODUCTION

In this chapter, a summary of the important results obtained and conclusions drawn during the course of this thesis will be presented. The chapter will include a discussion of the five major areas studied:

1) the time-resolved detection technique,

2) its application to the study of IRMPD mechanisms,

3) the use of the technique for the measurement of infrared linestrengths and bandstrengths of transient species,

4) the use of the technique in studying the reaction kinetics of transient species, and

5) its use in measuring the isotopic selectivity of the IRMPD process.

Where possible, prospects for further research in these areas will be discussed.

6.2 TIME-RESOLVED DETECTION WITH TDLs

During the course of this thesis, a time-resolved tunable diode laser technique for monitoring the products of IRMPD has been developed. It has been applied to the detection of the transient species CF_2 and CF_3, and has also been used for the short timescale detection of such species as HCl, DCl, CO, C_2F_6, COF_2, CF_4, and C_2F_4.

At present, the time resolution of the technique is limited to approximately 25 μs after the CO_2 laser pulse because of the interference of electrical noise associated with the firing of the CO_2 laser. The TDL can at present be modulated at 250 kHz, implying that a resolution of 2 μs could be obtained in the absence of this electrical noise.

The sensitivity of the technique has been shown to be detector noise limited.[36] That is, the sensitivity is not limited by any physical phenomenon (such as laser noise or optical fringing which often limit cw experiments) and the use of a more powerful diode laser or more sensitive detector would improve the sensitivity of the technique. To date, noise levels corresponding to a fractional absorbance of 10^{-5} have been obtained. Work is currently underway at McMaster to improve both the sensitivity and time resolution of the technique.

It is of interest to compare the sensitivity of our CF_2 creation and detection technique with the standard procedure of creating CF_2 in a microwave discharge and using TDLs for cw detection of the CF_2.[38] While Davies et al. do not report the fractional absorptions obtained or pathlength used in their microwave discharge experiment, peak CF_2 absorptions of 10% over a pathlength of 2.4 m are obtained in our microwave discharge system.[36] When this is compared with the absorptions obtained in the IRMPD/TDL technique (30% absorption over a 15 cm pathlength), it can be seen that the CF_2 partial pressure is about 50 times greater than that obtained in the microwave discharge. Thus, the creation of radicals by IRMPD and their subsequent time-resolved detection with TDLs should have application in high-resolution spectroscopic studies. For example, the CF_2 ν_2 bending mode, which to date has not been observed in microwave discharge systems, may be detected using our transient technique.

6.3 DETERMINATION OF IRMPD MECHANISMS

The detection of transients has been applied to the determination of the IRMP photolysis and post-photolysis mechanism of three halocarbons - CF_2HCl,

$(CF_3)_2CO$, and $CDCl_3$. The main advantage of the technique in studies of this sort is that the primary dissociation fragments can be monitored. That is, mechanistic information does not have to be inferred solely from the final product distribution which is often complicated by the presence of secondary reactions.

In the case of CF_2HCl (Chapter 3), it was well established that IRMPD resulted in the formation of CF_2 and HCl (the CF_2 had previously been detected by LIF and by time of flight mass spectrometry) and TDL detection of these fragments serves only as a confirmation of this mechanism. For hexafluoroacetone (Chapter 4), the situation is different, as it was not previously known whether dissociation occurred via direct production of C_2F_6, or via the production of two CF_3 fragments. However, CF_3 is directly detected by time-resolved TDL absorption spectroscopy following IRMPD of hexafluoroacetone. Further, C_2F_6 is shown to be absent immediately following the passage of the CO_2 laser pulse, but its concentration increases as the CF_3 decays. Therefore, hexafluoroacetone IRMPD must occur via the production of two CF_3 molecules, which subsequently combine to form C_2F_6. In the case of $CDCl_3$, time resolved hydrogen chloride detection, in conjunction with FT-IR detection of carbon-bearing products, has led to the

conclusion that CCl_4 production is the result of radical reactions involving chlorine atoms. The addition of a Cl scavenger (C_2F_4) lowers the yield of both CCl_4 and HCl in the IRMPD of $CDCl_3/CHCl_3$ mixtures. This may significantly improve the isotopic selectivity of the process, since such radical reactions are isotopically non-selective.

Obviously, the determination of dissociation mechanisms is not limited to the three molecules discussed here, and can be applied to any other molecule provided the absorption frequencies of the expected product fragments are known.

6.4 LINESTRENGTH AND BANDSTRENGTH CALCULATIONS

A major achievement in this thesis is the determination of an infrared linestrength and bandstrength for both CF_2 ν_1 (Chapter 3) and CF_3 ν_3 (Chapter 4). A linestrength for CF_2 is determined by comparing the time-resolved infrared absorption coefficients of CF_2 and HCl formed from the IRMPD of CF_2HCl. Since the concentrations of these species must be equal immediately following the photolysis, the ratio of their linestrengths can be obtained from the ratio of the measured absorption coefficients for the two species. Since linestrengths for

HCl are known, one can then obtain a linestrength for CF_2. This one measured linestrength is then used to calculate the ν_1 bandstrength and any other linestrength in this band. The CF_2 ν_1 bandstrength was found to be $(3.4\pm0.8) \times 10^{-18}$ cm molecule^{-1}, from the measured linestrength of $(9\pm2) \times 10^{-21}$ cm molecule^{-1} for the $^rQ_3(9)$ line at 1243.0185 cm^{-1}.

A similar method was used to obtain a linestrength and bandstrength for CF_3 from the time-resolved detection of CO, C_2F_6, and CF_3 produced in the IRMPD of hexafluoroacetone. The photolysis mechanism is determined to involve the production of 2 CF_3 molecules, and one CO molecule. The CF_3 linestrength is then obtained from a knowledge of the stoichiometry of the dissociation and from readily available CO linestrength data. From the experimentally determined linestrength of $(1.4\pm.3) \times 10^{-20}$ cm molecule^{-1} for the $^rR_{16}(20)$ transition at 1264.739 cm^{-1}, the CF_3 ν_3 bandstrength is determined to be $(8\pm2) \times 10^{-18}$ cm molecule^{-1}.

The availability of infrared linestrength or bandstrength data for transient species in the literature is very scarce. The general technique used in the measurements of CF_2 and CF_3 bandstrengths is of course applicable to many other transient species, with the limit being in the ability to find a suitable precursor

molecule. The precursor must first dissociate under the influence of a laser. Further, the precursor must dissociate into the desired fragment (for which the linestrength is to be measured) plus other fragment(s) for which linestrength information is available. For example, $CDCl_3$ dissociates into CCl_2 and DCl when irradiated near 910 cm^{-1}, and this molecule could then be used to obtain a linestrength for CCl_2. Other possibilities include the irradiation of CH_3NO_2 to obtain the bandstrength of CH_3, CH_3ONO for the determination of a bandstrength for CH_3O, or C_3H_6 or cyclo-C_3H_6 for a CH_2 bandstrength determination.

6.5 KINETIC STUDIES OF TRANSIENT SPECIES

Determination of the linestrength and bandstrength of the transient species CF_2 and CF_3 allows for a knowledge of their absorption concentration at any time following the passage of the CO_2 laser pulse. That is, their kinetics can be studied.

In the case of CF_2 (Chapter 3), the rate constant for recombination of two CF_2 molecules to C_2F_4 is measured to be $(2.3\pm0.7) \times 10^{-14}$ cm^3 $molecule^{-1}$ s^{-1} compared to the literature value of $(3.7\pm0.3) \times 10^{-14}$ cm^3 $molecule^{-1}$ s^{-1}.

For CF_3 (Chapter 4), the rate constant for recombination is determined to be $(2.2\pm0.5) \times 10^{-12}$ cm^3 $molecule^{-1}$ s^{-1} compared to the literature value of $(3.0\pm0.4) \times 10^{-12}$ cm^3 $molecule^{-1}$ s^{-1}. In addition, the third body rates of reaction of CF_3 with O_2 and NO have been measured. Values of $(2.1\pm0.5) \times 10^{-29}$ and $(2.8\pm0.7) \times 10^{-29}$ cm^6 $molecule^{-2}$ s^{-1} have been obtained for O_2 and NO, respectively. This agrees with the literature value of $(1.9\pm0.2) \times 10^{-29}$ cm^6 $molecule^{-2}$ s^{-1} recently reported for CF_3 with O_2, while no literature value for CF_3 and NO below the high pressure limit has yet been reported.

It is apparent that all the kinetic measurements made in this work agree within experimental error with the literature, with the exception of the fact that our CF_2 recombination rate constant is low. It may be significant that the quoted literature value for CF_2 recombination was measured in 1969. Obviously, then, this technique has been shown to be a viable one for the study of the reaction kinetics of transient species. It can obviously be extended to include the study of the reactions of CF_2 and CF_3 with other species of interest, or it may be used to make kinetic studies on other transients such as CCl_2. It should be pointed out that a similar technique has been employed to study the reaction rate of CF_2 with H_2, Cl_2 and Br_2.[79]

6.6 LASER ISOTOPE SEPARATION

A study of the feasibility of using TDLs for studies of the isotope selectivity of IRMPD has also been presented. While the sensitivity of TDL detection of hydrogen halides is impressive (as demonstrated by the detection of the DCl produced in the IRMPD of natural abundance $CDCl_3$ in $CHCl_3$), these measurements (taken over a timescale of minutes) are inaccurate due to wall effects. Preliminary experiments show that the use of time-resolved detection of hydrogen halides (over μs timescales to eliminate these wall effects) may be effective in measuring the isotopic selectivity of the IRMPD process. The technique is not limited to DCl and HCl measurements. For example, DF has been detected in our lab (by Carl Brown) from the IRMPD of CDF_3. Also, the technique may be extended to the detection of tritiated species, such as TCl and TF, produced in the IRMPD of $CTCl_3$ or CTF_3.

6.7 SUMMARY

The experiments in this thesis involve the TDL detection of the products of IRMPD, particularly the transient species CF_2 and CF_3. The technique has been employed to determine IRMPD photolysis and post-photolysis mechanisms, to measure CF_2 and CF_3 linestrengths and bandstrengths, to study the kinetics of these transient species, and to study isotope separation. The potential for further research in these areas, and in high resolution IR absorption spectroscopy of these and other transient species has been outlined.

REFERENCES

1. N.R. Isenor and M.C. Richardson, "Dissociation and breakdown of molecular gases by pulsed CO_2 laser radiation", Appl. Phys. Lett. 18, 224-226 (1971).

2. V.N. Bagratashvili, V.S. Letokhov, A.A. Makarov, E.A. Ryabov, "Multiple-photon infrared laser photophysics and photochemistry", Laser Chemistry 1, 211-342; 4, 1-103; 4, 171-274; 4, 311-423; 5, 53-105.

3. W. Fuss, K.L. Kompa, "The importance of spectroscopy for infrared multiphoton excitation", Prog. Quant. Elect. 7, 117-151 (1981).

4. R.V. Ambartzumian and V.S. Letokhov, "Multiple photon infrared laser photochemistry", in Chemical and Biochemical Applications of Lasers, ed. C. Bradley Moore, Academic Press, 1977.

5. R.V. Ambartzumian and V.S. Letokhov, "Selective dissociation of polyatomic molecules by intense infrared laser fields", Acc. Chem. Res. 10, 61-67 (1977).

6. N. Bloembergen and E. Yablonovitch, "Infrared laser-induced unimolecular reactions", Phys. Today 31, 23-30 (1978).

7. P.A. Schulz, Aa.S. Sudbo, D.J. Krajnovich, H.S. Kwok, Y.R. Shen, Y.T. Lee, "Multiphoton dissociation of polyatomic molecules", Ann. Rev. Phys. Chem. 30, 379-409 (1979).

8. V.S. Letokhov, "Laser separation of isotopes", Ann. Rev. Phys. Chem 28, 133-159 (1977).

9. V.S. Letokhov and C.B. Moore, "Laser Isotope Separation (review)", Sov. J. Quant. Elec. 6, 129-150 and 259-276 (1976).

10. I.P. Herman and J.B. Marling, "Ultrahigh single-step deuterium enrichment in CO_2 laser photolysis of trifluoromethane as measured by carbon-isotope labeling", J. Chem. Phys. 72, 516-523 (1980).

11. "Infrared spectroscopic applications and techniques", Reprint List, published by Spectra Physics, Laser Analytics Division, 25 Wiggins Ave., Bedford, MA, 01730.

12. H.I. Schiff, D.R. Hastie, G.I. Mackay, T. Iguchi, B.A. Ridley, "Tunable diode laser systems for monitoring trace gases in tropospheric air", Environ. Sci. Tech. 17, 352A-364A (1983).

13. E.D. Hinkley, "High-resolution infrared spectroscopy with a tunable diode laser", Appl. Phys. Lett 16, 351-354 (1970).

14. J.I. Steinfeld and P. Houston, "Double Resonance Spectroscopy", in Laser and Coherence Spectroscopy, Ed. J.I. Steinfeld, Plenum Press, New York, 1980.

15. R.V. Ambartzumian, Y.A. Gorokhov, V.S. Letokhov, G.N. Makarov, "Direct observation of the nonequilibrium excitation of high vibrational levels of the OsO_4 molecule by a high-power laser pulse, and separation of osmium isotopes", JETP Letters 22, 43-44 (1975).

16. V.N. Bagratashvili, Yu. G. Vainer, V.S. Dolzhikov, S.F. Kol'yakov, V.S. Letokhov, A.A. Makarov, L.P. Malyavkin, E.A. Ryabov, E.G. Silkis, V.D. Titov, "Intermolecular and intramolecular distribution of vibrational energy under multiphoton excitation by IR

laser radiation", Sov. Phys. JETP 53, 512-522 (1981).

17. J.W. Hudgens and J.D. McDonald, "Discrete and quasicontinuum level fluorescence from infrared multiphoton excitation of SF_6", J. Chem. Phys. 76, 173-188 (1982).

18. R.V. Ambartzumian, V.S. Letokhov, G.N. Makarov, A.A. Puretzky, "Characteristics of multiple-photon dissociation of OsO_4 molecule by two-frequency tunable CO_2-laser pulses", Opt. Comm. 25, 69-74 (1978).

19. I.P. Herman and J.B. Marling, "IR photolysis of CDF_3: A study in kinetics of multiple-photon dissociation with applications to deuterium separation", Chem. Phys. Lett. 64, 75-80 (1979).

20. D.M. Larsen and N. Bloembergen, "Excitation of polyatomic molecules by radiation", Opt. Comm. 17, 254-258 (1976).

21. V.T. Platonenko, "Mechanism of the excitation of high vibrational-rotational states and dissociation of polyatomic molecules by an infrared field", Sov. J. Quant.

Elec. 8, 1010-1013 (1978).

22. W. Fuss, "Rate equations approach to the infrared collisionless multiphoton excitation", Chem. Phys. 36, 135-144 (1979).

23. P. Mukherjee and H.S. Kwok, "Picosecond laser study of the quasicontinuum of chloropentafluoroethane", J. Chem. Phys. 84, 1285-1295 (1986).

24. P.J. Robinson and K.A. Holbrook. Unimolecular Reactions. John Wiley and Sons, Ltd. Toronto. 1972.

25. I. Oref and B.S. Rabinovitch, "Do highly excited reactive polyatomic molecules behave ergodically?", Acc. Chem. Res. 12, 166-175 (1979).

26. T.H. Richardson and D.W. Setser, "Laser induced decomposition of fluoroethanes", J. Phys. Chem. 81, 2301-2303 (1977).

27. D. Rayner and P.A. Hackett, "Direct measurement of ground state unimolecular decay rate in IRMPD of CF_3I and $C_6F_{13}I$", Chem. Phys. Lett. 110, 482-487 (1984).

28. Aa.S. Sudbo, P.A. Schulz, E.R. Grant, Y.R. Shen, Y.T. Lee, "Simple bond rupture reactions in multiphoton dissociation of molecules", J. Chem. Phys. 70, 912-929 (1979).

29. E.R. Grant, M.J. Coggiola, Y.T. Lee, P.A. Schulz, Aa. S. Sudbo, Y.R. Shen, "The extent of energy randomization in the infrared multiphoton dissociation of SF_6", Chem. Phys. Lett. 52, 595-599 (1977).

30. Aa. S. Sudbo, P.A. Schulz, Y.R. Shen, Y.T. Lee, "Three and four center elimination of HCl in the multiphoton dissociation of halogenated hydrocarbons", J. Chem. Phys. 69, 2312-2322 (1978).

31. J.A. Horsley, D.M. Cox, R.B. Hall, A. Kaldor, E.T. Maas, Jr., E.B. Priestley, G.M. Kramer, "Isotopic selectivity in the laser induced dissociation of molecules with overlapping absorption bands", J. Chem. Phys. 73, 3660-3665 (1980).

32. S.D. Rockwood and J.W. Hudson, "Laser driven synthesis of $BHCl_2$ from BCl_3 and H_2", Chem. Phys. Lett. 34, 542-545 (1975).

33. S.S. Penner. Quantitative Molecular Spectroscopy and Gas Emissivities. Addison-Wesley Pub. Co., Inc. 1959.

34. J. Reid and D. Labrie, "Second-harmonic detection with tunable diode lasers - Comparison of experiment and theory", Appl. Phys. B26, 203-210 (1981).

35. L.S. Rothman, "AFGL atmospheric absorption line parameter compilation: 1980 version", Appl. Opt. 20, 791-795 (1980).

36. P.H. Beckwith, C.E. Brown, D.J. Danagher, D.R. Smith, J. Reid, "High sensitivity detection of transient infrared absorptions using tunable diode lasers", Appl. Opt. 26, 2643-2649 (1987).

37. K. Sugawara, T. Nakanaga, H. Takeo, C. Matsumura, "Infrared diode laser spectroscopic detection of CF_2 carbene produced by CO_2 laser photolysis of $CHClF_2$", Chem. Phys. Lett 130, 560-564 (1986).

38. P.B. Davies, W. Lewis-Bevan, D.K. Russell, "Infrared diode laser spectrum of the ν_1 band of CF_2 (X^1A_1)", J. Chem. Phys. 75, 5602-5608 (1981).

39. C. Yamada and E. Hirota, "Infrared diode laser spectroscopy of the CF_3 ν_3 band", J. Chem. Phys. 78, 1703-1711 (1983).

40. J.C. Stephenson and D.S. King, "Energy partitioning in the collision-free multiphoton dissociation of molecules: Energy of X CF_2 from CF_2HCl, CF_2Br_2, and CF_2Cl_2", J. Chem. Phys. 69, 1485-1492 (1978).

41. R.C. Slater and J.H. Parks, "Non-thermal laser induced chemistry and high reactant gas pressures", Chem. Phys. Lett. 60, 275-278 (1979).

42. R. Dupperex and H. van den Bergh, "Time resolved measurement of CF_2 formation in the infrared multiphoton dissociation of CF_2HCl", J. Chem. Phys. 71, 3613-3619 (1979).

43. R.I. Martinez and J.T. Herron, "Real-time mass-spectroscopic study of the chemistry initiated by infrared laser photolysis: CF_2HCl", Chem. Phys. Lett. 84, 180-182 (1981).

44. M. Santos, R. Hernandez-Vara, J.M. Herreros, P.F. Gonzalez-Diaz, "Dependence of the unimolecular dissociation products on the fluence of the CO_2 laser beam", J. Mol. Structure 142, 533-536 (1986).

45. S.R. Leone, "Rate coefficients for vibrational energy transfer involving the hydrogen halides", J. Phys. Chem. Ref. Data 11, 953-996 (1982).

46. A.S. Pine, A. Fried, J.W. Elkins, "Spectral intensities in the fundamental bands of HF and HCl", J. Mol. Spec. 109, 30-45 (1985).

47. W.J.R. Tyerman, "Rate parameters for reactions of ground-state difluorocarbene and determination of the absolute intensity of the A $^1B_1$ - X $^1A_1$ absorption bands", Trans. Farad. Soc. 65, 1188-1198 (1969).

48. J.M. Birchall, R.N. Haszeldine, D.W. Roberts, "Cyclopropane Chemistry. Part II. Cyclopropanes as sources of difluorocarbene", J. Chem. Soc. Perkin I, 1071-1078 (1973).

49. P.A. Hackett, M. Gauthier, C. Willis, "Mechanism of multiphoton dissociation of hexafluoroacetone", J. Chem.

Phys. 69, 2924-2925 (1978).

50. P.A. Hackett, M. Gauthier, C. Willis, R. Pilon, "The selective decomposition of $CF_3{}^{13}COCF_3$ at natural abundance: multiphoton dissociation at threshold", J. Chem. Phys. 71, 546-548 (1979).

51. P.A. Hackett, C. Willis, M. Gauthier, "Multiphoton dissociation of hexafluoroacetone: effects of pressure, fluence, wavelength, and temperature on the decomposition yield and C-13 and O-18 isotopic selectivity", J. Chem. Phys. 71, 2682-2692 (1979).

52. P.A. Hackett, M. Gauthier, W.S. Nip, C. Willis, "Kinetic study of infrared multiphoton dissociation: two frequency irradiation of $CF_3{}^{13}COCF_3$ molecules at natural abundance", J. Phys. Chem. 85, 1147-1152 (1981).

53. O.N. Avatkov, E.B. Aslandi, A.B. Bakhtadze, R.I. Zainullin, Yu. S. Turischev, "Multiphoton absorption and dissociation of hexafluoroacetone in a strong infrared CO_2 laser field", Sov. J. Quant. Elec 9, 232-235 (1979).

54. W. Fuß, K.L. Kompa, F.M.G. Tablas, "Wavelength

dependence of multiphoton absorption and dissociation of hexafluoroacetone", Faraday Disc. 67, 180-187 (1979).

55. W. Batey, A.B. Trenwith, "The thermal decomposition of hexafluoroacetone", J. Chem. Soc. 1961, 1388-1392.

56. D.A. Whytock, K.O. Kutschke, "The primary process in the photolysis of hexafluoroacetone vapour. I. Photodecomposition studies", Proc. R. Soc. London Ser. A306, 503-510 (1968).

57. G.G.A. Perkins, E.R. Austin, F.W. Lampe, "The 147 nm photolysis of hexafluoroacetone", J. Chem. Phys. 68, 4357-4359 (1978).

58. N. Selamoglu, M.J. Rossi, D.M. Golden, "Absolute rate of recombination of CF_3 radicals", Chem. Phys. Lett. 124, 68-72 (1986).

59. G.A. Laguna, S.L. Baughcum, "Real-time detection of methyl radicals by diode laser absorption at 608 cm^{-1}", Chem. Phys. Lett. 88, 568-571 (1982).

60. F. Caralp, R. Lesclaux, A.M. Dognon, "Kinetics of the reaction of CF_3 with O_2 over the temperature range 233-273

K", Chem. Phys. Lett. 129, 433-438 (1986).

61. J.C. Amphlett, L.J. MacAuley, "Reactions of trifluoromethyl radicals with iodine and nitric oxide", Can. J. Chem. 54, 1234-1238 (1976).

62. W.S. Benedict, R. Herman, G.E. Moore, S.Silverman, "Infrared line and band strengths and dipole moment function in HCl and DCl", J. Chem. Phys. 26, 1671-1677 (1957).

63. I.P. Herman, "Two-frequency CO_2 laser multiple-photon dissociation and dynamics of excited state absorption in CDF_3", Chem. Phys. 75, 121-132 (1983).

64. S.A. Tuccio, A. Hartford, Jr., "Deuterium enrichment via selective dissociation of fluoroform-d with a pulsed CO_2 laser", Chem. Phys. Lett. 65, 234-239 (1979).

65. D.K. Evans, R.D. McAlpine, H.M. Adams, "The multiphoton absorption and decomposition of fluoroform-d: laser isotope separation of deuterium", J. Chem. Phys. 77, 3551-3558 (1982).

66. R.D. McAlpine, D.K. Evans, H.M. Adams, "CO_2 laser-induced multiphoton absorption of fluoroform-d: the effects of collisions", J. Chem. Phys. 78, 5990-5992 (1983).

67. V. Parthasarathy, S.K. Sarkar, K.V.S. Rama Rao, J.P. Mittal, "Selective IR laser chemistry of CDF_3 in natural fluoroform", Appl. Phys. B39, 187-190 (1986).

68. M. Gauthier, R. Pilon, P.A. Hackett, C. Willis, "Infrared multiphoton chemistry of fluoroform-d", Can. J. Chem. 57, 3173-3177 (1979).

69. K. Takeuchi, S. Satooka, Y. Makide, "Tritium isotope separation by CO_2-laser irradiation at low temperature", Appl. Phys B33, 83-90 (1984).

70. F. Magnotta, I.P. Herman, "Observations on the spectral dependence and T/D isotope selectivity in the CO_2 laser multiple-photon dissociation of trifluoromethane", Appl. Phys. B36, 207-212 (1985).

71. F. Magnotta, I.P. Herman, F.T. Aldridge, "Highly selective tritium-from-deuterium isotope separation by pulsed NH_3 laser multiple-photon dissociation of

chloroform", Chem. Phys. Lett. 92, 600-605 (1982).

72. I.P. Herman, F. Magnotta, F.T. Aldridge, "The status of the photochemistry and photophysics of tritium-from-deuterium isotope separation by infrared laser multiple-photon dissociation of chloroform", Israel J. Chem. 24, 192-196 (1984).

73. F. Magnotta, I.P. Herman, "Infrared laser multiple-photon dissociation of $CTCl_3$: wavelength dependence, collisional effects, and tritium/deuterium isotope selectivity", J. Chem. Phys. 81, 2363-2374 (1984).

74. R.D. McAlpine, J.W. Goodale, D.K. Evans, "Multiphoton absorption and decomposition studies of chloroform-d induced by a pulsed $^{13}CO_2$ laser", Can. J. Chem. 63, 2995-3000 (1985).

75. I.P. Herman, F. Magnotta, R.J. Buss, Y.T. Lee, "Infrared laser multiple-photon dissociation of $CDCl_3$ in a molecular beam", J. Chem. Phys. 79, 1789-1794 (1983).

76. J.J. Tiee, F.B. Wampler, W.W. Rice, Jr., "Reactions of chloromethylidyne, dichloromethylene, and

chlorofluoromethylene radicals", Chem. Phys. Lett. 73, 519-521 (1980).

77. I.C. Plumb, K.R. Ryan, "Gas phase reactions of CF_3 and CF_2 with atomic and molecular fluorine: their significance in plasma etching", Plasma Chem. and Plasma Processing 6, 11-25 (1986).

78. M.A.A. Clyne, R.F. Walker, "Absolute rate constants for elementary reactions in the chlorination of CH_4, CD_4, CH_3Cl, CH_2Cl_2, $CHCl_3$, $CDCl_3$, $CBrCl_3$", JCS Faraday I 69, 1547-1567 (1973).

79. K. Sugawara, T. Nakanaga, H. Takeo, C. Matsumura, "Reactions of CF_2 carbene with Br_2, Cl_2, and H_2 studied by means of CO_2 laser photolysis and infrared diode laser spectroscopy", Chem. Phys. Lett. 134, 347-349 (1987).

APPENDIX A

In this appendix, the kinetic equations used in the study of combination reactions will be developed.

Consider the general recombination reaction of two A radicals combining to form molecule B. In general, the reaction occurs in two steps: the (reversible) reaction of the two radicals forming vibrationally excited B^*, followed by collisional relaxation of the excited B^* molecule.

$$2\,A \underset{k_2}{\overset{k_1}{\rightleftharpoons}} B^* \qquad \ldots.(A.1)$$

$$B^* + M \xrightarrow{k_3} B + M \qquad \ldots.(A.2)$$

Applying a steady-state approximation to the B^* molecule, the following rate of reaction is obtained:

$$\text{Rate} = k_1 k_3 (A)^2 (M)/[k_2 + k_3(M)] \qquad \ldots.(A.3)$$

At high pressure $k_3(M)$ exceeds k_2 and the rate of reaction at the high-pressure limit is obtained:

$$\text{Rate} = k_1 (A)^2 \qquad \ldots\ldots(A.4)$$

At low pressure, where k_2 exceeds $k_3(M)$, the rate of reaction involves a third-body:

$$\text{Rate} = k_1 k_3 (A)^2 (M)/k_2 \qquad \ldots\ldots(A.5)$$

At the pressures employed in this thesis, it can be concluded that the recombination of CF_2 will be at the high pressure limit,[78] while the recombination of CF_3 is also at or very near the high pressure limit.[58] Hence, kinetic studies on these reactions were done using equation (A.4). On the other hand, the reaction of CF_3 and O_2 is not at the high pressure limit at the pressures used in this study,[60] and therefore the third-body effect had to be taken into account.